

**HIGH - GRADIENT MAGNETIC CAPTURE**

**OF**

**MINERAL PARTICLES**

**by**

**Glenn S. Dobby**

A thesis submitted to the Faculty of Graduate Studies  
and Research in partial fulfillment of the require-  
ments for the Degree of Master of Engineering.

**Department of Mining and Metallurgical Engineering**

**McGill University**

**Montreal, Canada**

**August, 1976**

i.  
Glenn S. Dobby

Department of Mining  
and Metallurgical  
Engineering

McGill University

A B S T R A C T

High-Gradient Magnetic Capture of Mineral Particles

The relevant parameters affecting particle capture in an M.I.T. high-gradient magnetic separator were closely controlled and tested on a superconducting, batch separator. Parameters studied were particle size, particle susceptibility, field strength, fluid velocity, fluid viscosity and feed weight. Particle susceptibility was controlled by the preparation of mineral samples to narrow susceptibility ranges on the Frantz Isodynamic Separator. Two modes of high-gradient separator operation, drainage and constant flow, were employed. Matrix length effect upon magnetic recovery was also investigated.

The test data was used to develop empirical models of particle capture which described magnetic recovery in terms of field strength, particle size and susceptibility, fluid velocity and feed weight.

From the empirical model, a methodology of predicting high-gradient separation of mineral samples was developed and demonstrated. The methodology was shown to be capable of handling complex samples with wide size and susceptibility distribution.

R E S U M ESEPARATION DE PARTICLES MINÉRALES PAR FORT CHAMP MAGNÉTIQUE

L'effet des principaux paramètres qui affectent l'efficacité du triage de particules par champ magnétique a été étudié. Ces paramètres sont la taille et la susceptibilité magnétique des particules, l'intensité du champ, la longueur de la zone de séparation, la vitesse et la viscosité du fluide et le poids de la charge introduite. La séparation est effectuée sous un champ magnétique intense fourni par un diamant à enroulement superconducteur construit au M.I.T. La préparation d'échantillons ayant un domaine étroit de susceptibilité magnétique a été réalisée grâce à un Séparateur Isodynamique Frantz. L'efficacité du triage a été évaluée sous deux conditions : écoulement libre de la charge et pression constante.

Les résultats expérimentaux ont permis de construire un modèle du processus de séparation magnétique qui tient compte des principales variables. Une méthode permettant de prédire l'efficacité de la séparation dans le cas d'échantillons possédant une grande diversité de taille de particules et de susceptibilité magnétique a été mise au point et vérifiée expérimentalement.

ACKNOWLEDGEMENTS

The author wishes to express his sincere gratitude to Dr. J. A. Finch for his constant help and enthusiasm during the course of the research, and for his critical comments in the preparation of this thesis.

Special appreciation is extended to Mr. Jan Nasset for his help in the testwork and enthusiastic discussion of the topic. Thanks are due to the people in the Physics Department, whose aid in the setting up and use of the cryogenic equipment was invaluable.

Financial support from the National Research Council of Canada and the Quebec Iron and Titanium Corporation is gratefully acknowledged. Thanks are also extended to Sala Magnetics for their supply of the basic apparatus.

TABLE OF CONTENTS

	<u>Page</u>
ABSTRACT	i
RESUME	ii
ACKNOWLEDGEMENTS	iii
TABLE OF CONTENTS	iv
NOMENCLATURE	viii
GLOSSARY	x
LIST OF FIGURES	xi
LIST OF TABLES	xv
CHAPTER 1 - INTRODUCTION	1
1.1 Introduction to High Intensity Wet Magnetic Separation	2
1.1.1 The Jones Separator	3
1.1.2 The Carpco Separator	7
1.1.3 The M.I.T. High-Gradient Magnetic Separator	9
1.2 Basic Principles of Magnetic Capture of Paramagnetic Particles	14
1.2.1 Field Gradient	14
1.2.2 Magnetic Force	18
1.2.3 Competing Forces	21
1.2.4 Force Balance	22
1.2.5 Matrix Length Effect	23
1.3 Aim of Thesis	25

<b>CHAPTER 2 - APPARATUS AND EXPERIMENTAL TECHNIQUE</b>	26
2.1 Apparatus	27
2.1.1 Description of Superconducting High-Gradient Separator	27
2.1.2 Calibration of Solenoid	35
2.1.3 Operation of Superconducting Magnet	40
2.1.4 Permanent Magnet	47
2.1.5 Frantz Isodynamic Separator	50
2.2 Sample Preparation	55
2.2.1 Uni-Mineral Samples	55
2.2.2 Multi-Mineral Samples	61
2.3 Experimental Technique	69
2.3.1 Constant Head System	69
2.3.2 Drainage System	71
2.3.3 Permanent Magnet Operation	72
2.3.4 Analysis of Test Products	72
<b>CHAPTER 3 - RESULTS</b>	74
3.1 Susceptibility Measurements	75
3.1.1 Uni-Mineral Samples	75
3.1.2 Effect of $d$ and $\theta$ Upon Measured $k$	75
3.1.3 Multi-Mineral Samples	78
3.2 Effect of Parameters on HGMS Particle Capture - Constant Head System	82
3.2.1 Zero Field Tests	82
3.2.2 Effect of Particle Size	85
3.2.3 Effect of Velocity	85
3.2.4 Effect of Viscosity	91
3.2.5 Effect of Matrix Loading	91

	<u>Page</u>
3.2 (Cont'd)	
3.2.6 Sphalerite and Chalcopyrite Recovery	91
3.2.7 Effect of Matrix Length	97
3.3 An Empirical Model of Capture - Constant Head System	97
3.4 Effect of Parameters on HGMS Particle Capture - Drainage System	100
3.4.1 Zero Field Tests	100
3.4.2 Effect of Particle Size	100
3.4.3 Effect of Velocity	100
3.4.4 Effect of Viscosity	107
3.4.5 Effect of Matrix Loading	107
3.4.6 Sphalerite and Chalcopyrite Recovery	107
3.5 An Empirical Model of Capture - Drainage System	112
 CHAPTER 4 - EMPIRICAL MODEL PREDICTIONS	 115
4.1 Recovery of a Size Range of Hematite <sup>A</sup>	116
4.2 Hematite - Silica Separations	116
4.3 Prediction of Mineral Separation - A Methodology	121
4.3.1 Predicted and Measured Metallurgy of Tin Concentrate Separations	123
4.3.2 Predicted and Measured Metallurgy of Copper Concentrate Separation	124
4.4 Predictions Using Shorter Matrix	128
 CHAPTER 5 - DISCUSSION	 131
5.1 Susceptibility Measurements	132
5.2 Force Balance Model of Capture	133

	<u>Page</u>
5.3 Empirical Models of Capture	134
5.3.1 Form of the Models	136
5.3.2 Parameter Effects	137
5.3.3 Precision of Separation	140
5.4 Matrix Length and the Empirical Model	141
5.5 Separation Predictions and the Use of the Frantz Isodynamic Separator	142
CHAPTER 6 - CONCLUSIONS AND FUTURE WORK	145
6.1 Conclusions	146
6.2 Claims for Original Research	149
6.3 Suggestions for Future Work	150
APPENDIX 1 Effect of Matrix Length	151
APPENDIX 2 Cross-sectional Diagram of Helium Dewar	153
APPENDIX 3 Tabulated Results	154
APPENDIX 4 Step-wise Multiple Regression of Data	162
APPENDIX 5 Methodologies for Predicting Metallurgy from Tin Concentrate and Copper Concentrate Separations	175
APPENDIX 6 Precision of Separation	189
REFERENCES	192

NOMENCLATURE

$F_M$	= magnetic force
$F_C$	= competing forces
$F_x$	= magnetic force acting in the x direction
$F_D$	= drag force
$F_G$	= force due to gravity
H	= magnetic field strength, gauss or kG
$\frac{dH}{dx}$	= field gradient
	= $\frac{\Delta H}{\Delta X}$
$2M_w$	= wire magnetization, kG
	= 10 if $H > 10$ kG
	= H if $H < 10$ kG
$M_p$	= particle magnetization, kG
$\rho$	= mineral density, gm/cm <sup>3</sup>
$\rho_L$	= liquid density, gm/cm <sup>3</sup>
k	= volume susceptibility, emu/cm <sup>3</sup> - Oe
$\chi$	= mass susceptibility, emu/gm - Oe
	= $k/\rho$
d	= particle size (arithmetical mean), $\mu\text{m}$
V	= particle volume, cm <sup>3</sup>
U	= fluid velocity, cm/sec
$\eta$	= fluid viscosity, cp
a	= matrix filament diameter, $\mu\text{m}$
L	= matrix length, cm
$\rho_m$	= matrix packing density
$L_m$	= matrix loading
	= ratio of feed weight to matrix weight

$f_d$	=	fraction of feed of size d
$f_a$	=	fraction of feed of mineral a
$r$	=	electrical resistance, ohm
$I$	=	current, Amps
$I_{50\%}$	=	current on Frantz at which 50 wt. % of the sample has been magnetically removed, Amps.
$\theta$	=	side slope on Frantz, degrees
$n$	=	number of matrix segments of equal weight and length
$R_{Mn}$	=	magnetic recovery with n pads, %
$R_{Mx}$	=	magnetic recovery with a matrix weight x, %
$R_{My}$	=	magnetic recovery with a matrix weight y, %
$R_M$	=	recovery by magnetic capture, %
$R_{aM}$	=	magnetic recovery of mineral a, %
$R_{Md}$	=	magnetic recovery of particles of size d, %
$R_p$	=	recovery by physical entrapment, %
$R_{ap}$	=	physical entrapment recovery of mineral a, %
$R_{pd}$	=	physical entrapment recovery of particles of size d, %
$R_T$	=	total recovery to mags, %
$R_{aT}$	=	total recovery to mags of mineral a, %
$R_{Td}$	=	total recovery to mags of particles of size d, %
$\Delta R_T$	=	difference between measured and predicted $R_T$ , %
$R_{\text{fract}}$	=	fractional magnetic recovery
$W_a$	=	weight % of mineral a in feed
$G_{a \text{ Mags}}$	=	grade of mineral a in mags, %
$G_{a \text{ Non-mags}}$	=	grade of mineral a in non-mags, %

GLOSSARY

susceptibility - the amount of attraction exerted on a given substance by a magnetic field, expressed as the ratio of the intensity of magnetization to the magnetic field strength.

permeability - the measure of the ease with which magnetic lines of force are carried by a particular material.

paramagnetic - a material with a small, positive susceptibility, and a permeability slightly greater than 1.

diamagnetic - a material with a small, negative susceptibility, and a permeability slightly greater than 1.

ferromagnetic - a material with a susceptibility and a permeability that are both large and positive.

field gradient - a spatial variation of magnetic field intensity.

working volume - the separating zone of a magnetic separator: in the case of a high-intensity wet magnetic separator, the volume element of the magnetic field in which is placed the matrix.

matrix - ferromagnetic material which creates sites of high field gradient, and on to which attaches the magnetic material, or mags product.

mags - material removed in a magnetic separator as a result of magnetic capture or physical entrainment.

non-mags - material that passes through a magnetic separator without being captured.

magnetic response curve - a plot of weight percent to mags fraction vs current, as derived from testing a material on the Frantz Isodynamic Separator.

LIST OF FIGURES

<u>Figure Number</u>	<u>Caption</u>	<u>Page</u>
1	Basic design of a continuous high intensity separator. The design of the magnetic circuit will vary.	5
2	Schematic diagram of the continuous Jones high-intensity wet magnetic separator.	6
3	Schematic diagram of a 4-pole CarpcO separator employing ferro-magnetic steel spheres as matrix material.	8
4	Schematic diagram of the cyclic M.I.T. high-gradient magnetic separator.	10
5	Schematic diagram of the continuous high-gradient magnetic separator.	12
6	Simplified situation of a spherical, paramagnetic particle approaching a cylindrical, ferromagnetic wire in an HGMS.	15
7	Schematic illustration of the field distribution around a cylindrical, ferromagnetic wire whose axis is perpendicular to a uniform magnetic field.	16
8	Magnetization curves for (a) diamagnetic, (b) paramagnetic, and (c) ferromagnetic materials.	20
9	Photograph of superconducting solenoid.	28
10	Photograph of dewar (with solenoid inside), vacuum system (rotary pump out of picture at bottom), vacuum gauge, power supply, head tank, and water line.	31
11	Schematic diagram of sample handling system (not to scale).	34
12	(a) Photograph of steel wool matrix. (b) Photograph of a single piece of expanded metal matrix.	37
13	Calibration of Hall probe mV output to field strength.	38
14	Calibration of solenoid current supply to field strength generated in the bore of the superconducting solenoid.	39
15	Distribution of field strength along the axis of the superconducting solenoid.	41
16	Schematic diagram of evacuation system (not to scale).	42

17	Schematic diagram of valve employed to pump liquid helium from the He <sub>L</sub> transfer container into the dewar	44
18	Photograph of transfer procedure. Photo shows the He <sub>L</sub> container, the He gas cylinder, the transfer line, and the valve which was schematically shown in Figure 17.	46
19	Photograph of permanent magnet with the matrix cannister, containing an expanded metal matrix. The matrix and magnet are in the mags flush position.	48
20	Field distribution along the axis of the permanent magnet	49
21	Photograph of the Frantz Isodynamic Magnetic Separator.	51
22	Schematic diagram of a paramagnetic particle between the pole pieces of the Frantz Separator. The particle is moving in the (+)z direction along the chute.	52
23	Calibration of current applied to the electromagnets of the Frantz to the maximum field strength generated between the pole pieces.	54
24	Size distribution of the as received tin concentrate, with estimated pyrrhotite distribution. Data points derived through the use of the cyclosizer were calculated for the S.G. of SnO <sub>2</sub> . The equivalent pyrrhotite size are noted.	63
25	Magnetic response curves, for several size intervals of the tin concentrate, including the -325m sample. $\theta = 20^{\circ}$ .	64
26	Size distribution of the copper concentrate sample (a) as received, (b) ground for 25 min., and (c) the cyclone U/F of the ground material. Data points derived through the use of the cyclosizer were calculated for a S.G. of 4.4	67
27	Magnetic response curves for the first three cyclosizer cone products of the copper concentrate. $\theta = 20^{\circ}$ .	68
28	Magnetic response curves of the four uni-mineral samples. $\theta = 20^{\circ}$ .	76
29	Measured volume susceptibility vs field strength at which the measurement was made, for the side slopes indicated, for (a) sphalerite and chalcopyrite, and (b) hematite and ilmenite. #1 cyclone material was used in all cases.	80
30	$R_p$ vs $d$ for ilmenite, hematite and silica at various velocities. Constant head system.	83
31	$R_p$ vs $L_m$ for ilmenite at 3 velocities. Constant head system.	84

	<u>Page</u>
32	$R_M$ vs H for five particle sizes of hematite. Constant head system. 86
33	$R_M$ vs d for hematite at various field strengths. Constant head system. 87
34	(a) $R_M$ vs $H^2 d^2$ for hematite data of Figures 32 and 33 (b) $R_M$ vs $\log H^2 d^2$ . 88
35	$R_M$ vs H for 21 $\mu\text{m}$ ilmenite at four velocities. Constant head system. 89
36	(a) $R_M$ vs $H^2/U$ for data of Figure 35 (b) $R_M$ vs $\log H^2/U$ for data of Figure 35. 90
37	$R_M$ vs $L_m$ for ilmenite at 9.9 cm/sec. Constant head system. 93
38	$R_M$ vs $\log \frac{H^2 d^2}{L_m}$ for the data of Figure 37. 94
39	$R_M$ vs H for three particle sizes of sphalerite and chalcopyrite at three velocities. Constant head system. 95
40	$R_M$ vs $\log \frac{HMwd^2}{U}$ for sphalerite and chalcopyrite data (tests 74 to 96, constant head system, Appendix 3). 96
41	$\log (1 - R_{Mn})$ vs n for matrix length tests performed on the permanent magnet with 22 $\mu\text{m}$ hematite at 3 cm/sec 99
42	Plotted regression results (equation 27) for constant head system. 101
43	$R_D$ vs d for ilmenite and sphalerite at several velocities. Drainage system. 102
44	$R_p$ vs $L_m$ for 21 $\mu\text{m}$ ilmenite at 10 cm/sec. Drainage system. 103
45	$R_M$ vs H for 5 particle sizes of hematite at 10 cm/sec. Drainage system. 104
46	(a) $R_M$ vs Hd for the data of Figure 45. (b) $R_M$ vs $\log Hd$ for the data of Figure 45. 105
47	$R_M$ vs H for 21 $\mu\text{m}$ ilmenite at five velocities. Drainage system. 106
48	(a) $R_M$ vs H/U for the data of Figure 47 (b) $R_M$ vs $\log (H/U)$ for the data of Figure 47. 108
49	(a) $R_M$ vs H for 21 $\mu\text{m}$ ilmenite at 10 cm/sec and five matrix loadings. Drainage system. (b) $R_M$ vs $\log (H^2/L_m)$ for the same data. 110

Page

50	$R_p$ vs $H$ for 22 $\mu$ m chalcopyrite and sphalerite at two velocities. Drainage system.	111
51	Plotted regression results (equation 28) of drainage system tests including all four minerals.	113
52	Plotted regression results (equation 29) of drainage system ilmenite and hematite tests.	114
53	Predicted and measured grades and recoveries for $Fe_2O_3$ from synthetic $Fe_2O_3 - SiO_2$ mixtures as a function of feed % $Fe_2O_3$ .	120

LIST OF TABLES

<u>Table Number</u>	<u>Heading</u>	<u>Page</u>
1	Helium well dimensions.	30
2	Matrix dimensions for steel wool matrix and two expanded metal matrices.	36
3	Size and weight of hematite samples.	56
4	Size analysis of hematite cyclone underflow and overflow.	57
5	Size and weight of ilmenite samples.	59
6	Size and weight of sphalerite and chalcopyrite samples.	60
7	Size of silica samples.	62
8	Size and pyrrhotite distribution of -325 tin concentrate. Also, the metallurgy from separation on the Frantz of -325 tin concentrate.	66
9	Metallurgy of separation on the Frantz of copper concentrate.	70
10	Mass and volume susceptibilities of uni-mineral samples. Measured at $\theta = 20^\circ$ using #1 cyclone material.	77
11	Effect of d upon measured k for hematite and sphalerite. Measured at $\theta = 20^\circ$ .	79
12	Susceptibilities of tin and copper concentrates at selected currents. Measured at $\theta = 20^\circ$ .	81
13	Magnetic recovery vs viscosity for constant head tests with ilmenite.	92
14	Results of matrix length tests employing seven successive matrix segments.	98
15	Magnetic recovery vs viscosity for drainage tests with hematite.	109
16	Predicted and measured $R_T$ of a size range of hematite - constant head system.	117
17	Predicted and measured $R_T$ of a size range of hematite - 3 drainage system tests.	118

		<u>Page</u>
18	Predicted and measured $\text{Fe}_2\text{O}_3$ recovery and grade in separations of synthetic $\text{Fe}_2\text{O}_3 - \text{SiO}_2$ mixtures.	119
19	Predicted and measured metallurgy of tin concentrate separations.	125
20	Copper concentrate separation results, including predicted and measured $R_T$ .	127
21	Predicted and measured $R_T$ for five constant head tests employing the shorter expanded metal matrix.	129
22	Predicted and measured $R_T$ for a constant head test employing the shorter expanded metal matrix and hematite cyclone underflow as feed.	130

#### APPENDIX

3-1	Data from constant head system tests.	155-158
3-2	Data from drainage system tests.	159-161
4-1	Step-wise regression data - hematite and ilmenite, constant head system.	168
4-2	Sphalerite and chalcopyrite data - constant head system.	169
4-3	Linear regression - constant head system.	170
4-4	Step-wise regression data - hematite and ilmenite, drainage system.	171
4-5	Step-wise regression - data from all four samples, drainage system.	172
4-6	Linear regression - all data, drainage system.	173
4-7	Linear regression - hematite and ilmenite data only, drainage system.	174

CHAPTER 1

INTRODUCTION

### 1.1 Background to High Intensity Wet Magnetic Separation

Wet magnetic separation, until about ten years ago, was mainly applied to the concentration of minerals of high magnetic susceptibility such as magnetite, at relatively coarse sizes. The number of different separators capable of treating these highly magnetic minerals was substantial (1, 2). At that time the principles of high gradient magnetic capture were understood, as evidenced by the development in the 1940's of the Frantz Ferro-filter (1).

However, inadequacy of the contemporary magnet technology prevented the economic production of high intensity magnetic fields over large volumes, and thus prevented treatment of lower susceptibility minerals. Rapid advancements in magnet design over the past ten to fifteen years has led to development of high-intensity magnetic separators. Not only have these separators been able to treat weakly paramagnetic minerals, but they have also extended the range of treatable particle size down to about one micrometre.

The improved magnets offer two primary advantages. First, the higher field strengths produced will inherently increase the magnetization of para- and dia-magnetic particles, making them more responsive to a magnetic field gradient. Second, the magnets are capable of magnetizing to saturation large volumes of ferromagnetic "matrices", such as spheres, rods, grooved plates and fibres. It is the perturbation of the magnetic field by the magnetized matrices that create large gradients in magnetic field, which in turn help to create magnetic forces large enough to capture fine paramagnetic particles from a slurry flow.

High-intensity wet magnetic separation has been reviewed by Lawver and Hopstock (3) and by Oberteuffer (4). Several types of high-intensity separators have been developed, the variations being mainly in the design of the magnetic circuit and in the type of matrix employed. It is not the intention now to discuss the attributes of each separator, but to review the more important ones and to discuss their main differences in design and use.

#### 1.1.1 The Jones Separator

G. H. Jones first patented the Jones separator (5-7) in 1955 as a cyclic device with an automatic operation of 10-15 cycles per minute. The three operating stages per cycle are: (1) magnetic capture of particles from a slurry flow on to vertical, grooved, ferromagnetic plates placed in a strong magnetic field; (2) flushing at high \* velocity with the magnetic field still present, to collect a middlings product; and (3) flushing with the field off to collect the magnetic product. The separating zone, or working volume, is the air gap between the poles of a strong electromagnet in which is placed the salient pole plates.

The machined points of the magnetized plates create points of high field gradient and sites for magnetic collection of particles. Inter-plate spacing can be adjusted to accommodate various particle sizes. An advantage in the use of plates as matrix material is that, since the air gaps are very small, the magnetic flux is easily conducted through the working volume. This is economically beneficial. However, a major disadvantage in the use of plates is a large capacity restriction due to the plates occupying a substantial fraction of the working volume.

Cyclic, or batch, separators are suitable for the processing of material in which the magnetics comprise a small weight fraction of the feed. However, if a large fraction of the feed is magnetically captured, as is the case with iron ore concentration, the matrix will quickly become loaded to capacity. Frequent shutting down of the field and flushing out of the magnetics will consume much of the processing time. This capacity loss would be economically unattractive. Unit batch operations also cause material handling difficulties in continuous process plants. Continuous high-intensity wet magnetic separators were, therefore, developed.

The essential design feature of the continuous high-intensity separators is a ring, or carousel, of matrix material revolving through a magnetic field, as schematically shown in Figure 1. The sample is fed in a slurry at the beginning of the working volume. As each section of the carousel passes through the magnetic field, the ferromagnetic matrix becomes magnetized and the magnetic minerals in the passing feed are captured and carried along with the matrix, while the less magnetic minerals pass through. The matrix with the magnetics revolves out of the working volume (and the magnetic field) and a high velocity water flush removes the magnetic product (or mags). High velocity flushes may also be used in the working volume to clean out physically entrained particles and produce a middlings product. A schematic diagram of a continuous, 4-pole Jones separator is shown in Figure 2.

Presently, the largest single application of high-intensity magnetic separation is at Itabira, Brazil, where 28 Jones DP-317 separators have been installed to treat the finer fractions of a hematite ore (8, 9). Rated capacity per separator is 120 TPH. The Jones separator has also been tested for the production of iron ore superconcentrates (<2% silica)

**FIGURE 1**

Basic design of a continuous high intensity separator (3).

The design of the magnetic circuit will vary

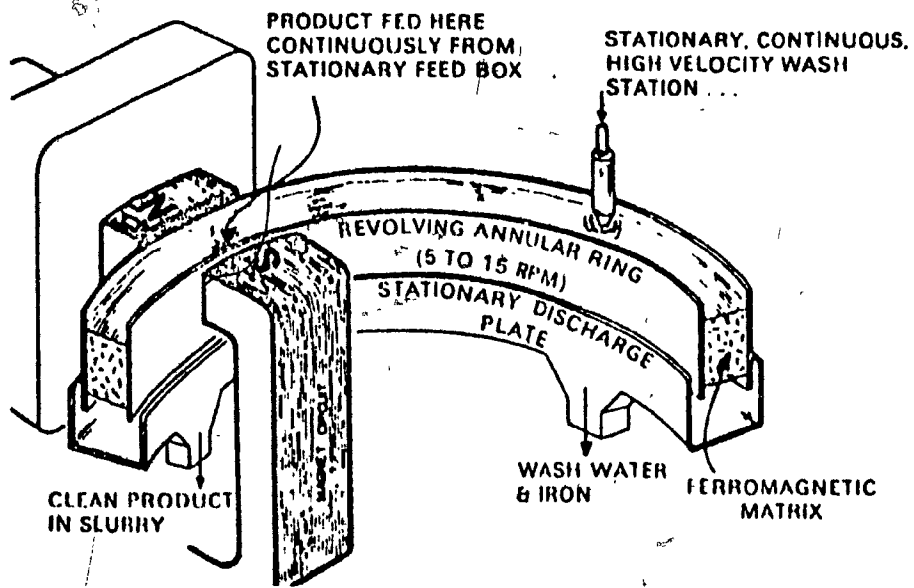
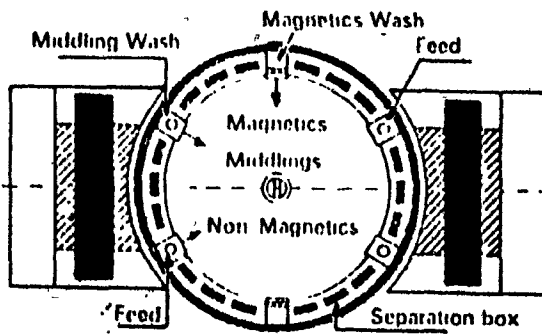
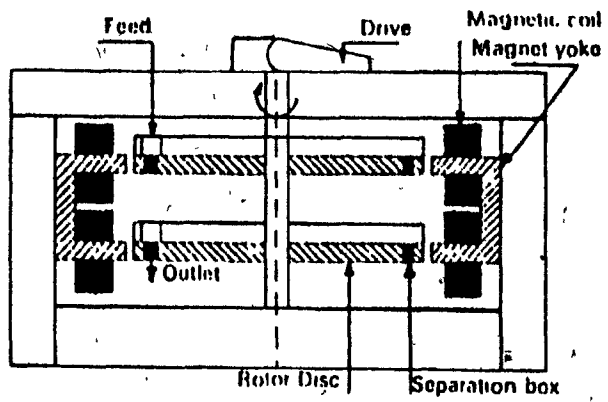


**FIGURE 2**

Schematic diagram of the continuous Jones high-intensity wet magnetic separator (3).



for direct reduction (8). The use of plates is advantageous in this respect, as the plates are parallel to the direction of slurry flow and thus provide minimum obstruction to the flow-through of non-magnetics. Bridges of highly magnetic particles between the plates is the main source of physical entrainment of non-magnetic particles (10).

### 1.1.2 The Carpco Separator

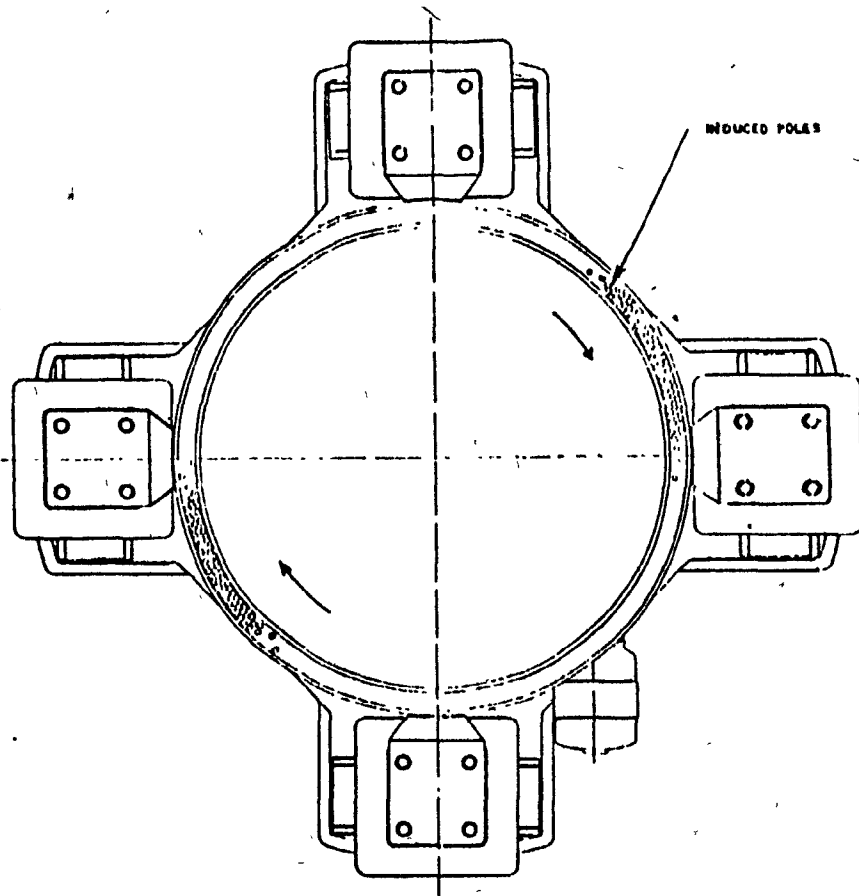
The Carpco separator (11, 12) was the first commercially applied continuous high-intensity magnetic separator. It differs from the Jones in the design of its magnetic circuit and in the use of spheres (or rods or cubes) as the matrix material. A schematic diagram of a four-pole Carpco separator is shown in Figure 3. The basic differences between the Jones and Carpco magnetic circuits can be observed by comparing Figures 2 and 3. It should be noted that the Jones circuit uses the carousel to conduct the flux between poles.

The spheres used in the Carpco separator to perturbate the magnetic field and generate points of high field gradient, range in diameter from 3/8 inch to 1 inch. A matrix of packed spheres, like plates, conducts the magnetic flux very well, and, like plates, spheres also occupy a large fraction of the working volume. Physical entrainment of non-magnetics is obviously a greater problem in a geometry of packed spheres, as opposed to one of parallel plates. The field gradients produced in the Jones separator are, on average, at least an order of magnitude higher than those in the Carpco separator. These latter two points have made the Jones a more attractive high-intensity separator for the iron-ore industry.

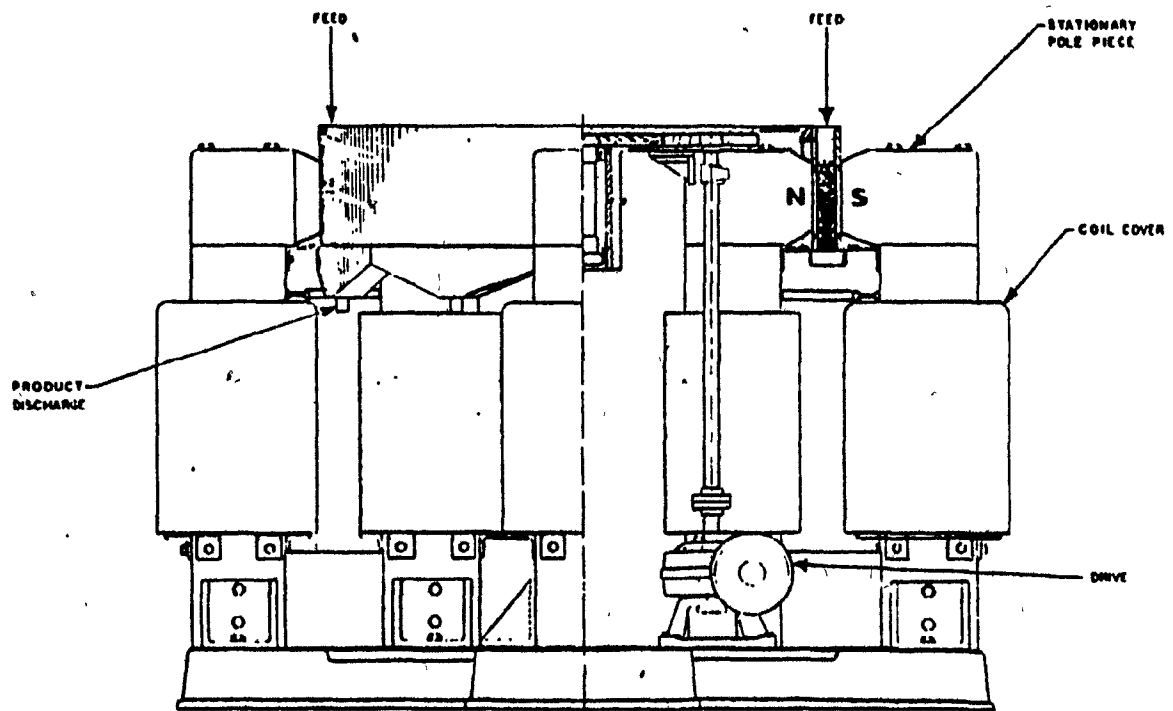
The Jones and Carpco separators use conventional magnetic circuits to create a magnetic field in the working volume and magnetize the matrix. This means that iron yokes are used to conduct the magnetic flux, created by electromagnetic coils, through the gap of the working

## FIGURE 3

Schematic diagram of a 4-pole Carpc separator employing ferromagnetic steel spheres as matrix material.



PLAN



ELEVATION

volume. The use of ferromagnetic iron intensifies the resultant field through the air gap, as that field is a combination of the field created by the electromagnets, plus the magnetization of the iron (13). Electric power consumption is reduced when iron is used to conduct the flux from the coils and produce high fields in the working volume. The result however, is a very heavy and large device in relation to its capacity.

### 1.1.3 The M.I.T. High-Gradient Magnetic Separator

An alternative to the high-intensity separator employing a conventional magnetic circuit is the M.I.T. high-gradient magnetic separator (HGMS), developed by Kolm and Marston (14, 15, 16). The separator consists basically of an iron-clad solenoid surrounding the matrix material - a fine, ferromagnetic steel wool or expanded metal lath. A schematic diagram of the high-gradient separator is shown in Figure 4. The magnet steel facilitates the return of the flux and aids in producing a uniform field over a greater portion of the length of the bore. Feed can be pumped from the bottom of the separator, or gravity fed.

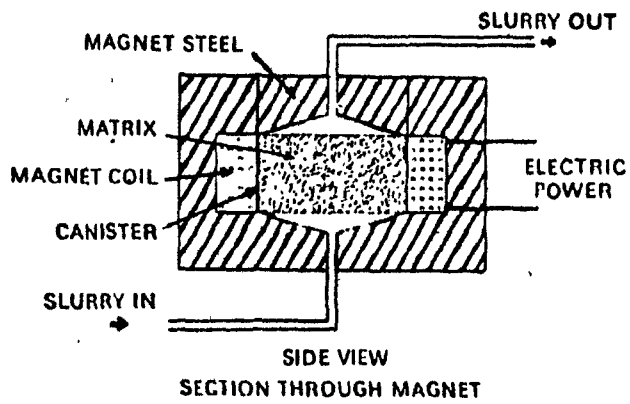
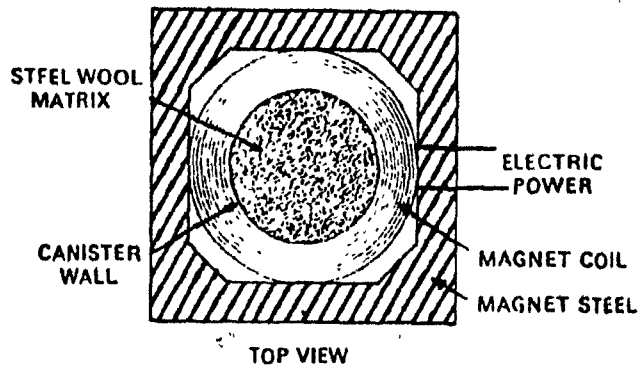
The advantage in using steel wool as the matrix material is that extremely high field gradients can be produced through the perturbation of the magnetic field by the ferritic steel fibres. The gradients produced are much higher than those of the Jones and CarpcO separators.<sup>1.</sup>

---

1. Thus the distinction of the M.I.T. separator as a "high-gradient" device, even though the gradients produced by other high-intensity separators are large compared to those of the low-intensity magnetic separators.

## FIGURE 4

Schematic diagram of the cyclic M.I.T. high-gradient magnetic separator(3).



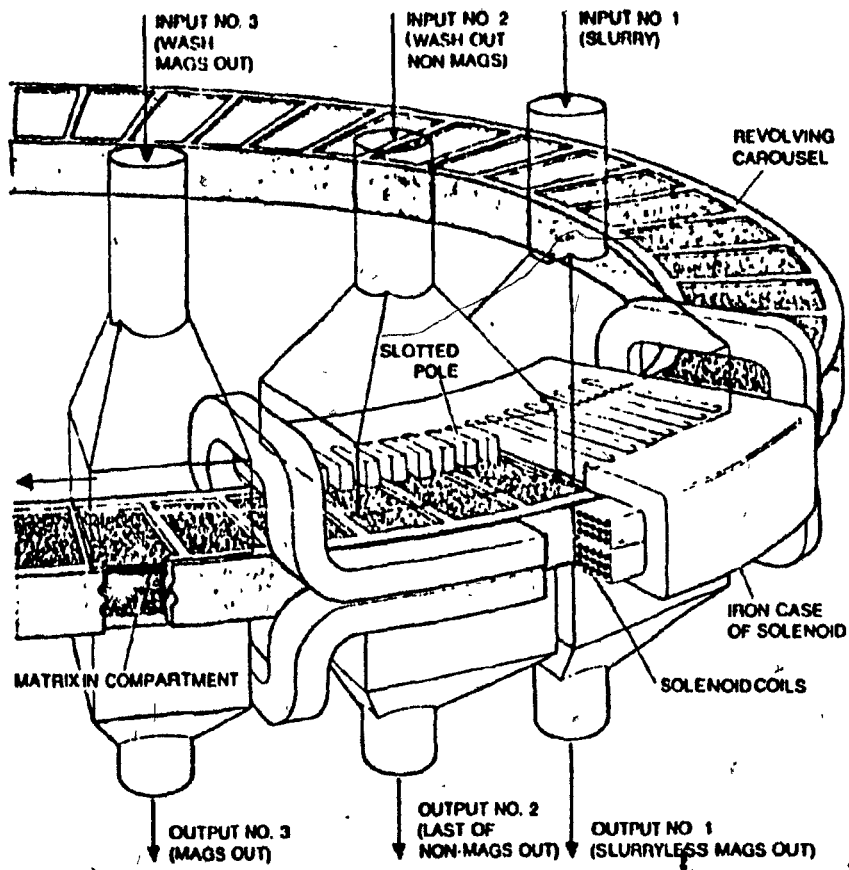
Steel wool also provides a large number of high-gradient sites for particle capture, and offers little resistance to slurry flow. Since the particle size and wire diameter should be of similar magnitude for maximization of magnetic forces, as will be explained in Section 1.3, the high-gradient separator is ideally suited for fine particles. With the use of a fine matrix, weakly paramagnetic particles as small as  $1\mu\text{m}$  can be captured in an HGMS.

In the 1940's, Frantz realized the potential advantages of a solenoid separator and the use of steel wool as matrix material. The mass of the steel wool only occupies a small portion of the total working volume. Even when tightly compressed, steel wool has a packing density of less than 10%, i.e. 90% void. Since it is mostly void, a steel wool matrix is very difficult to magnetize. Magnets, at the time of Frantz, were not capable of economically producing the high field strengths over large volumes required to saturate the ferromagnetic filaments. Marston applied Frantz's use of a solenoid surrounding steel wool and, with improved magnet design, developed a separator capable of generating up to 20,000 gauss in a large volume, easily enough to magnetize steel wool to saturation. Fundamental differences between the HGMS and the other high-intensity separators, and the improvement in process economics offered by the high-gradient separator have been discussed (14).

The HGMS described above is a batch separator. For reasons previously mentioned, a continuous device is essential for treatment of such feeds as iron ore. A continuous HGMS is presently in an advanced pilot plant stage, with test results of batch and continuous separations in good agreement (17, 18). Figure 5 is a schematic diagram of the continuous HGMS. The solenoid is elongated with the ends bent at  $90^\circ$

## FIGURE 5

Schematic diagram of the continuous high-gradient magnetic separator(15).



to allow the carousel to pass through. Note that the magnetic field produced is parallel to the slurry flow, while the fields produced by the Carpco and Jones separators are perpendicular to the slurry flow. As previously mentioned and seen in Figure 2, the magnetic field of the Jones separator is directed through the carousel. Residual magnetism of the Jones plates at the mags wash causes problems when dealing with highly magnetic particles. This is avoided with the HGMS design.

In summary, the main advantages of HGMS over other high-intensity devices are: (1) the generation of a higher background field, with the capability of magnetizing paramagnetic particles to a greater extent, (2) the creation of much larger field gradients, and, thus, larger magnetic forces, and (3) from (1) and (2), the capability of treating micrometre sized, weakly magnetic particles.

High-gradient magnetic separation has much potential in several industrial applications. Some of these are: 1. brightening and purification of kaolin clay through removal of micrometre sized titanium dioxide (19), 2. desulfurization of coal and coal slurries (20,) 3. removal of suspended solids and phosphates from sewage water (21), and 4. steel mill water treatment for removal of fine iron particles (22). Many ores, concentrates and tailings are potentially amenable to concentration by HGMS. With the general trend of having to mine ores with decreasing head grades there comes an increasing need to treat fines. Current technology is often incapable of adequately handling fine particles. Some of the present techniques of fines treatment and their associated difficulties have been discussed (23-29). With its capability of handling paramagnetic particles as fine as one micrometre HGMS may prove to be the solution for some of the fine particle problems.

## 1.2 Basic Principles of Magnetic Capture of Paramagnetic Particles

Theories of magnetic capture of paramagnetic mineral particles in a high-gradient separator have been proposed and discussed by several authors (4, 30-33). For the purpose of initially analysing the forces involved without going into a complex theory, an idealized situation describing the separation process can be applied. Consider Figure 6. A spherical paramagnetic particle, in a fluid moving at constant velocity, approaches a ferromagnetic wire of circular cross section. A uniform magnetic field applied perpendicular to the wire axis magnetizes the wire and the particle. A field gradient is created near the cylindrical wire and a magnetic force acting on the particle is developed. If the magnetic force is large enough to overcome the competing hydrodynamic and gravitational forces the particle will adhere to the wire.

The nature of the field gradient and the extent of the forces involved in this simplified situation can now be discussed.

### 1.2.1 Field Gradient

The magnetic permeability of a ferromagnetic material is much greater than that of air or water. As a result, the magnetic flux in the vicinity of a ferromagnetic body placed in a uniform magnetic field will be diverted through the body. The net effect is a change in the previously uniform distribution of magnetic flux. This field disturbance is schematically illustrated in Figure 7 for the case of the ferromagnetic cylindrical wire. The field strength at the top and bottom of the cylinder (point A) is greater than the uniform background field strength (point B), while the field strength at the sides (point C)

## FIGURE 6

Simplified situation of a spherical, paramagnetic particle approaching a cylindrical, ferromagnetic wire in an HGMS.

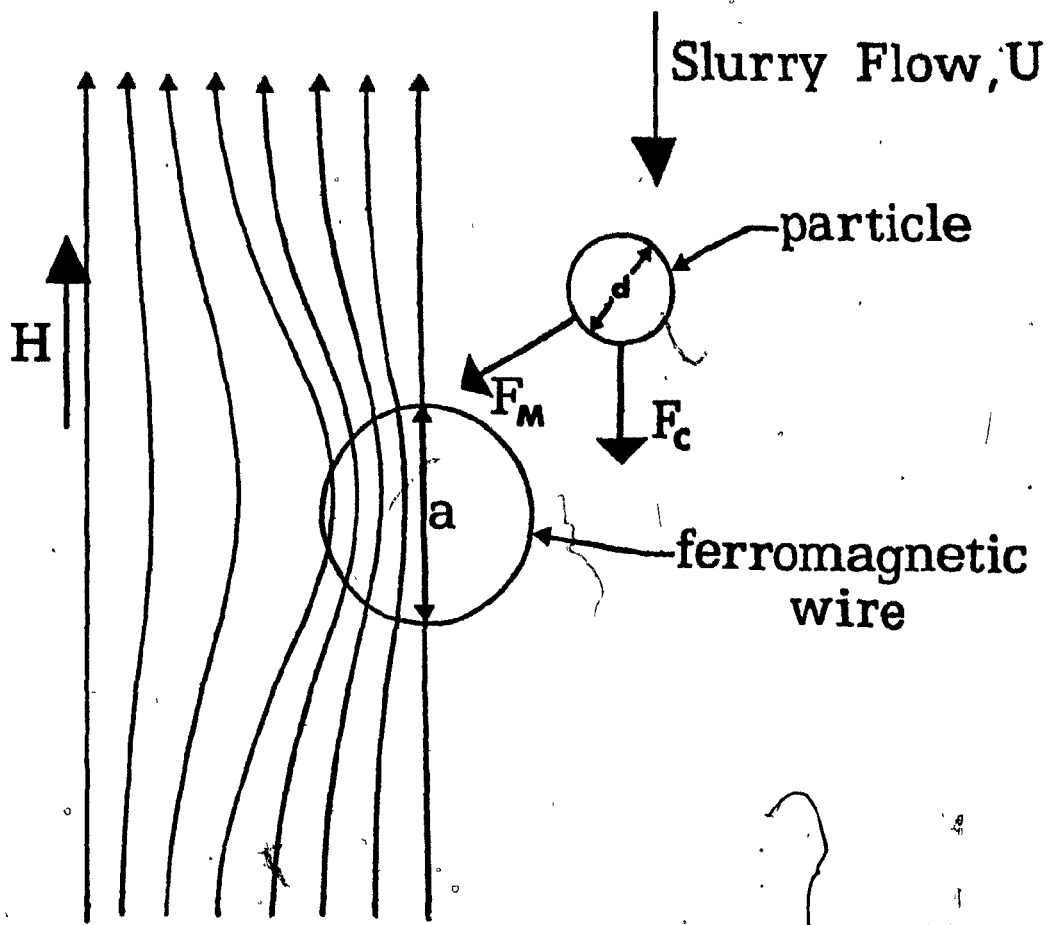
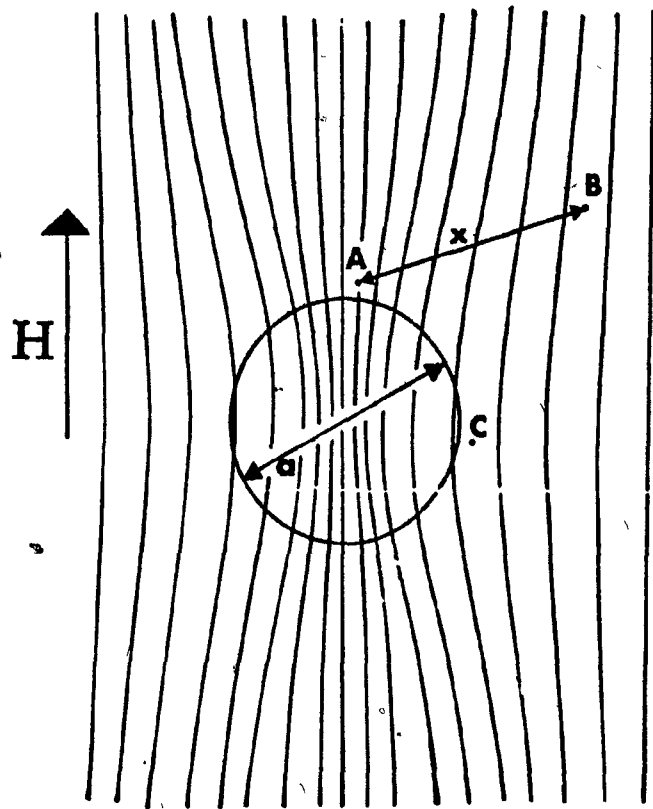


## FIGURE 7

Schematic illustration of the field distribution around a cylindrical, ferromagnetic wire whose axis is perpendicular to a uniform magnetic field.



is actually reduced. Field gradients, or localized spacial variations in the field intensity, have been created.

Determination of the actual field distribution around the wire over three dimensions can be made from elementary electromagnetic theory (34). Oberteuffer (35), however, has made an order of magnitude estimate for the value of the field gradient for the case of the cylindrical wire. Referring again to Figure 7, the intensity of the field at A is approximately equal to the sum of the background field intensity and the wire magnetization,  $2\pi M_w$ . Thus,

$$H_A \sim H + 2\pi M_w \quad (1)$$

At B, a distance  $x$  from A, the effect of the wire magnetization is minimal, so,

$$H_B \sim H \quad (2)$$

The field variation from B to A can therefore be expressed by:

$$\frac{H_B - H_A}{x} \sim \frac{2\pi M_w}{x} \quad (3)$$

where  $x$  is of the same magnitude as the wire diameter,  $a$  (35). Thus, an approximation to the magnitude of the field gradient around the wire is given by:

$$\frac{dH}{dx} \sim \frac{2\pi M_w}{a} \quad (4)$$

This equation expresses a noteworthy relationship - the smaller the diameter of wire employed, the larger the resulting field gradients.

### 1.2.2 Magnetic Force

The attractive or repulsive force acting along a given direction on a paramagnetic or diamagnetic particle in a magnetic field is given by,

$$F_x = VM_p \frac{dH}{dX} \quad (5)$$

The force is thus proportional to three terms: the volume of the particle, the particle magnetization, and the field gradient over the dimensions of the particle. A paramagnetic particle placed in a uniform magnetic field would become aligned with the field, but, since the gradient is zero, there would be no net magnetic force acting on the particle. In simple terms, the magnetization of the two ends of the particle, which acts as a dipole, are equal and opposite, thus cancelling each other. Only when there is a change in field intensity over the dimensions of the particle will the particle experience a net magnetic force.

Maximization of the magnetic force requires a maximization of the field gradient across the dimensions of the particle. Since the gradient around the cylindrical wire extends approximately one wire diameter from the edge of the wire, maximization of the gradient across the particle requires the particle diameter to be of the same order of magnitude as the wire diameter.

If the particle size is considerably larger than the wire diameter, a substantial portion of the particle will remain in a relatively uniform field. The larger particle will then not have as high a gradient acting across its total dimension as a particle whose size is matched to the wire size. A particle considerably smaller than the wire

diameter will also not experience as high a gradient across its diameter (35). Therefore, the very high field gradients produced through the use of fine, ferromagnetic wire are only effective in producing strong magnetic forces when the particle size is of the same magnitude as that of the wire. For maximization of the magnetic force,  $a = 2.7d$  (4). When this is so, the system is said to be matched.

Magnetic force is also maximized by maximizing the particle magnetization,  $M_p$ . Figure 8 (b) is a magnetization curve for a paramagnetic material. Its magnetization increases linearly with field strength, and the slope of the line is the particle susceptibility. Therefore,

$$M_p = kH \quad (6)$$

Combining Eqs. (4), (5), and (6), then, for a spherical particle the magnetic force can be estimated by:

$$F_M \sim \frac{\pi}{6} d^3 kH \frac{2\pi M_w}{a} \quad (7)$$

Unlike the magnetization of the paramagnetic particle, the magnetization of the ferromagnetic wire is nonlinear with field strength, as shown in the magnetization curve of Fig. 8(c). At sufficiently high values of  $H$  a ferromagnetic material will become saturated. The wire magnetization will therefore increase with  $H$  until it reaches a saturation level. For steel fibres, saturation occurs at between 7 and 10 kilogauss<sup>(3)</sup>.

To simplify, let

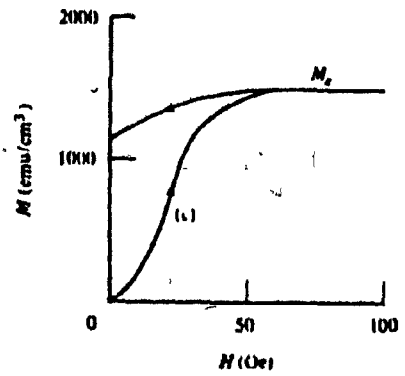
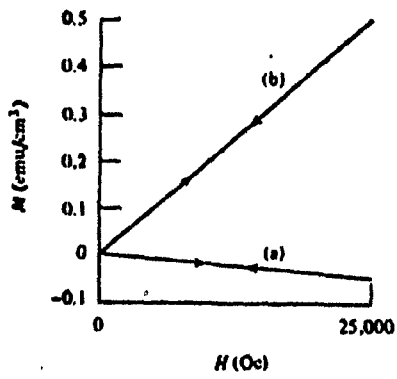
$$2\pi M_w = H, \text{ if } H < 10 \text{ kG} \quad (8)$$

and

$$2\pi M_w = 10, \text{ if } H > 10 \text{ kG} \quad (9)$$

## FIGURE 8

Magnetization curves for (a) diamagnetic, (b) paramagnetic, and (c) ferromagnetic materials (13).



The field gradient will, therefore, increase up to about 10 kG, whereupon a further increase in H will not affect the gradient. Increasing H above the wire saturation value only serves to increase the particle magnetization. The magnetic force can now be expressed by:

$$F_M \propto \frac{d^3 k H^2}{a}, \text{ if } H < 10 \text{ kG} \quad (10)$$

$$F_M \propto \frac{d^3 k H}{a}, \text{ if } H > 10 \text{ kG} \quad (11)$$

### 1.2.3 Competing Forces

An expression for the drag force acting on the spherical particle will vary with flow regime (d and U). A Stokesian regime will be assumed, where the hydrodynamic drag is given by:

$$F_D = 3\pi\eta dU. \quad (12)$$

The gravitational force acting on the spherical particle is:

$$F_G = \frac{1}{6} \pi d^3 g (\rho - \rho_L). \quad (13)$$

Other competing forces include interparticle effects such as electrostatic attraction, friction and magnetic attraction. They play an increasing role only when handling particles less than 5  $\mu\text{m}$ . The gravitational force is proportional to d, indicating that gravity will be an important consideration only at relatively coarse sizes. When handling particles between about 5 and 50  $\mu\text{m}$  in an HGMS, the predominant competing force is hydrodynamic drag.

#### 1.2.4 Force Balance

Capture of a paramagnetic particle in the HGMS will depend upon the relative magnitudes of the magnetic and drag forces. A force balance can therefore be set up:

$$\frac{F_M}{F_C} \sim \frac{F_M}{F_D} \propto \frac{d^2 kH(2\pi M_w)}{\eta Ua} \quad (14)$$

If a matched system can be approximated, then,

$$\frac{F_M}{F_D} \propto \frac{dkH(2\pi M_w)}{\eta U} \quad (15)$$

It would be expected that the recovery of paramagnetic particles to the magnetically captured fraction would be related to the value of the ratio of Eq. (14), or,

$$R_M = f \left[ \frac{F_M}{F_D} \right] \quad (16)$$

If the relationship is assumed to be linear, then,

$$R_M = C \left[ \frac{d^2 kH(2\pi M_w)}{\eta Ua} \right] \quad (17)$$

where C is a constant. This equation will be referred to as the force balance model.

The above discussion shows that the magnetic capture of a paramagnetic particle is a function of several variables - particle size and susceptibility, field strength, wire magnetization, and fluid velocity and viscosity. There are three other operating parameters that are of practical importance in an HGMS. They are: the matrix loading,  $L_m$ , (or the amount of sample fed to a fixed matrix weight); the matrix length,  $L$ ; and the matrix packing density,  $\rho_m$ .

The force balance model, although derived through several simplifying assumptions, is useful in indicating the basic relationship of the variables involved. A more general expression of how recovery to the magnetics fraction is related to the particle and operating parameters would be:

$$R_M = f(d^A k^B H^C \eta^D U^E L_m^F L^G \rho_m^J) \quad (18)$$

In summary, optimum use of the magnetic forces created in the high-gradient separator requires that the wire diameter employed be closely matched to the particle size of the material being handled. Maximizing the magnetic force means maximizing the particle magnetization and the field gradients across the particle, both of which are attained through increasing the background field strength. However, maximum field gradients will be attained at  $\sim 10$  kG, and increasing the field beyond this value only serves to increase particle magnetization. Hydrodynamic drag is increased through an increase in fluid velocity. Therefore, given a particular set of particle parameters ( $d$  and  $k$ ) and matrix parameters ( $L_m$ ,  $L$ , and  $\rho_m$ ), magnetic capture of the particles can be controlled through a selective balancing of field strength and fluid velocity.

#### 1.2.5 Matrix Length Effect

As a first attempt at understanding the role of matrix length in magnetic recovery, assume that the length of a matrix has been divided into  $n$  segments of equal weight and length. Knowing the recovery,  $R_{M1}$ , in the first segment ( $n = 1$ ), predictions of the recoveries for  $n > 1$  can be made by applying the equation (36):

$$R_{Mn} = 1 - (1 - R_{M1})^n \quad (19)$$

where all  $R_M$  values are fractional recoveries. Eq. (19) results from the application of probability theory, where  $R_{M1}$  is the probability of capture on any segment and is assumed to be independent of the number of the segment (see Appendix 1). To confirm the assumption the following technique was suggested (36). Re-arranging Eq. (19) the recovery to non-mags is:

$$1 - R_{Mn} = (1 - R_{M1})^n. \quad (20)$$

Thus,

$$\log (1 - R_{Mn}) = n \log (1 - R_{M1}). \quad (21)$$

If  $R_{M1}$  is independent of  $n$ , then a plot of  $\log (1 - R_{Mn})$  vs  $n$  should be linear with slope  $\log (1 - R_{M1})$ . The feed weight to each successive segment decreases, so that if the assumption of  $R_{M1}$  being independent of  $n$  is proved correct, then the implication is that  $R_M$  is independent of feed weight.

Appendix 1 also shows that if  $R_{Mx}$  represents the magnetic recovery of a mineral using the matrix weight  $x$ , then  $R_{My}$ , the recovery with matrix weight  $y$ , can be predicted by:

$$R_{My} = 1 - (1 - R_{Mx})^{y/x}. \quad (22)$$

### 1.3 Aim of Thesis

- ° The general aim of the thesis is to determine the effects of the controlling process parameters upon magnetic recovery in an HGMS. Control of the particle parameters will be obtained by preparation of samples to narrow particle size and susceptibility ranges. Operating parameters studied will include field strength, fluid velocity, viscosity, matrix loading and matrix length.

The data derived from testing the individual variables will be used to develop an empirical model of capture, encompassing all the variables studied.

Finally, the predictive capabilities of the empirical model will be examined through its application to the separation of several test samples.

CHAPTER 2  
APPARATUS  
AND  
EXPERIMENTAL TECHNIQUE

## 2.1 Apparatus

### 2.1.1 Description of Superconducting High Gradient Separator

The high-gradient separator used for experimentation was a laboratory batch separator. Its two basic components were:

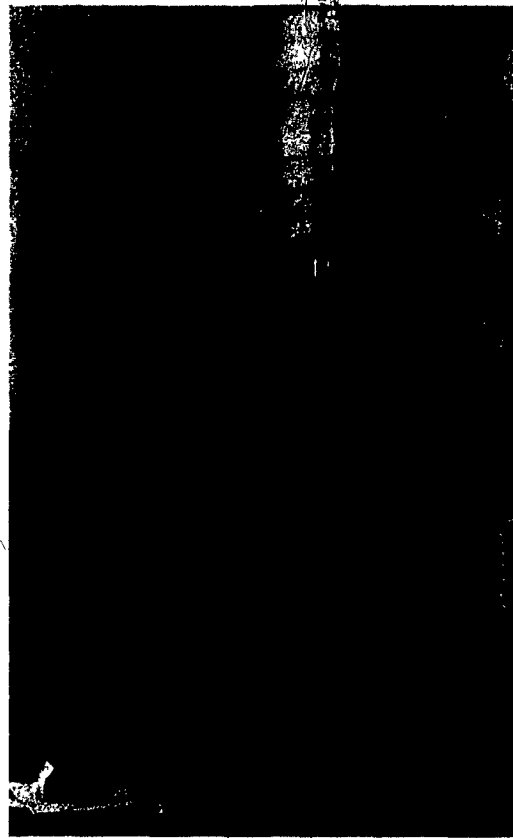
(a) the magnet, and (b) the matrix and sample handling system.

(a) The Magnet. The magnet used to generate the high background field was a superconducting solenoid. The property of major interest of a superconducting material is that below a certain critical temperature,  $T_c$ , and below a critical field strength the electrical resistance of the material drops to zero. Since  $r = 0$ , the power, or heat loss,  $I^2 r$ , equals zero. Currents can therefore be passed through a superconducting solenoid without the generation of large amounts of heat and without the large power loss caused by resistance heating. The magnetic field generated in the bore of a solenoid is directly proportional to the current. Strong magnetic fields can thus be produced in the bore of a superconducting solenoid without the need for the large currents or the large amounts of cooling water that conventional magnets demand. Theory of superconductivity and its practical applications can be found in the literature (37, 38). A superconducting high-gradient separator has also been described by Stekly (39).

The magnet used was a zirconium-niobium alloy, with a critical temperature,  $T_c$ , between 5 and 15°K. To keep it below  $T_c$  the solenoid was immersed in a bath of liquid helium, at 4.2°K. At that temperature the solenoid had a limiting field strength of about 22 kG and an inductance of 7.5 henry. The coil had an I.D. of 8.2 cm, an O.D. of 11.4 cm, and was 30.5 cm long. Figure 9 is a photograph of the solenoid.

FIGURE 9

Photograph of superconducting solenoid.



A cryostat, or dewar, was required to contain the bath of liquid helium, in which the solenoid sat. The dewar was basically a multi-walled, stainless steel, cylindrical container. A cross-sectional diagram of the dewar is shown in Appendix 2. Its overall length was 1.37 metres with a 30 cm O.D. The outside annulus was evacuated; the next annulus was filled with liquid nitrogen (77.4 K); the next was also evacuated; and the following larger space contained the liquid helium and the solenoid. On the other side of the helium well was an evacuated double wall. The 5.0 cm bore of the dewar was thus at room temperature. Table 1 lists some of the helium well dimensions and its capacity. The liquid nitrogen reservoir had approximately a 15 L capacity.

The diagram in Appendix 2 indicates a coupling for the pressure gauge, and the outlet and valve to the vacuum system. The walls of the dewar were pumped out with a water cooled oil diffusion pump backed by a  $\frac{1}{2}$  H.P. rotary pump. The ultimate vacuum before helium transfer was not known, as the vacuum gauge used did not have a scale low enough for an accurate reading. Figure 10 is a photograph showing the dewar (with the solenoid in place), power supply, diffusion pump, and slurry head tank.

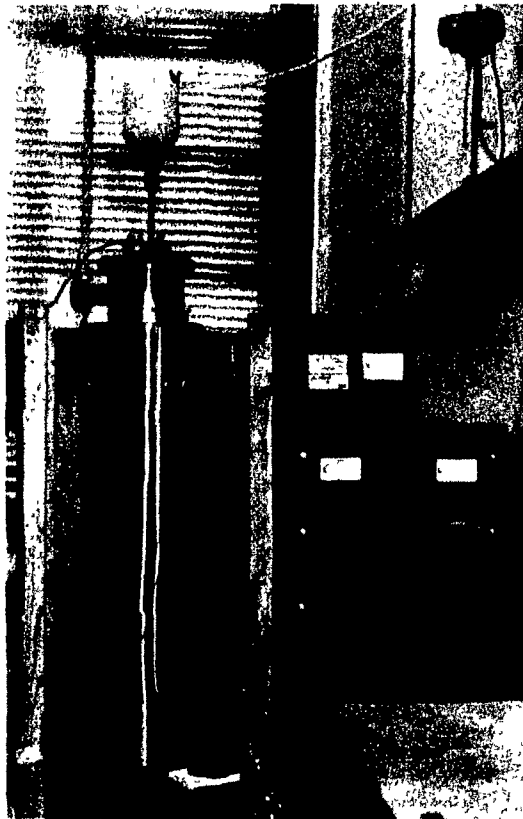
Liquid helium was transported in a 25 or 30 L portable dewar. The 25 L dewar was a conventional container with an insulation design similar to the magnet dewar (vacuum walls and liquid nitrogen shield). The newer, 30 L aluminium container did not require liquid nitrogen shielding. It employed super-insulation and recovered sensible heat by an ultra-shielding system in a high vacuum (40). Flexible, helical copper tubing with an outer evacuated wall was used to transfer the liquid helium from the helium container to the helium well of the

TABLE 1 - HELIUM WELL DIMENSIONS

O.D. of Helium Well, cm	20
I.D. of Helium Well, cm	7.6
Cross-sectional Area of Helium Well, cm <sup>2</sup>	280
Depth of 1 Liter of He <sub>L</sub> , cm	3.6
Volume of He <sub>L</sub> to cover solenoid, L	9.7
Total He Well Capacity, L	30

## FIGURE 10

Photograph of dewar (with solenoid inside), vacuum system (rotary pump out of picture at bottom), vacuum guage, power supply, head tank and water line.



magnet dewar. The two "legs" of the transfer line (one "leg" in either dewar) were 1.2 and 1.4 m long.

Depth of liquid helium in the dewars was determined by measuring the position of the top of the helium bath. This was done with a "dip stick", a 2.5 mm O.D., thin-walled stainless-steel tube 1.3 m in length. The dip stick was slowly lowered into the helium bath. When the bottom tip of the stick was in liquid helium, or the cold gas just above the liquid, strong vibrations up the tube were produced, perhaps due to the great temperature difference between the two ends of the thin tube. When the tip passed through the liquid-gas boundary, there was a very noticeable abrupt change in the frequency of the vibrations. Thus, by calibrating the stick length with the dimensions of the dewars, and noting the level at which there was a frequency change, the depth of liquid helium could be easily determined.

The maximum D.C. output of the power supply was 50 Amps at 6 Volts. However, a resistance of 0.2 $\Omega$  was connected in series between the power supply and magnet, to give a maximum normal current of about 30 Amps. This maximum increased slightly upon heating of the resistors.

When setting the current, it was important not to overshoot the required value. If the current was increased beyond the required value and then brought back down, a back emf would be induced in the coil. This would result in a generated field with a strength slightly different from that had the current been simply brought up to the desired value with no overshoot.

(b) Matrix and Sample Handling System

The matrix was held in a 25 cm long cannister placed in the room temperature bore of the solenoid. Two cannisters were used: plexiglass, with a 3.7 cm

I.D.; and copper, with a 3.8 cm I.D. The cannister was connected at either end to 1.3 cm I.D. copper tubing. Slurried sample was gravity fed via the tubing from a head-tank, through the separating zone (or working volume), and into a collecting bucket. Figure 11 is a schematic diagram of the sample transport system.

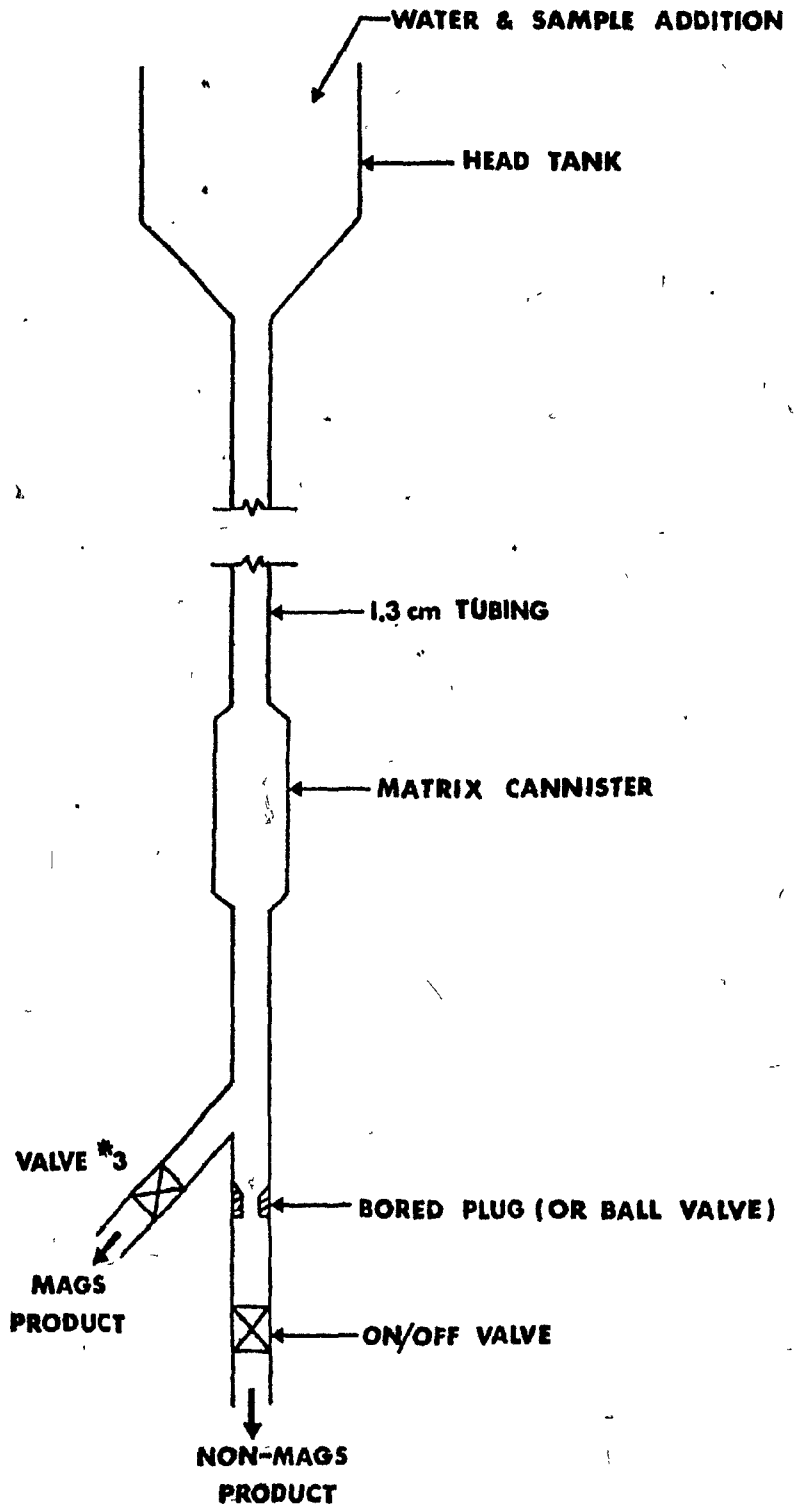
For tests run at constant velocity, i.e. constant head, a 2.5 L plastic head-tank sat directly above the matrix, resulting in a 1.35 m static head from the bottom of the head-tank to the centre of the matrix. A ball valve was placed approximately 20 cm below the cannister to act as an on/off valve. 1.3 cm I.D. Tygon tubing was attached to the valve and flow rate was controlled through the use of a set of bored, brass plugs placed in the line. Each plug had a different I.D. so that the velocity through the cannister and matrix was different for each of the 6 plugs. Reproducible velocities were thus quickly and reliably attained. Total head from the bottom of the head-tank to the end of the Tygon tubing (running into a bucket) was approximately 1.8 m.

A series of tests was performed using a drainage method of operation, whereby the slurry head was not held constant and the system was allowed to drain completely. For those tests a 2 L glass head-tank, approximately 3.0 m above the slurry outlet was employed. Instead of bored plugs, a second ball valve was used to control the flow rate. Velocities quoted in test work were determined from the flow rate of the first 500 cc of flow.

To develop a maximum velocity flush, the on/off valve was closed and valve 3 was opened. In this manner, there was no need to remove the velocity control plug, or readjust the flow control valve, each time a full velocity flush was employed.

## FIGURE 11

Schematic diagram of sample handling system( not to scale).



Two types of matrix material were used; stainless steel wool and expanded metal lath. Table 2 summarizes the dimensions and use of both types. Note that the expanded metal is considerably larger in cross section than the steel wool. Figure 12 (a) is a photograph of a section of steel wool inside a plexiglass cannister, and Figure 12 (b) is a photograph of a single piece of the expanded metal lath. Each piece of the expanded metal weighed about 1.5 gms. 39 pieces were stacked one on top of another within the cannister to yield the 59 gm (longer) matrix, and 21 pieces were employed to yield the 32 gm (shorter) matrix. The two expanded metal matrices were not packed at the same density, so that the ratio of their weights was not equal to the ratio of their respective lengths.

#### 2.1.2 Calibration of Solenoid

The magnetic field strength in the bore of a solenoid is directly proportional to the electric current passed through the solenoid. To calibrate the field strength of the superconducting magnet with the D.C. input a Hall probe (41), model HR-66, was employed. It was used in an open circuit with an input of 200 mAmps. The probe was first calibrated with a variable field strength electromagnet and a gaussmetre. The relationship between the gaussmetre readings and mVolt output of the Hall probe is plotted in Figure 13. Maximum field strength of the electromagnet was 13.2 kG.

The solenoid was then calibrated by placing the Hall probe in the centre of the solenoid, and recording the millivolt output at set current inputs from the magnet power supply. These millivolt readings were converted to field strength values using Figure 13. The linear relationship between solenoid field strength and current through the solenoid is shown in Figure 14 and is expressed by:

$$H = 0.15 + 0.63 I .$$

**TABLE 2**  
**Matrix Dimensions**

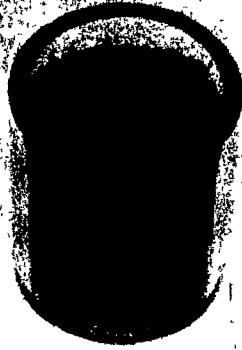
	Stainless Steel Wool	Expanded Metal	
		Longer	Shorter
Approx. dimensions of Cross-Section, $\mu\text{m}$	50 x 250	500 x 600	500 x 600
Weight, gms	30	59	32
Length, L, cm	24	8	3.5
Occupied Volume, $\text{cm}^3$ (I.D. = 3.7 cm)	260	86	38
Matrix Packing Density, $\rho_m$ , % ( $\rho_{\text{Fe}} = 7.85$ )	1.5	8.9	10.7

**FIGURE 12(a)**

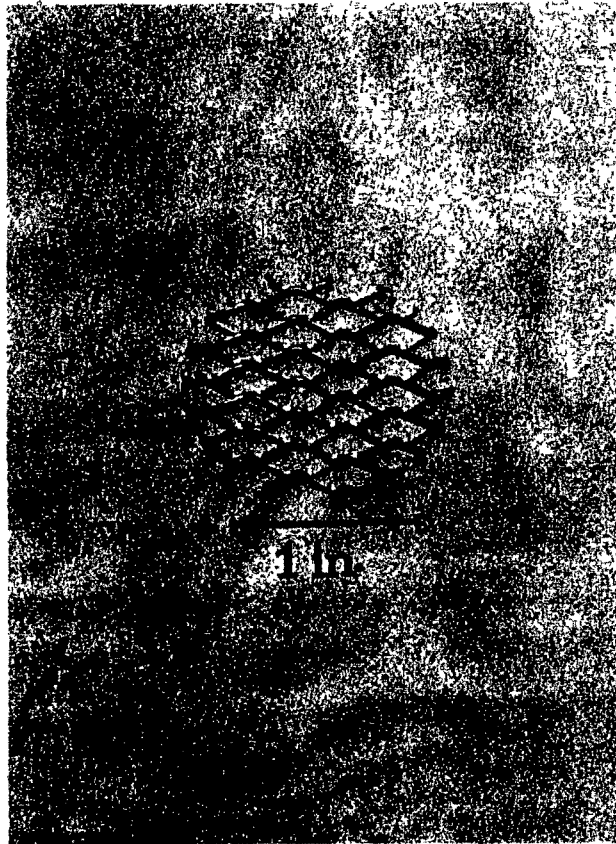
Photograph of steel wool matrix.

**FIGURE 12(b)**

Photograph of a single piece of expanded metal matrix.



1 in.



1 in.

## FIGURE 13

Calibration of Hall probe mV output to field strength.

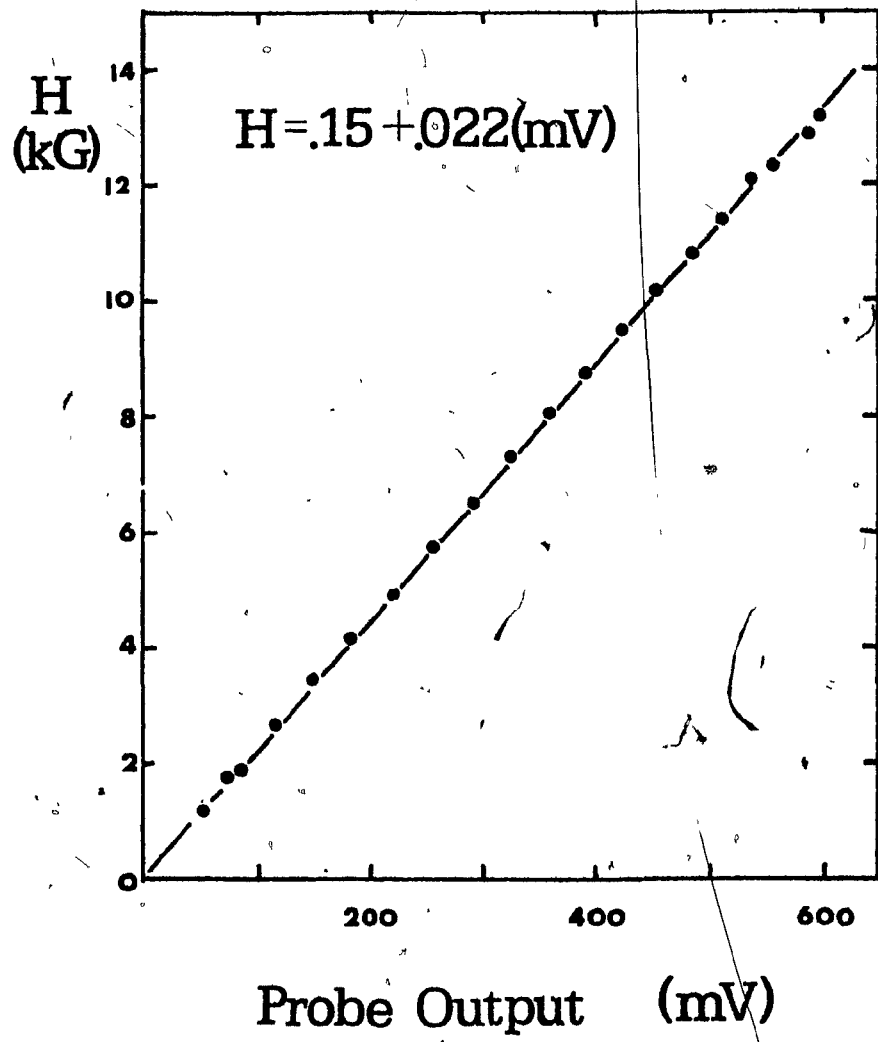
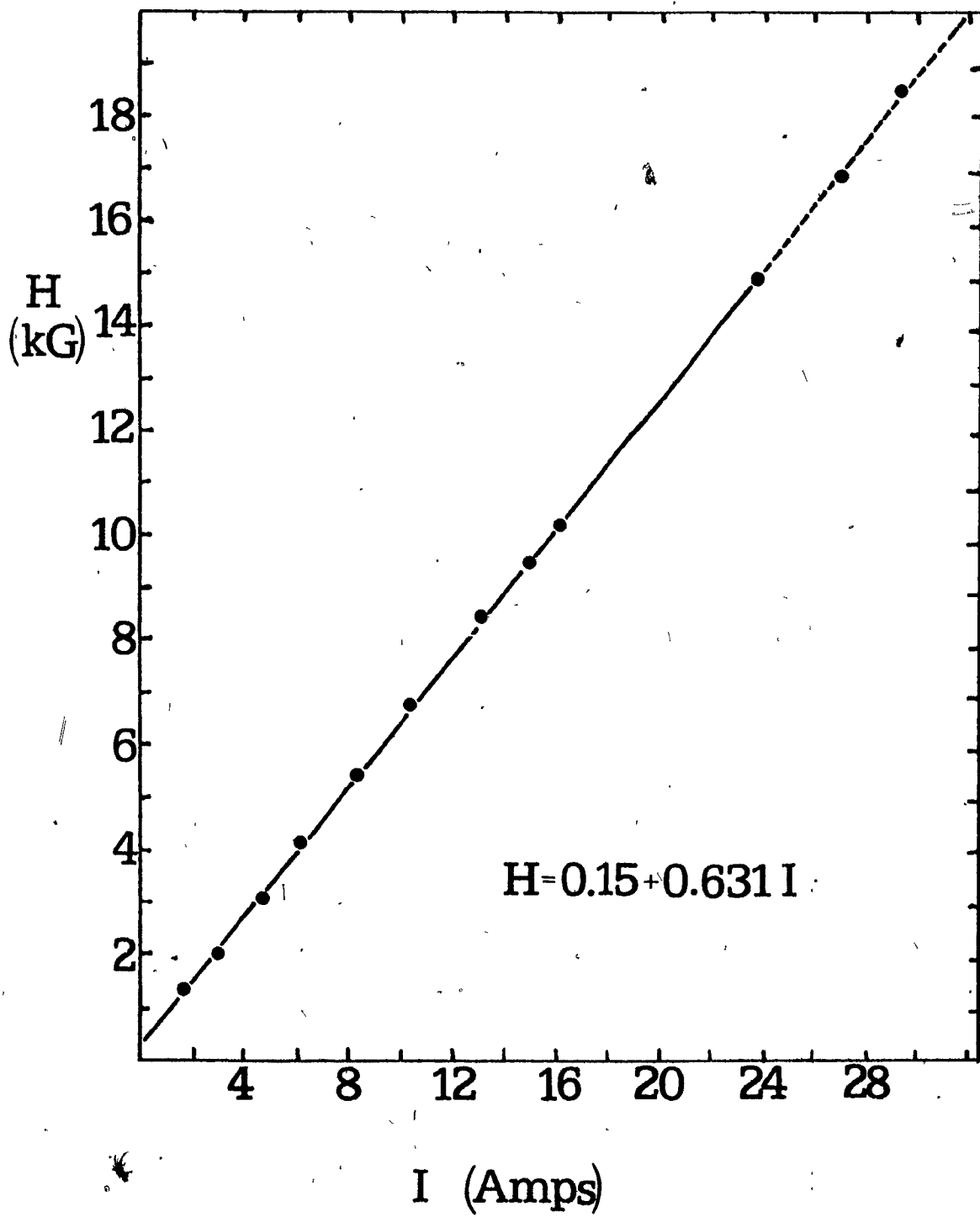


## FIGURE 14

Calibration of solenoid current supply to field strength generated in the bore of the superconducting solenoid.



H is in kG and I is in Amps. Since the probe was only calibrated to 13.2 kG, Figure 14 has been extrapolated from 13.2 to 20 kG. Current readings were accurate to approximately  $\pm 0.2$  Amp.

The Hall probe was also used to determine the distribution of field strength along the solenoid axis. This distribution is plotted in Figure 15 and indicates that the field is very uniform over the centre 20 cm of the bore.

### 2.1.3 Operation of Superconducting Magnet

Operation of the magnet for test purposes meant filling the dewar with liquid helium and keeping the helium boil-off rate at a low value. The operating procedure consisted of: 1. evacuating the walls of the dewar, 2. filling the nitrogen reservoir, 3. cooling the solenoid to liquid nitrogen temperature, and 4. placing the solenoid in the dewar and filling the liquid helium reservoir.

1. The dewar was pumped out over the period of 1 to 3 days with the use of the oil diffusion pump and rotary pump. A schematic of the evacuation system is shown in Figure 16. The initial procedure was as follows:

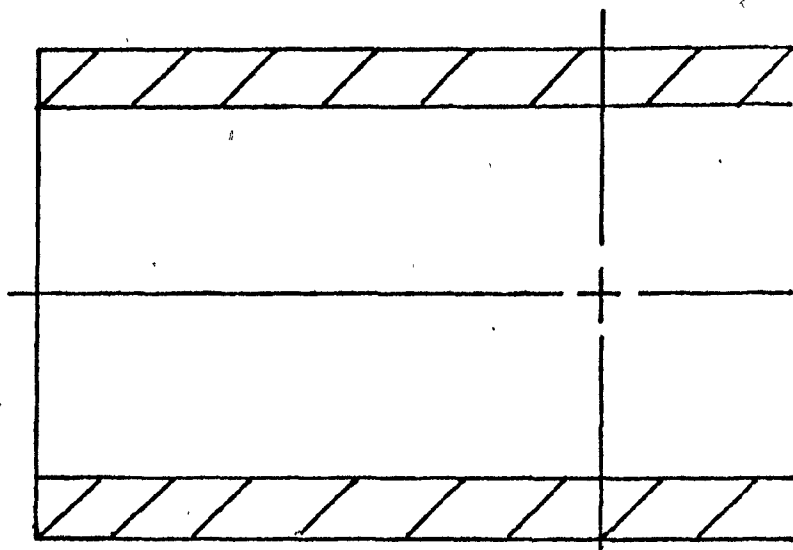
- (a) With valves 1 and 2 closed and the release valve open, switch rotary pump on.
- (b) Close release valve and open valves 1 and 2.
- (c) Switch heater of oil diffusion pump on.
- (d) Turn on water to cool diffusion pump.

If the dewar was already at the roughing vacuum (about 100  $\mu\text{m}$ ), the following procedure was used:

- (a) Switch rotary pump on.
- (b) Close release valve and open valve 1.
- (c) Switch diffusion pump and water line on.

## FIGURE 15

Distribution of field strength along the axis of the superconducting solenoid.



$$\frac{H}{H_C}$$

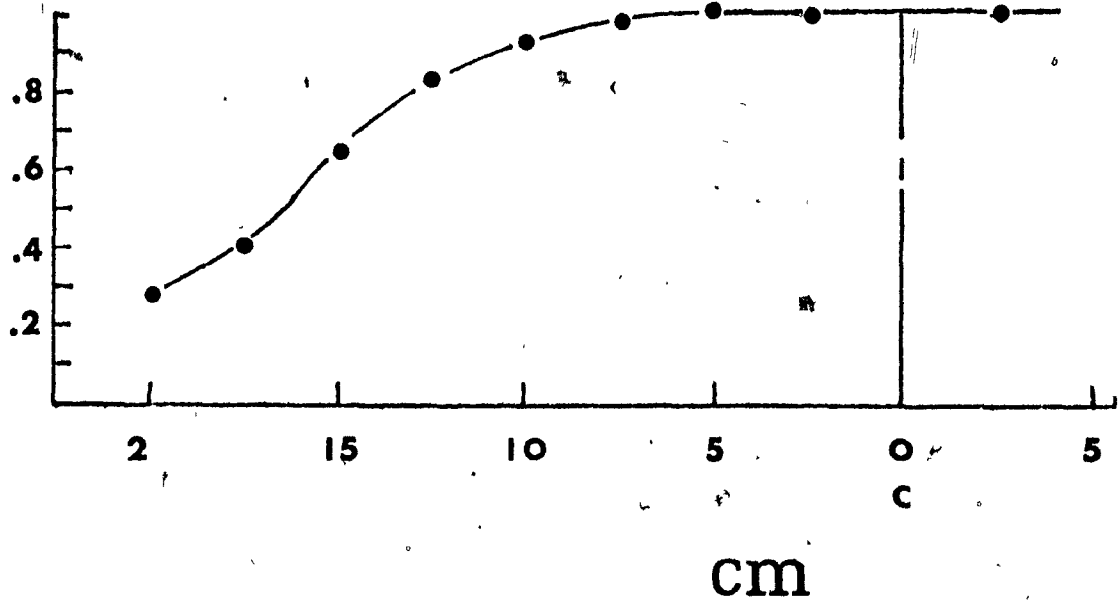
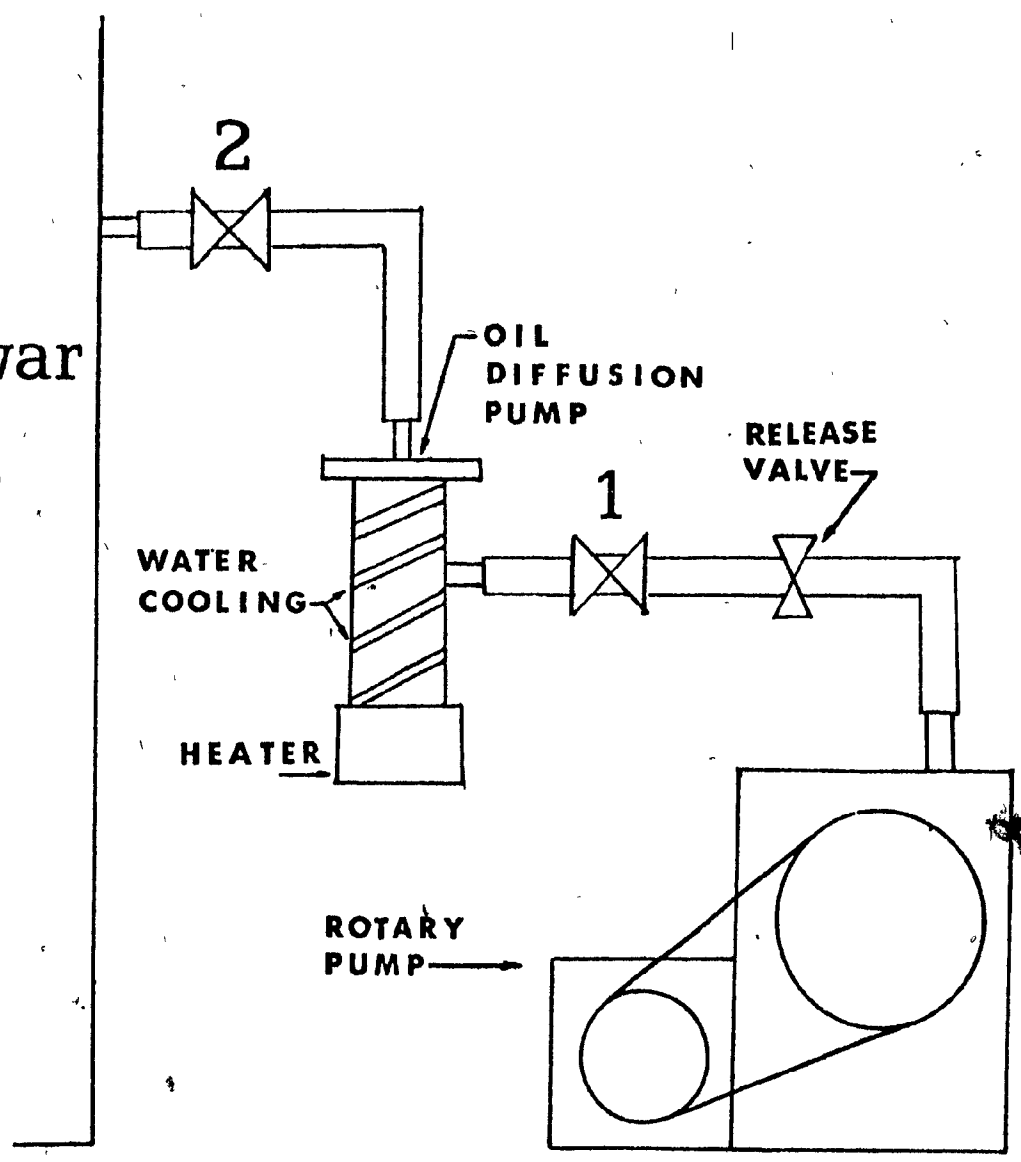


FIGURE 16.

Schematic diagram of evacuation system (not to scale).

Dewar



- (d) When oil heater is at maximum temperature, open valve 2.

The pumping system was shut down by the following procedure:

- (a) Close valve 2.  
(b) Switch heater of diffusion pump off (leave the cool water running).  
(c) When diffusion pump has cooled to room temperature (about 30 min.) close valve 1.  
(d) Switch rotary pump off and open release valve.

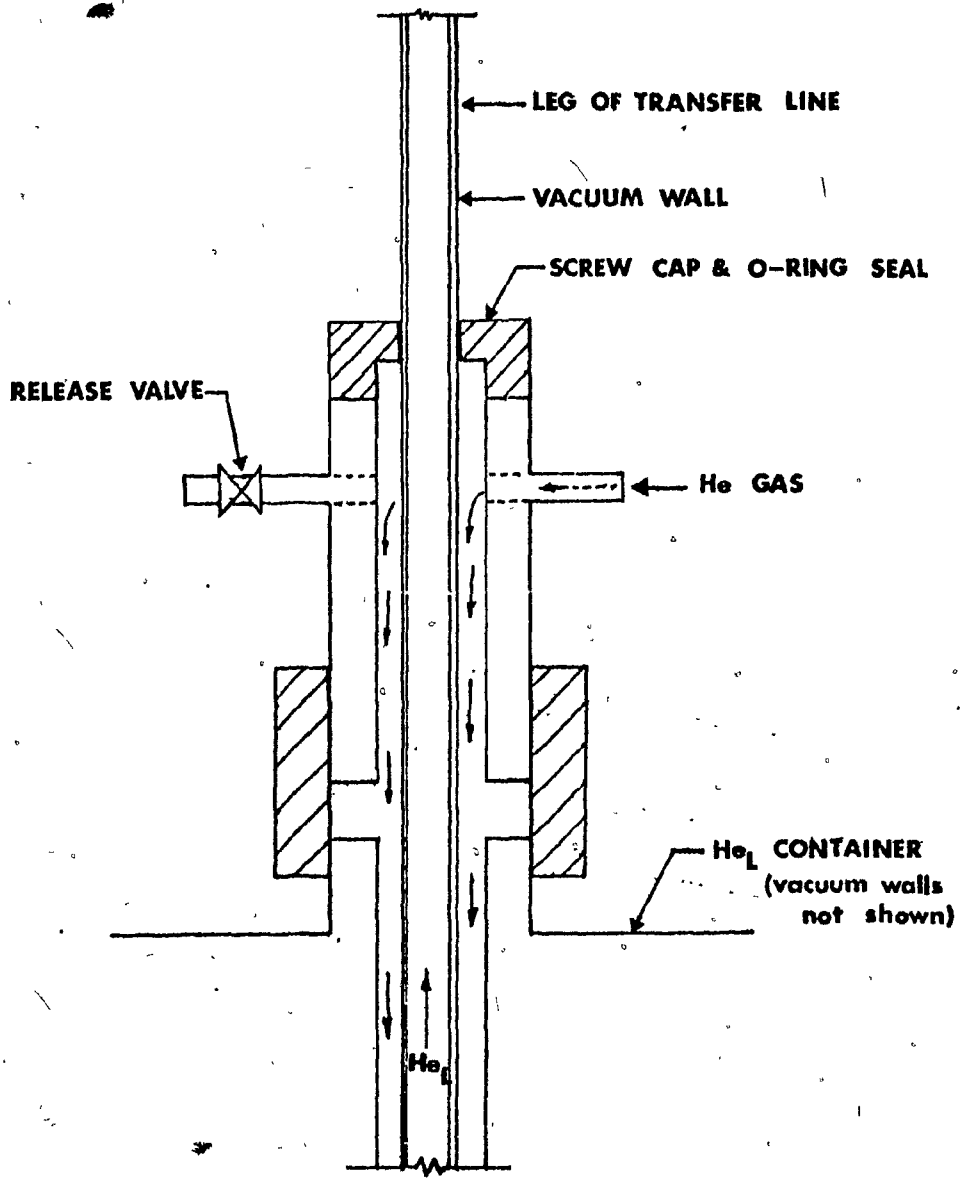
2. Nitrogen was transported from the main filling tank in a 30 L dewar. A valve was fitted to the  $N_L$  dewar (similar to that used on the liquid helium dewar, see Figure 17) such that an applied nitrogen gas flow into the  $N_L$  dewar would pressurize the vessel and force the liquid nitrogen out. Approximately 40 L of  $N_L$  was required to fill the nitrogen reservoir, and it was periodically topped up during the test run.

3. The price paid for  $N_L$  was \$0.30 per liter, while  $He_L$  cost between \$4.00 and \$6.00 per liter. Thus it was economically beneficial to precool the magnet with liquid nitrogen to  $N_L$  temperature, before cooling it the rest of the way in the helium bath. This was done by placing the coil in a styrofoam container and filling the container with nitrogen. Room temperature resistance of the coil was  $450\Omega$  and its resistance at  $N_L$  temperature ( $77.4^\circ K$ ) was  $70\Omega$ . Resistance was monitored and used to indicate when the coil had reached  $N_L$  temperature. This procedure consumed approximately 10 L of liquid nitrogen.

4. When the magnet had reached a resistance of  $70\Omega$  it was placed in the dewar and at this point the vacuum system was closed to the dewar (valve 2 of Figure 16 was closed). The legs of the flexible transfer line was simultaneously placed right to the bottom of the dewar and the helium

## FIGURE 17

Schematic diagram of valve employed to pump liquid helium from the  $\text{He}_L$  transfer container into the dewar.



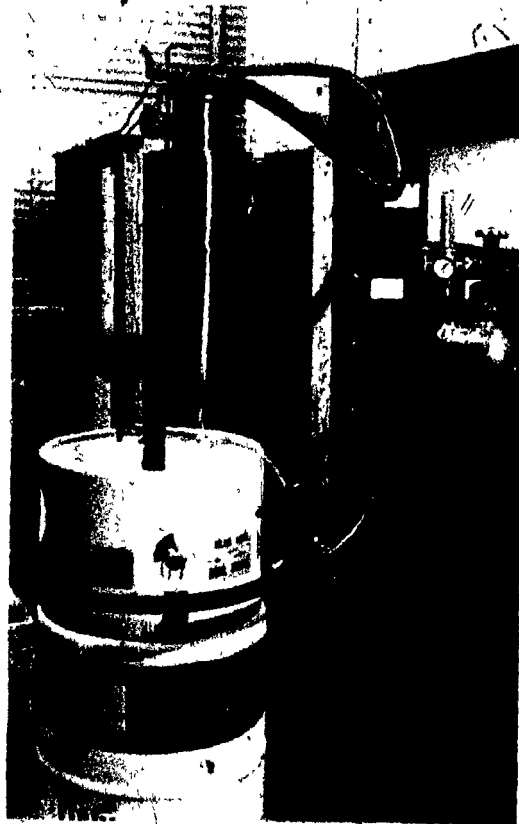
container. The top of the helium container was fitted with a valve, schematically drawn in Figure 17, that fit tightly around the leg of the transfer line. It allowed the entrance of a flow of helium gas to pressurize the helium dewar, thus forcing liquid helium through the transfer line and into the helium well of the magnet dewar. A flow metre and pressure gauge on the helium gas cylinder controlled the over-pressure in the helium container, and thus controlled the rate of transfer. A photograph of the helium transfer equipment and procedure is shown in Figure 18.

The first several litres of liquid helium were boiled off by cooling the transfer line, solenoid, and helium well to the  $\text{He}_L$  temperature ( $4.2^\circ\text{K}$ ). Gas molecules in the vacuum walls ( $\text{O}_2$ ,  $\text{N}_2$ , etc.) are solidified by the helium on the other side of the wall, thus producing the ultra high vacuum in the walls. The importance of closing the vacuum system off from the dewar before transfer is effected can thus be appreciated. The vacuum in the dewar becomes lower than that in the diffusion pump. Consequently, if the valve is left open, air molecules will be "cryo-pumped" into the dewar and solidified by the liquid helium, resulting in a large (and eventually total) consumption of liquid helium.

As helium transfer continued, the coil resistance was monitored. A steady drop in resistance occurred as the coil and dewar were cooled to  $\text{He}_L$  temperature, until the coil temperature reached  $4.2^\circ\text{K}$  and the resistance dropped to zero. At this point the solenoid had gone superconducting and the helium reservoir began to fill with liquid. Depth of helium was then monitored with the dip stick. Transfer continued until the point at which there was no noticeable increase in the height of the helium bath over a time span of a few minutes. This indicated that the helium dewar was empty, so transfer was discontinued. This was done by releasing the

## FIGURE 18

Photograph of transfer procedure. Photo shows the He<sub>L</sub> container, the He gas cylinder, the transfer line, and the valve which was schematically shown in Fig. 17.



pressure in the helium container and removing the transfer line from the two dewars. Total time of helium transfer varied from 45 to 90 minutes.

On the average, 20 L of liquid helium was required to cool the magnet and dewar, and fill the helium well to a height of about 44 cm, or about 8 cm above the top of the coil. Boil off rate was generally 1 to 1.5 cm per hour (0.3 to 0.45 L/hr). The magnet was operated until the level had dropped about 8 cm below the top of the coil, as the solenoid went normal (non-superconducting) at a level between 8 and 15 cm below the top of the coil. Therefore, if the dewar was filled with liquid helium to about 8 cm above the top of the coil, 10 to 16 hours of magnet operating time was available for testwork.

2.1.4 Permanent Magnet

A small, permanent magnet (solenoid) was used to perform some initial tests. It was 10 cm high with an O.D. of 15 cm and a bore of 5.7 cm. Figure 19 is a photograph of the magnet and the glass cannister used to hold the matrix (expanded metal matrix in this case). I.D. of the cannister was 3.7 cm when expanded metal was used, and a 5.0 cm I.D. cannister was employed when a steel wool matrix was used. A 2 L glass head-tank held the slurry about 40 cm above the magnet. Two ball valves below the cannister were employed to control the flow rate.

Field strength of the magnet was measured along the axis of the bore using the same Hall probe, and probe calibration, used to calibrate the larger magnet. The field distribution, shown in Figure 20, indicates a reasonable uniformity in field strength over the centre 5 cm of the bore. When steel wool was packed in the bore the maximum field strength was increased from 0.9 to 1.0 kG and was constant at 1 kG over the centre 5 cm.

## FIGURE 19

Photograph of permanent magnet with the matrix cannister, containing an expanded metal matrix. The matrix and magnet are in the mags flush position.

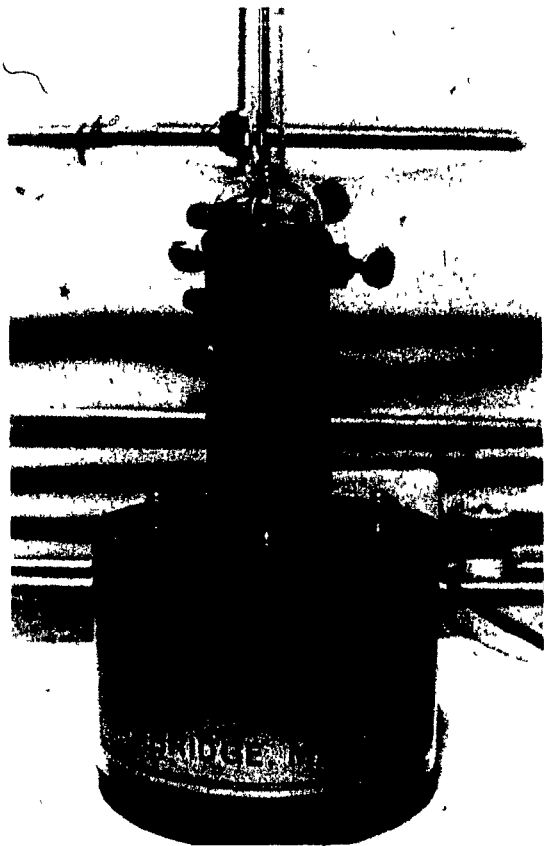
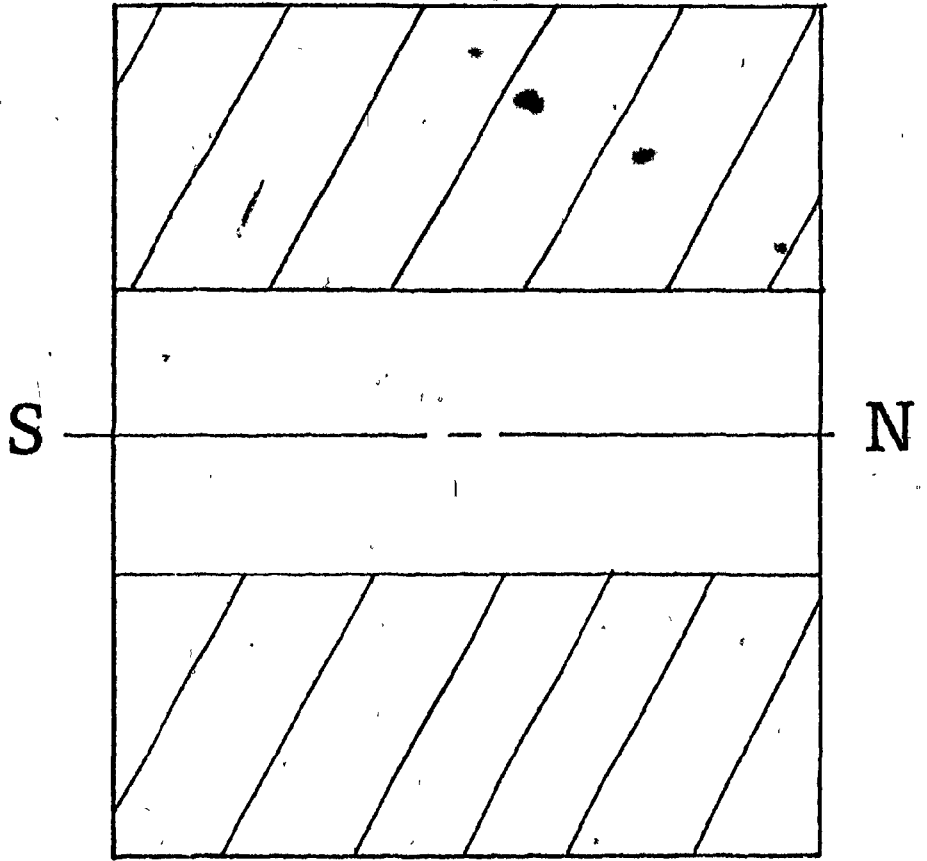
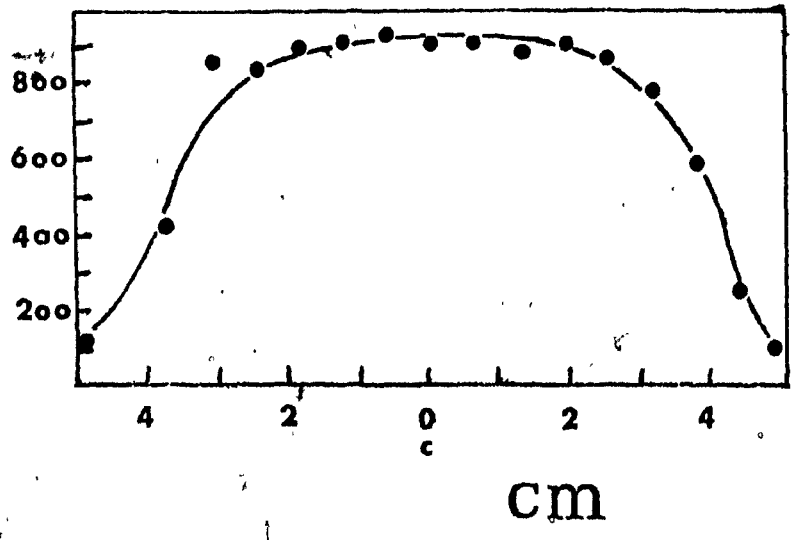


FIGURE 20

Field distribution along the axis of the permanent magnet.



H  
(gauss)



### 2.1.5 Frantz Isodynamic Magnetic Separator

The Frantz Isodynamic Magnetic Separator (42, 43) was used for sample preparation and mass susceptibility measurements. A photograph of this device is shown in Figure 21. Basically, it consists of an inclined chute placed between long, specially shaped pole pieces of a powerful electromagnet. The dry sample to be separated is fed down the chute parallel to the length of the pole pieces. The electromagnet and chute are also slightly tilted to one side, causing the particles to flow down one side of the chute when no magnetic field is applied. However, when current is passed through the electromagnets and a magnetic field is produced between the pole pieces, the diverging shape of the poles causes a magnetic force to act on a paramagnetic particle in a direction opposite to the gravitational force. This is illustrated in Figure 22, a cross section of the chute and pole pieces. A field gradient is produced in the (+)x direction, thus producing the  $F_M$  in a direction opposite to the  $F_G$ .

The main feature of the pole shape, however, is that a constant field gradient (and thus a constant  $F_M$ ) acts on a particle regardless of its position across the chute. Thus, the ratio of magnetic to gravitational forces is relatively constant for a given particle. It can also be shown that the net motion of the particles is virtually independent of particle size (4). Because of the long operating space parallel to the sample flow, the separator provides a long period of magnetic action on the particles rather than a short impulse. The direction of motion of the particles is consequently a resultant of the combined magnetic and gravitational forces.

The Frantz produces a separation based mainly on the relative mass susceptibilities of the particles, and, due to the pole shape, it makes

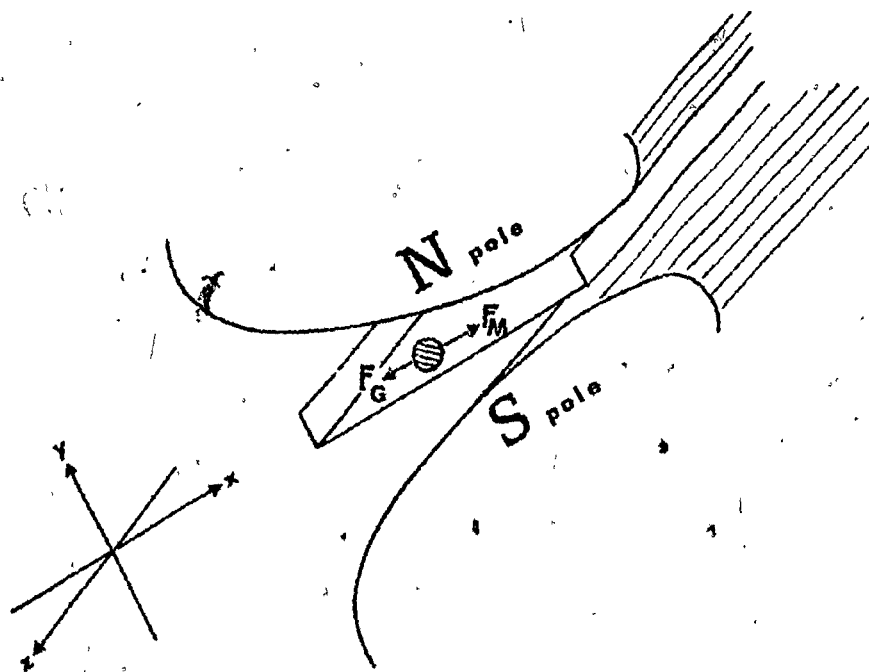
FIGURE 21

Photograph of the Frantz Isodynamic Magnetic Separator.



## FIGURE 22

Schematic diagram of a paramagnetic particle between the pole pieces of the Frantz Separator. The particle is moving in the (+)z direction along the chute.



very precise separations between particles of close susceptibility. Half way down the chute a splitter divides the separated particles into magnetic and non-magnetic fractions. Magnetic force is increased by increasing the current through the electromagnet and gravitational force is increased by increasing the side tilt. The minimum particle size treatable is about 20  $\mu\text{m}$ . All samples should be clean, and free of dust on the mineral grains.

A "magnetic response curve" of a given sample can be generated by passing the sample through the Frantz at a set side slope and a low current. The mags product is weighed and the non-mags become the feed for the next pass at a higher current. This is repeated several times, increasing the current each time. Cum. Wt. % reporting to the magnetics chute can then be plotted against current.

An approximate determination of the mass susceptibility of any paramagnetic material passed through the separator can be made from the following relationship:

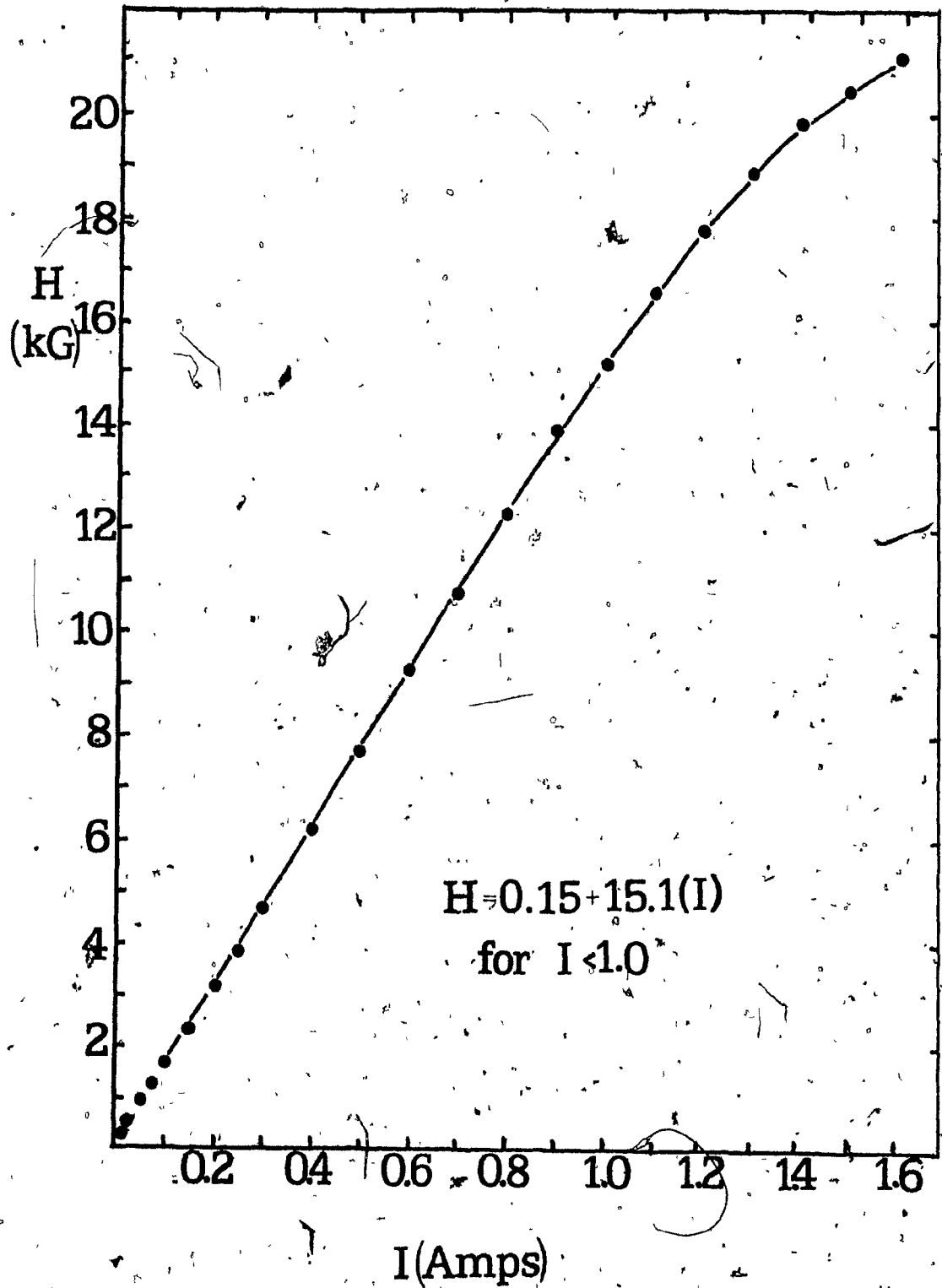
$$\chi = \frac{20 \sin\theta}{I^2} \times 10^{-6} \frac{\text{emu}}{\text{gm} - \text{Oe}} \quad (24)$$

This equation is derived from a force balance between  $F_M$  and  $F_G$ . The  $I$  used is the lowest current at which the particles report to the "magnetics" side of the chute.

The Hall probe was also employed to calibrate the field strength of the Frantz with the applied current. The relationship between  $H$  and  $I$ , shown in Figure 23, is linear to 1.0 Amp. (15 kG). It also indicates that Eq. (24) would be applicable up to about 1.3 Amp before excessive effects of magnetic saturation occur.

## FIGURE 23

Calibration of current applied to the electromagnets of the Frantz to the maximum field strength generated between the pole pieces.



## 2.2 Sample Preparation

Five uni-mineral samples were prepared for use in experiments designed to test the operating and particle parameters. Two multi-mineral samples (concentrates) were also prepared for separations on the HGMS.

### 2.2.1 Uni-mineral Samples

The test program as outlined in Section 1.3 called for a close control of particle size and magnetic susceptibility. Therefore, samples of narrow size range and narrow susceptibility range were required. To meet these two requirements the Warman cyclosizer and the Frantz Isodynamic Magnetic Separator were employed for sample preparation.

Several kilograms of -400m hematite had been prepared by Partridge (44) from the Carol Lake iron ore deposit of the Iron Ore Company of Canada. Analysis of the hematite on the Frantz showed the coarser material (30  $\mu\text{m}$ ) to be approximately 99% hematite - 1% silica, and to have a very narrow susceptibility range (see Section 3.1). Closely sized samples were produced with the use of the cyclosizer. Several samples of 60 gms each were cyclosized. The minus #5 cone material was recovered for the first 3-5 minutes of operation. Table 3 lists the range of particle sizes for each cone, the average particle size of each fraction, and the accumulated weight of samples collected.

To produce a hematite sample with a wider size distribution some of the sample prepared by Partridge was cycloned at 5 psi on a 1-in. laboratory cyclone. The size analysis of both the U/F and O/F material is given in Table 4.

A clean ilmenite sample (98-99%  $\text{FeTiO}_3$ ) was obtained from Quebec Iron and Titanium Corp., Sorel. It also had a narrow susceptibility range. The coarse sample was dry ground in a 23 cm Abbé ball mill employing a

TABLE 3  
Hematite Samples

Cyclone #	Size Range ( $\mu\text{m}$ )	$d_{\text{Ave}}$	Collected Sample Weight (gms)
1	23 → 37	30	90
2	17.6 → 25.4	22	90
3	13.1 → 19.3	16	70
4	9.0 → 14.4	12	90
5	7.1 → 9.9	8.5	50
5	8		70

TABLE 4

Size Analysis of Hematite Cyclone  
Underflow and Overflow

Cone #	d <sub>Ave</sub> ( $\mu$ m)	Cyclone U/F		Cyclone O/F	
		Wt %	Cum Wt %	Wt %	Cum Wt %
1	32	7.4	7.4	-	-
2	24.7	23.6	31.0	1.5	1.5
3	18.7	31.2	62.2	4.1	5.6
4	13.5	20.6	82.8	6.4	12.0
5	9.8	9.7	92.5	9.7	21.7
~ 5	~5	7.5		78.3	

10 kgm steel ball grinding media. Stage grinding was employed with screening at 325 m. Approximately 1000 gms of -325 m ilmenite thus produced was cyclosized in 60 gm samples. The second and third cone cyclosizer products were combined, as were the fourth and fifth cone products. Minus #5 cone material was collected for the first 3-5 minutes of operation. The size ranges, average sizes, and accumulated sample weights are listed in Table 5.

Copper concentrate, with chalcopyrite as the primary Cu mineral, was obtained from Geco Mines, Ontario. The sample was first cleaned and de-slimed in alcohol using a decanting technique (45), then dried and screened down to 325 m.

30 to 40% of the concentrate consisted of minerals with susceptibilities substantially different from that of the chalcopyrite. To produce a sample with a narrow susceptibility range, minerals other than chalcopyrite had to be removed. Therefore, sized fractions (-270 +325m, -200 + 270m, and -150 + 200m) were passed through the Frantz Isodynamic Separator at a current setting of 0.95 Amp and a side slope of 20°. The material reporting to the "non-magnetics" side of the chute was a very pure chalcopyrite, while the "magnetics" consisted mainly of pyrrhotite and sphalerite.

The cleaned chalcopyrite fractions were stage ground in a 23 cm Abbé ball mill to produce samples in the 10 to 40  $\mu$ m size range. A one minute grind was used, followed by screening at 325 m. +325 m Material was returned to grinding-screening, and -325 m chalcopyrite was accumulated for cyclosizing. Table 6 lists the particle sizes, size ranges, and weights of the cone products from the cyclosizer.

TABLE 5  
Ilmenite Samples

Size Interval	Range in d ( $\mu\text{m}$ )	d Ave ( $\mu\text{m}$ )	Collected Sample Wgt. (gms)
+325 - 270 m	44 - 53	49	100
#1 Cone*	26 - 53	44*	80
#1 cone	26 - 44	35	200
#2 & 3 cones	15 - 26	21	460
#4 & 5 cones	8 - 15	11	180
- #5 cone	<8		60

\* Weighted ave. of wide size distribution

TABLE 6

Sphalerite and Chalcopyrite Samples

Cyclone #	Range in d ( $\mu\text{m}$ )	d <sub>Ave</sub> ( $\mu\text{m}$ )	Collected Sample Wts. (gms)	
			(Zn, Fe)S	CuFeS <sub>2</sub>
1	28 - 44	36	35	25
2 & 3	16 - 28	22	40	70
4 & 5	9 - 16	12	25	30

Zinc concentrate containing sphalerite (or marmatite) was obtained as well from Geco Mines. The sample was cleaned and deslimed in alcohol, then dried and screened. As with the Cu concentrate, minerals with susceptibility different from that of sphalerite were present in large amounts, and the Frantz was employed to produce a cleaned sphalerite concentrate with a narrow range of susceptibility. It was operated at a  $\theta$  of  $20^\circ$  and current settings of 0.85 and 0.95 Amp. Material that reported to the magnetics side of the chute between 0.85 and 0.95 Amp was primarily sphalerite. This cleaned sphalerite was stage ground, screened at 325 m, and cyclosized in the same manner as was the chalcopyrite. Table 6 also lists the size data of the sphalerite samples so prepared.

50 gm samples of Indusmin Ltd. silica were cyclosized to produce samples with narrow size ranges. The size data of the cyclosized silica is given in Table 7. The presence of two sets of samples was due to the operation of the cyclosizer at two different water temperatures.

### 2.2.2 Multi-Mineral Samples

A tin concentrate ( $\text{SnO}_2$ ) containing 15% pyrrhotite ( $\text{Fe}_7\text{S}_8$ ) was obtained from a gravity concentration circuit at the Sullivan Concentrator, Cominco Ltd., Kimberly, B.C. A size analysis of the as received concentrate is shown in Figure 24 along with estimated pyrrhotite distribution. The pyrrhotite grades shown were roughly determined from Frantz magnetic response curves for a few selected size intervals, Figure 25. They indicate the predominant occurrence of pyrrhotite in the coarser fractions, as would be expected in a gravity concentration product containing two minerals of quite different density ( $\rho_{\text{SnO}_2} = 7.0$ ,  $\rho_{\text{Fe}_7\text{S}_8} = 4.6$ ).

Observations at low magnification of the products of each pass through the Frantz, indicated that the material magnetically captured up to 0.6 Amp

TABLE 7  
Silica Samples

Cyclone #	$d_{\text{Ave A}}$ ( $\mu\text{m}$ )	$d_{\text{Ave B}}$ ( $\mu\text{m}$ )
1	37.3	
2	28.4	42.4
3	21.2	32.0
4	14.6	23.2
5	11.4	16.7

## FIGURE 24

Size distribution of the as received tin concentrate, with estimated pyrrhotite distribution. Data points derived through the use of the cyclosizer were calculated for the S.G. of  $\text{SnO}_2$ . The equivalent pyrrhotite sizes are noted.

Wt % 80  
Finer

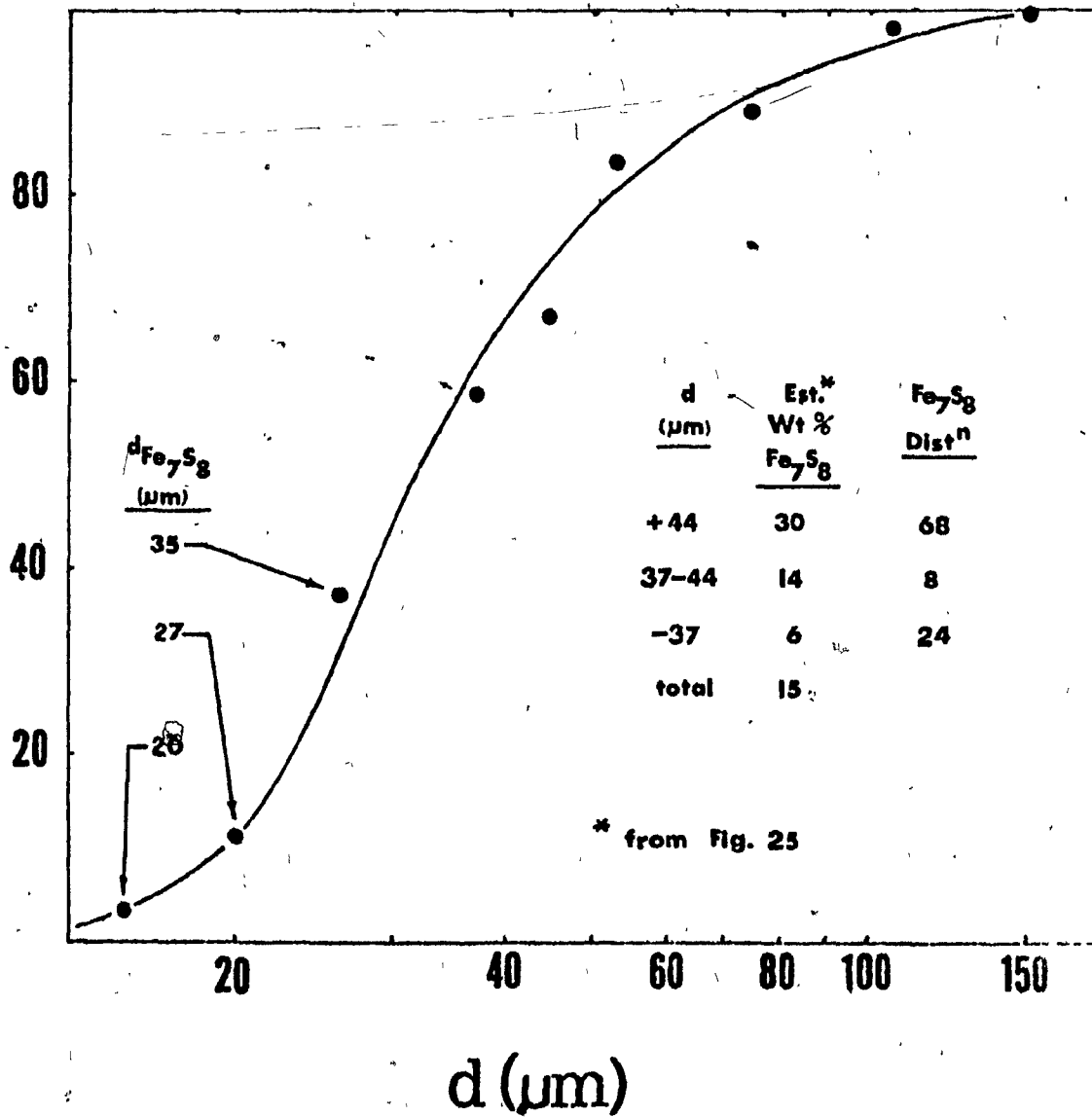
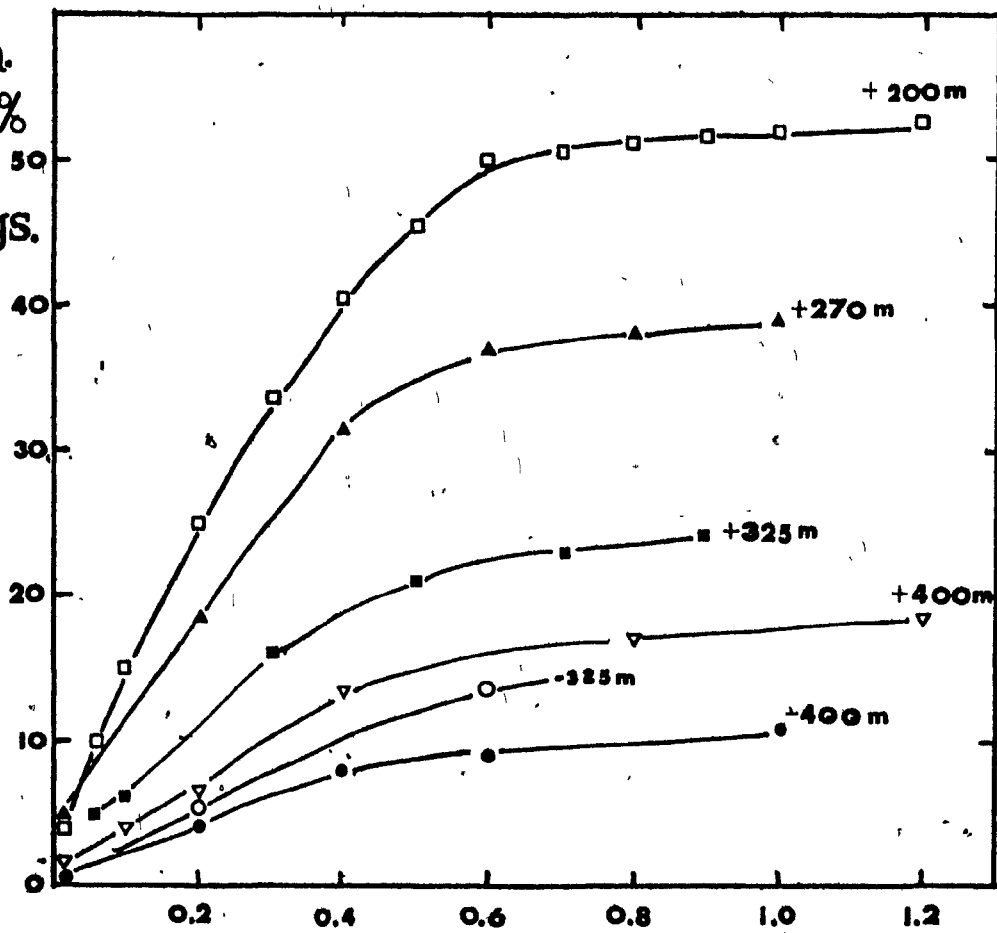


## FIGURE 25

Magnetic response curves, for several size intervals,  
of the tin concentrate, including the -325m sample.  
 $\theta=20^\circ$ .

Cum.  
Wt. %  
to  
Mags.



I (Amps)

was primarily pyrrhotite with 20-40% locked  $\text{SnO}_2$ .

To produce a sample with a size distribution in the range in which the HGMS was tested (8 to 50  $\mu\text{m}$ ) some of the tin concentrate was screened at 325 m. The size and pyrrhotite distributions for the -325 m material are given in Table 8. A representative sample of the -325m material was passed through the Frantz at 0.6 Amp and a side slope of  $20^\circ$ . The Fe assays and distribution of  $\text{Fe}_7\text{S}_8$  for the two products at  $I = 0.6$  Amp are also given in Table 8.

A low grade copper concentrate was obtained from Vihanti Mine, Outokumpu Oy, Finland. The as received sample assayed 26.7% Fe, 19.4% Cu, 2.2% Zn and 1.2% Pb; with the principal minerals being chalcopyrite, pyrrhotite, pyrite, galena, marmatite and gangue minerals.

Figure 26 plots the size analysis of the as received sample and the sample after 25 minutes of dry grinding. Grinding was performed in a 8-cm Abbé ball mill with a 50 gm feed and a 300 gm charge. Some of the ground material was cycloned at 5 psi on the laboratory cyclone, to produce a sample with a size distribution within the range of particle size tested on the HGMS. The size analysis of the cyclone U/F is also shown in Figure 26.

Samples from the first three cyclosizer cones of the cyclone U/F were individually tested on the Frantz. Their magnetic response curves were plotted in Figure 27. Mineralogical observation at high magnification of some of the Frantz products showed a large degree of finely disseminated locking. Material reporting to the mags at a current of 0.7 Amp or less consisted mainly of pyrrhotite with finely disseminated chalcopyrite-pyrite grains. Material above 0.7 Amp was mainly chalcopyrite and pyrite with a large amount of locking between the two. Sphalerite was also

TABLE 8

-325m Tin Concentrate

Cyclone #	$d_{\text{AveSnO}_2}$ ( $\mu\text{m}$ )	$d_{\text{AveFe}_7\text{S}_8}$ ( $\mu\text{m}$ )	Wt %	% $\text{Fe}_7\text{S}_8$	$\text{Fe}_7\text{S}_8$ Units	$\text{Fe}_7\text{S}_8$ Distribution
1	34.0	38.0	40.4	6.1	246	28.7
2	21.5	28.0	49.0	10.3	505	58.9
3	16.2	21.2	6.5	10	65	7.6
4	~12.0	~15.0	4.1	10	41	4.8
Feed				8.57	857	

Separation on Frantz

Conditions: / Sample: -325 m Tin Concentrate

Current: 0.6 Amp

$\theta$ : 20°

Product	Wt %	% Fe	% $\text{Fe}_7\text{S}_8$	$\text{Fe}_7\text{S}_8$ Units	$\text{Fe}_7\text{S}_8$ Distn
Mags	13.5	37.8	62.3	841	94.4
Non-Mags	86.5	0.35	0.58	50	5.6

## FIGURE 26

Size distribution of the copper concentrate sample (a) as received, (b) ground for 25 min., and (c) the cyclone U/F of the ground material. Data points derived through the use of the cyclosizer were calculated for a S.G. of 4.4.

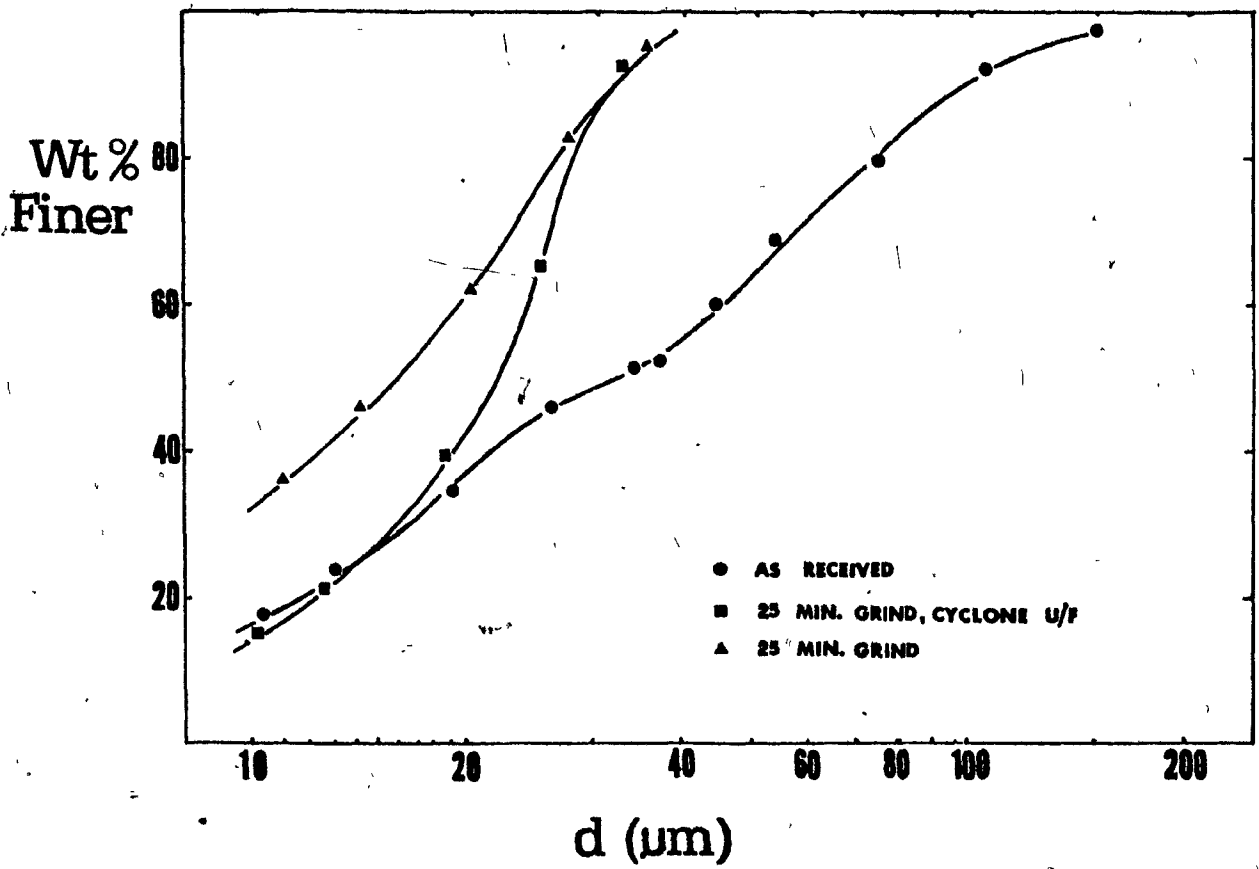
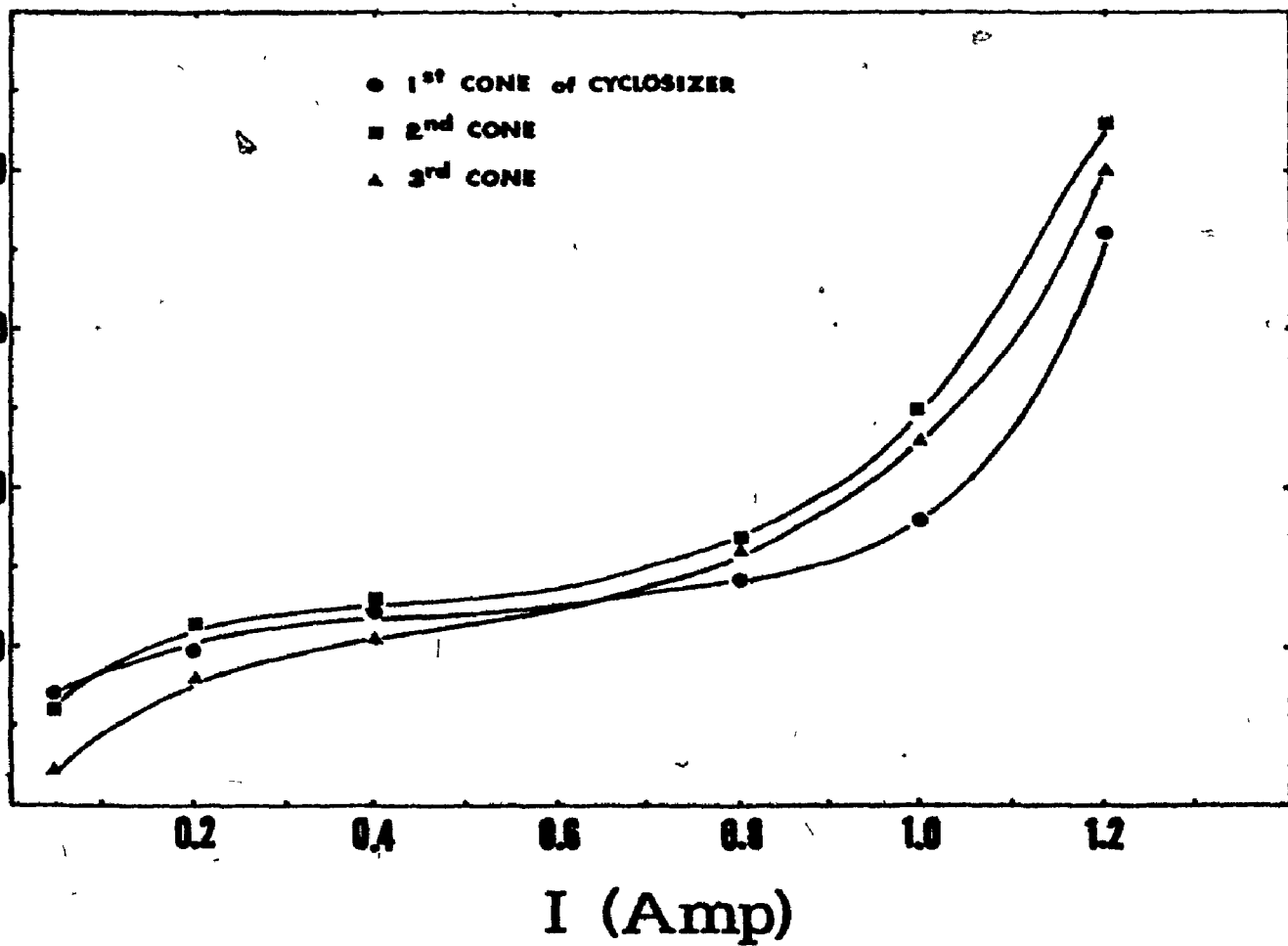


## FIGURE 27

Magnetic response curves for the first three cyclosizer cone products of the copper concentrate.  $\theta=20^\circ$ .

Cum.  
Wt.%  
to  
Mags



present.

A sample from the second cone of the cyclosizer was passed through the Frantz at a current of 0.4 Amp, and  $\theta = 20^\circ$ . The two products at this current setting were assayed for Cu and Fe. The assays and distribution of the Cu and Fe in the two products is reported in Table 9.

### 2.3 Experimental Technique

The uni-mineral samples had been prepared to narrow particle size and susceptibility ranges. As well, the operating parameters  $H$ ,  $U$ ,  $\eta$ ,  $L_m$  and  $L$  could be easily controlled. To study the effects of these particle and operating parameters upon magnetic recovery, individual samples of the closely sized samples were passed through the separator under selected operating conditions. The experimental technique was that of holding all variables constant except the one to be studied. Two experimental methods were employed; the constant head system, and the drainage system.

#### 2.3.1 Constant Head System

Tests performed with this system, where the hydrostatic head was maintained, all employed the expanded metal matrix described in Section 2.1.1. The procedure for each test run was as follows:

1. Velocity through the matrix was set by placing the required velocity control plug in the line.
2. The matrix and sample carrying line were filled with water.
3. Field strength was set to the desired value, by adjusting the current to its corresponding value.
4. A selected mass of the uni-mineral sample was slurried and well wetted by agitation in 500 cc of water.
5. The on/off valve was opened. As the slurry passed through the magnetized matrix into a bucket, water was added at the

TABLE 9Separation on Frantz

Conditions:      Sample: Copper Concentrate  
                         Size : #2 Cyclosizer Cone  
                         Current: 0.4 Amp  
                          $\theta$ : 20<sup>o</sup>

Product	Wt %	% Cu	Cu Distn.	% Fe	Fe Distn.
Mags	26.0	7.7	9.4	46.0	42.1
Non-Mags	74.0	26.0	90.6	22.2	57.9

head tank to maintain a constant head.

6. When the discharge was observed to be free of mineral particles the valve was closed.
7. Current was shut off, thus removing the magnetic field.
8. Two full velocity top flushes were applied to wash out the mags product into a separate bucket.

Slurry density through the matrix was 2% or less, and the total volume of water passed through the matrix in steps 5 and 6 was about 7 litres, or about 80 times the working volume.

#### 2.3.2 Drainage System

Hydrostatic head was not maintained during an individual test in this system, and all experiments employed the steel wool matrix described in Section 2.1.1. The basic procedure was as follows:

1. Velocity through the matrix was set to the desired value by adjusting the ball valves below the matrix.
2. The matrix and sample carrying line were filled with water.
3. Field strength was set to the desired value.
4. A selected mass of the sample was slurried and well wetted by agitation in 500 cc of water.
5. The slurried sample was washed into the head tank and the bottom valve opened, draining the slurry column through the matrix and into a bucket.
6. The bottom valve was closed and about 1.5 L of wash water was slowly fed to the system from the head tank.
7. Valve 3 (Figure 11) was opened and the wash water was flushed into the bucket.

8. Repeat of steps 6 and 7.
9. Current was shut off to remove the magnetic field.
10. Two full velocity top flushes were applied to wash out the mags product into a separate bucket.

Slurry density through the matrix was 3% or less. Total volume of water passed through the matrix in steps 5 to 8 was generally 5 L or about 20 times the working volume.

### 2.3.3 Permanent Magnet Operation

Tests were performed with the permanent magnet using both the drainage and constant head systems. Operation was basically the same as described above, except that the introduction and removal of the magnetizing field was by moving the magnet.

### 2.3.4 Analysis of Test Products

For all tests performed with both systems of operation two products were produced - a non-mags product and a mags product. The non-mags consisted of mineral particles which passed through the matrix without being captured. The mags fraction consisted of particles that were either magnetically captured or physically entrapped in the matrix.

The two products from each uni-mineral test run were filtered, dried and weighed. Total losses were generally less than 5%.  $R_T$  was defined as the weight % of the feed, minus losses, reporting to the mags.

If  $R_M$  represented the magnetic recovery of particles, and  $R_p$  the recovery due to physical entrainment, then:

$$R_T = R_M + R_p \quad (25)$$

$R_p$  was experimentally determined by performing a series of tests with  $H = 0$ . In these tests  $R_M = 0$ , so that  $R_p = R_T$ .

The procedure used for separation tests was the same as described above, depending upon the system used. Products were filtered, dried, weighed, and assayed.

CHAPTER 3

RESULTS

### 3.1 Susceptibility Measurements

#### 3.1.1 Uni-Mineral Samples

The magnetic response curves of the prepared uni-mineral samples are shown in Figure 28. The magnetic susceptibility of the samples was determined using the response curves and Eq. (24). Measurements were made with #1 cyclone material at a side slope,  $\theta$ , of  $20^\circ$ .

Since each sample had a relatively narrow susceptibility range each could be characterized by a single susceptibility value. This value was taken to be that at 50% cumulative weight recovery. The current on the Frantz corresponding to 50% cumulative weight recovery,  $I_{50\%}$ , and  $\theta = 20^\circ$  were substituted in Eq. (24) to yield the mass susceptibility of the sample. Volume susceptibility is related to mass susceptibility by:

$$k = \rho \chi \quad (26)$$

The values of mass and volume susceptibility of the four uni-mineral samples as determined by the above method are given in Table 10, along with the range of volume susceptibility within which 90% of each sample reported.

Most of the silica (90%) was magnetically recovered on the Frantz when  $I = 1.0$  Amp and was between  $2^\circ$  and  $5^\circ$ . The volume susceptibility of the silica was therefore approximated by the single value of  $0.03 \times 10^{-4}$  emu/cm<sup>3</sup>Oe.

#### 3.1.2 Effect of d and $\theta$ Upon Measured k

To determine if the particle size of the sample affected the value of the susceptibility as measured on the Frantz, three different sizes

FIGURE 28

Magnetic response curves for the four uni-mineral samples.  
 $\theta = 20^\circ$ .

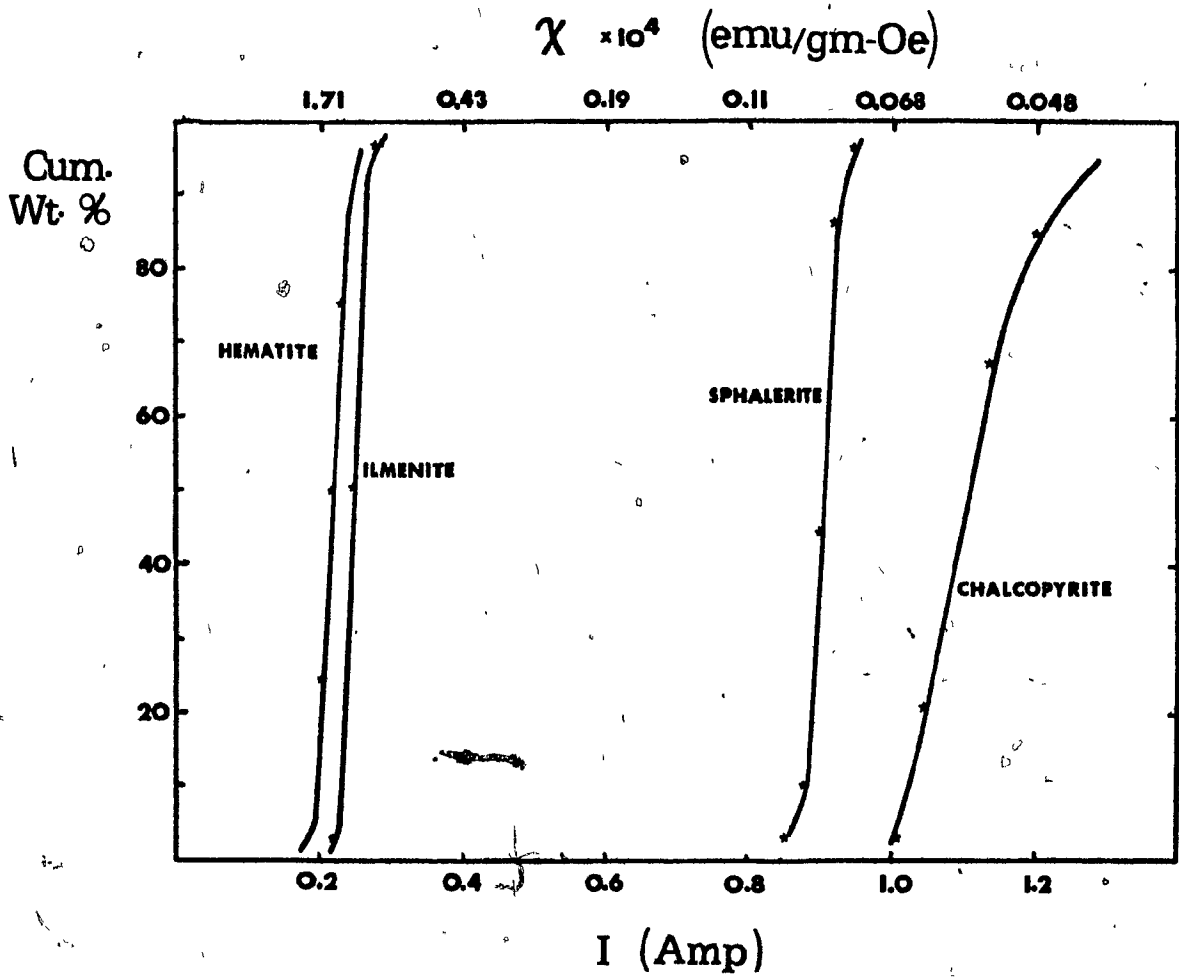


TABLE 10  
Susceptibilities of Uni-Mineral Samples

Mineral	$\chi \times 10^6$ $\left(\frac{\text{emu}}{\text{gm-Oe}}\right)$	$\rho$ $\left(\frac{\text{gm}}{\text{cm}^3}\right)$	$k \times 10^4$ $\left(\frac{\text{emu}}{\text{cm}^3\text{-Oe}}\right)$	90% Range
Hematite	152	5.2	8.0	6.7-9.9
Ilmenite	116	4.8	5.6	4.2-6.8
Sphalerite	8.4	4.1	0.34	.31-.38
Chalcopyrite	5.5	4.3	0.25	.17-.28

of hematite and sphalerite were tested (at  $\theta = 20^\circ$ ) and the susceptibility measured. The results, shown in Table 11, indicate very little effect of particle size upon  $k$  with the sphalerite, but a more pronounced effect with the hematite. The range of measured  $k$  values for the various hematite particle sizes was of the same magnitude as the 90% range of a single size interval (see Table 10). Further study of this aspect of susceptibility measurement was not pursued.

The effect of side slope,  $\theta$ , upon the value of susceptibility as determined from Eq. (24) was also studied. The susceptibilities of the hematite, ilmenite, chalcopyrite, and sphalerite samples were determined from the results of several tests on the Frantz, with each test employing a different side slope. As the slope increases, so does the gravitational force acting on the particles. A higher field strength (ie current) will then be required to pull the particles to the magnetics side of the chute.  $I_{50\%}$  and the particular  $\theta$  employed were substituted in Eq. (24) to determine the susceptibility for each  $\theta$ . The field strength,  $H$ , at the measured  $I_{50\%}$  was also calculated using Figure 23.  $k$  vs  $H$  was then plotted for each mineral, as shown in Figure 29. As can be seen,  $k$  decreased with increasing  $H$ .

### 3.1.3 Multi-Mineral Samples

The magnetic response curves from the Frantz (at  $\theta = 20^\circ$ ) for the two samples (Figures 25 and 27) indicate a wide range of susceptibility in each sample. The samples were therefore characterized by 3 or 4 susceptibility values, which are given in Table 12 along with the corresponding currents. Note that different specific gravities have been used for the same sample. This was to try to allow for locked

TABLE 11  
Effect of d Upon Measured k

Mineral	d ( $\mu\text{m}$ )	$I_{50\%}$ (Amp)	$k \times 10^4$ $\left(\frac{\text{emu}}{\text{cm}^3 \cdot 0e}\right)$
Hematite	30	0.211	8.0
	22	0.217	7.6
	16	0.225	7.1
Sphalerite	49	0.880	0.34
	36	0.878	0.34
	22	0.874	0.34

## FIGURE 29

Measured volume susceptibility vs field strength at which the measurement was made, for the side slopes indicated, for (a) sphalerite and chalcopyrite, and (b) hematite and ilmenite. #1 cyclone material was used in all cases.

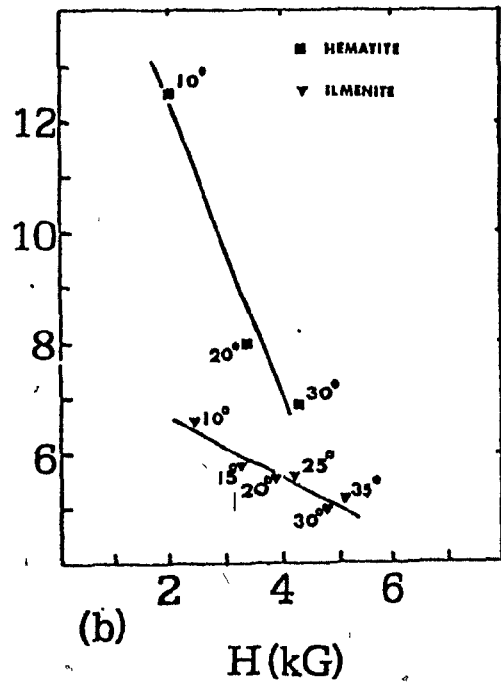
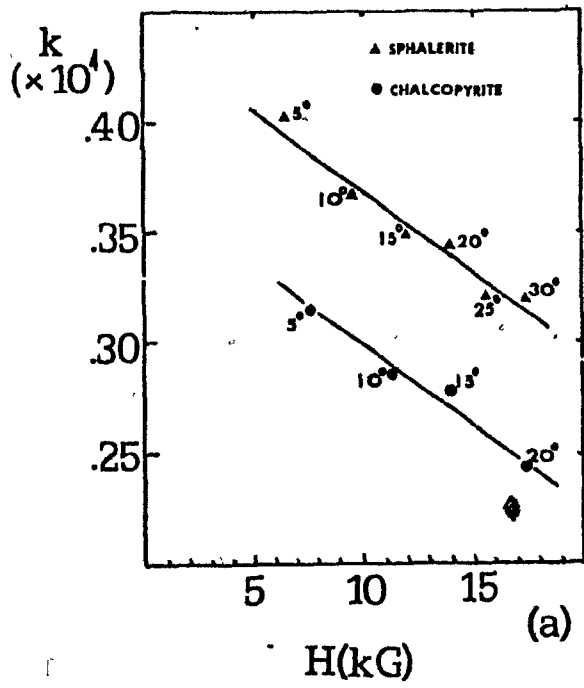


TABLE 12

## Susceptibilities of Tin and Copper Concentrates at Selected Currents

	I (Amps)	$\chi \times 10^4$ $\left(\frac{\text{emu}}{\text{gm-Oe}}\right)$	$\rho$ $\left(\frac{\text{gm}}{\text{cm}^3}\right)$	$k \times 10^4$ $\left(\frac{\text{emu}}{\text{cm}^3\text{-Oe}}\right)$
Tin Conc.	0.1	6.84	5.0	34.2
	0.3	0.76	5.5	4.2
	0.55	0.23	6.0	1.4
	0.8	0.11	6.0	0.66
Copper Conc.	0.05	27.4	4.6	125
	0.2	1.71	4.6	7.8
	0.4	0.43	4.5	1.92
	0.6	0.19	4.5	0.86
	1.05	0.067	4.3	0.29

$$\rho_{\text{Fe}_7\text{S}_8} = 4.6$$

$$\rho_{\text{SnO}_2} = 7.0$$

$$\rho_{\text{CuFeS}_2} = 4.3$$

particles of intermediate specific gravity.<sup>2</sup> For example, the tin concentrate values of 5.0, 5.5 and 6.0 represented locked particles of varying pyrrhotite ( $\ell = 4.6$ ) and cassiterite ( $\ell = 7.0$ ) proportions.

### 3.2 Effect of Parameters on HGMS Particle Capture - Constant Head System

Individual test data and results for all constant head system tests is given in Appendix 3. Unless otherwise indicated, all of the following test results are for a feed weight of 20 gm, ie  $L_m = 0.33$ .

#### 3.2.1. Zero Field Tests

To determine the extent of physical entrapment,  $R_p$ , of the uni-mineral samples a series of tests was run at zero field strength under various conditions of velocity and particle size. Figure 30 is a plot of  $R_p$  vs  $d$  for ilmenite at four velocities, silica at two velocities, and hematite at one velocity. As can be seen,  $R_p$  is decreased through a decrease in  $d$  or an increase in  $U$ . Comparing the hematite, ilmenite and silica data at 5.7 cm/sec, note that  $R_p$  of hematite ( $\ell = 5.2$ ) was slightly greater than  $R_p$  of ilmenite ( $\ell = 4.8$ ), while that of silica ( $\ell = 2.6$ ) was considerably lower.

The effect of matrix loading upon  $R_p$  is shown in Figure 31 for 21  $\mu\text{m}$  ilmenite at three velocities.  $R_p$  appeared to remain constant with  $L_m$  until the low loading of 0.083 was employed, whereupon  $R_p$  increased significantly.

---

<sup>2</sup> The net susceptibility of a particle containing two or more different minerals is the sum of the products of the susceptibility and volume fraction of each mineral.

## FIGURE 30

$R_p$  vs  $d$  for ilmenite, hematite and silica at various velocities. Constant head system.

- 2.9 cm/sec ilmenite
- 5.7 cm/sec ilmenite
- 9.9 cm/sec ilmenite
- 15.6 cm/sec ilmenite
- ▽ 9.9 cm/sec silica
- △ 5.7 cm/sec silica
- ▲ 5.7 cm/sec hematite

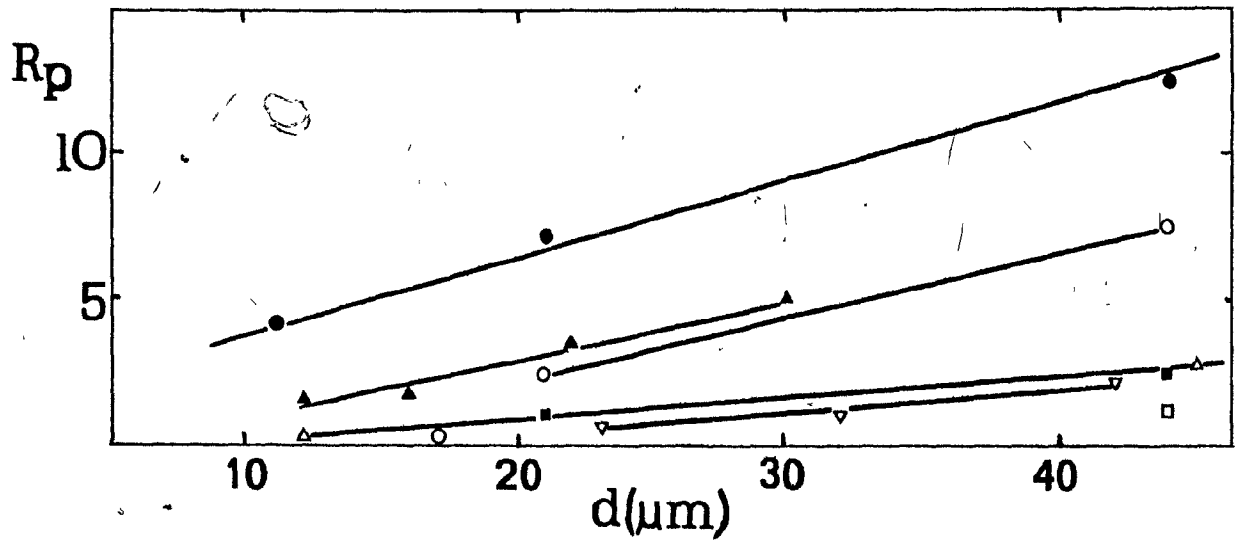




FIGURE 31

$R_p$  vs  $L_m$  for ilmenite at three velocities. Constant head system.

ILMENITE

● 2.9 cm/sec

□ 5.7 cm/sec

▲ 9.9 cm/sec

$R_p$

15

10

5

.083

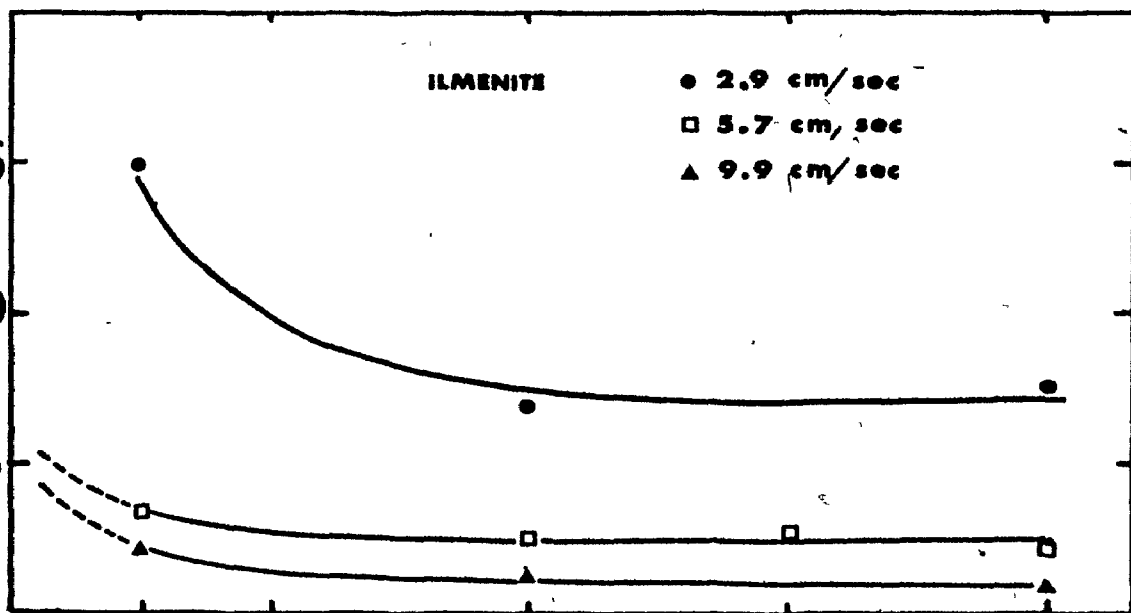
.17

.33

.50

.67

$L_m$



.083

.17

.33

.50

.67

$L_m$

### 3.2.2. Effect of Particle Size

The effect of particle size was tested using all four uni-mineral samples, with the more extensive work being done with the hematite samples, which is reported here.

Figure 32 shows the results of  $R_M$  vs  $H$  for five sizes of hematite at 9.9 cm/sec. In general accordance with Eq. (17),  $R_M$  increased with increasing  $H$  and  $d$ . Figure 33 plots  $R_M$  vs  $d$  for the same data.

In both figures, a family of curves was evident. The force balance model suggests that  $R_M$  is proportional to  $H^2 d^2$  (for  $H > 10$  kG) and, to test this,  $R_M$  vs  $H^2 d^2$  was plotted, Figure 34 (a). A log plot of the same data, Figure 34 (b), indicated an approximately linear relationship. Note that in the plots of Figure 34, the data points derived from the smaller particle sizes, 8.5 and 12  $\mu\text{m}$ , fell below the average data line, while the data points from the coarser particle sizes, 22 and 30  $\mu\text{m}$ , lay above it.

### 3.2.3 Effect of Velocity

The influence of velocity upon recovery was tested with all four uni-mineral samples.  $R_M$  vs  $H$  for 21  $\mu\text{m}$  ilmenite is plotted in Figure 35 for 4 different velocities. As would be expected from Eq. (17),  $R_M$  increased when  $U$  decreased. A family of curves was again evident, so, in conforming with Eq. (17),  $R_M$  vs  $\frac{H^2}{U}$  was plotted, as in Figure 36 (a). If  $R_M$  vs  $\log \frac{H^2}{U}$  was plotted, as in Figure 36 (b), an approximately linear relationship was indicated. In Figure 36 (a) and (b) the high velocity (15.6 cm/sec) data points lay considerably below the average data line.

## FIGURE 32

$R_M$  vs H for five particle sizes of hematite. Constant head system.

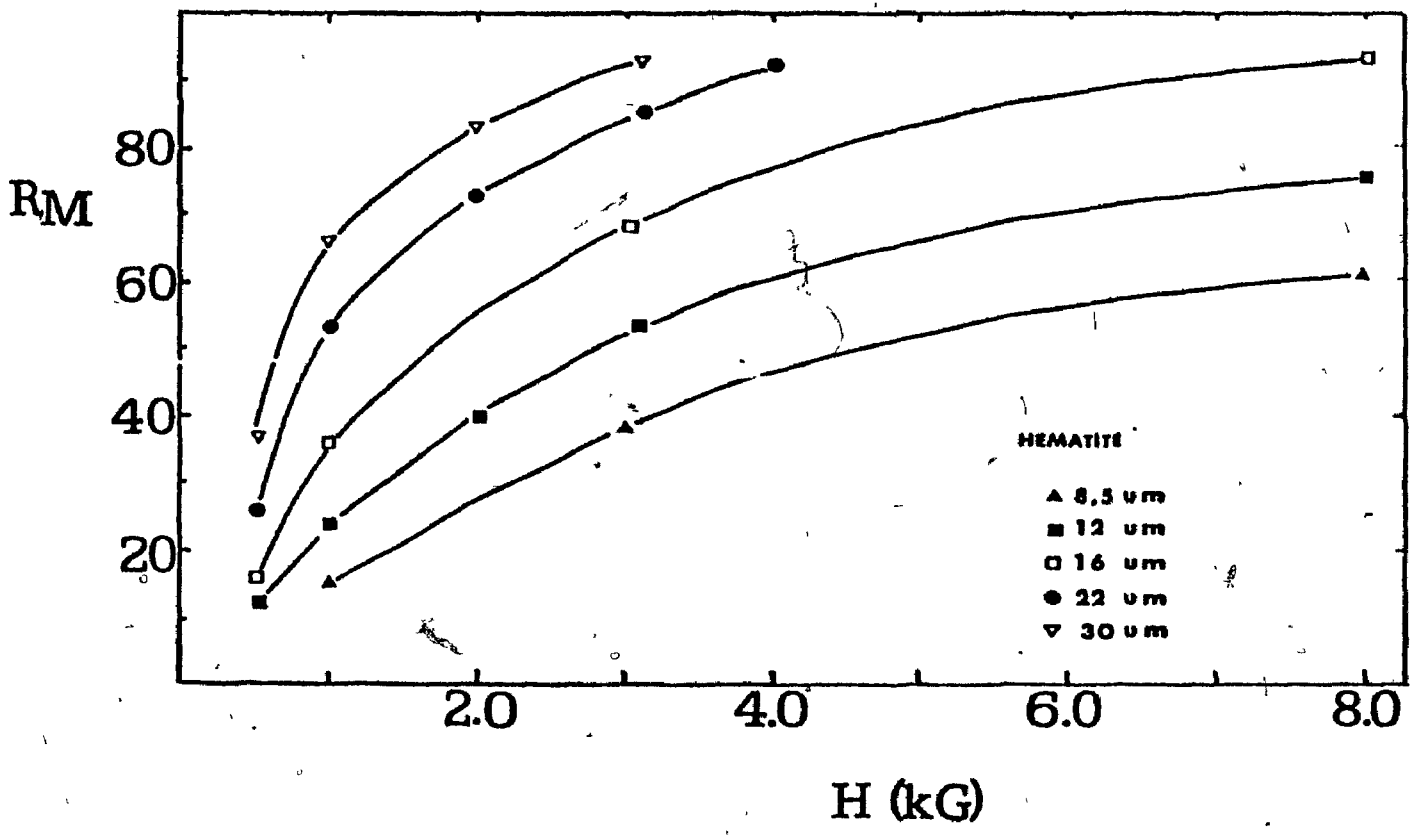


FIGURE 33

$R_M$  vs  $d$  for hematite at various field strengths.  
Constant head system.

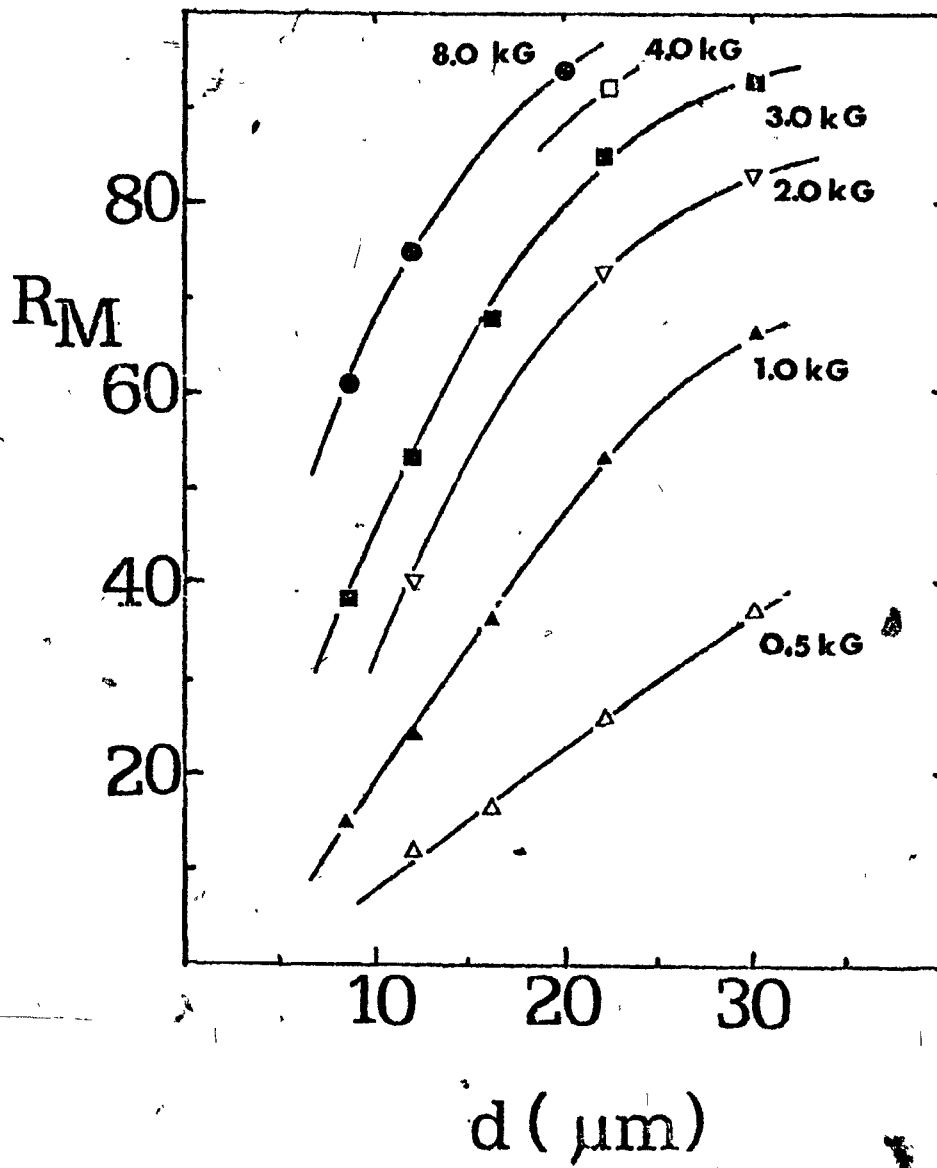
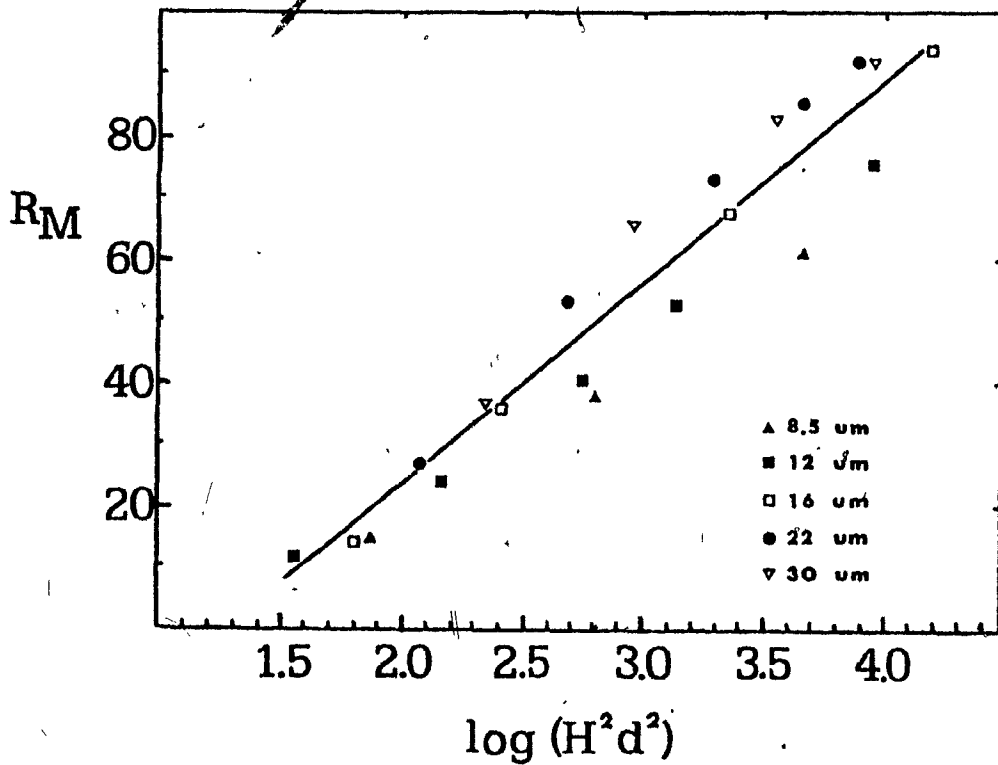
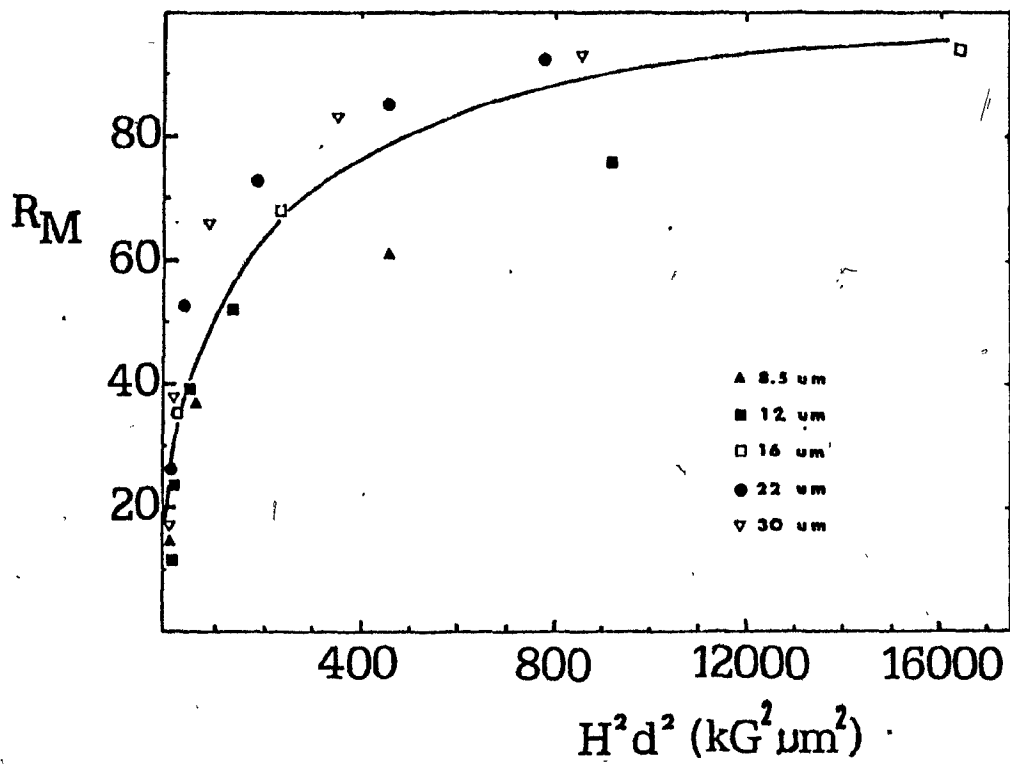


FIGURE 34(a)

$R_M$  vs  $H^2 d^2$  for hematite data of Fig.'s 32 and 33.

FIGURE 34(b)

$R_M$  vs  $\log( H^2 d^2 )$ .



## FIGURE 35

$R_M$  vs H for 21  $\mu\text{m}$  ilmenite at four velocities. Constant head system.

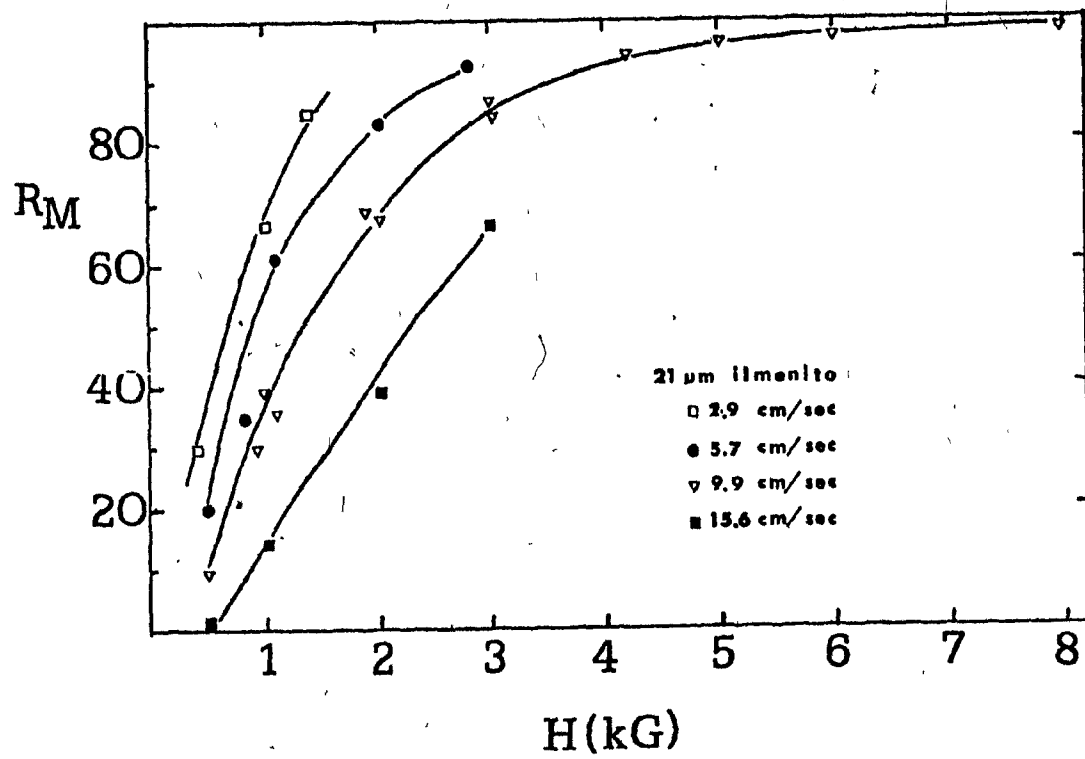
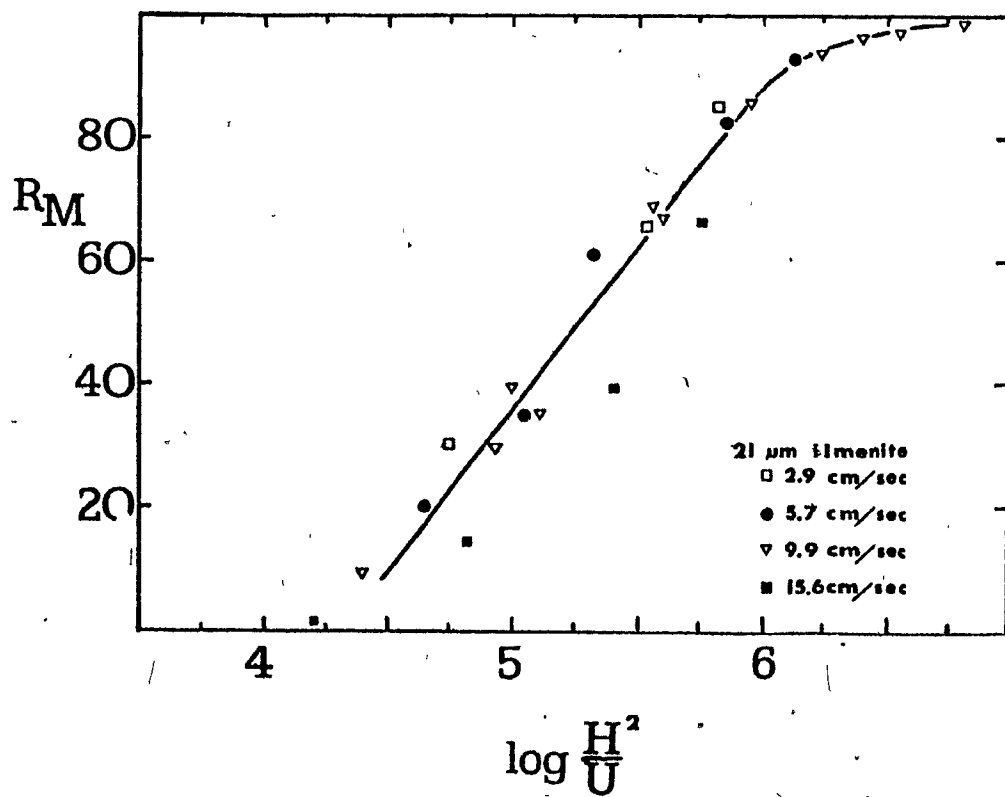
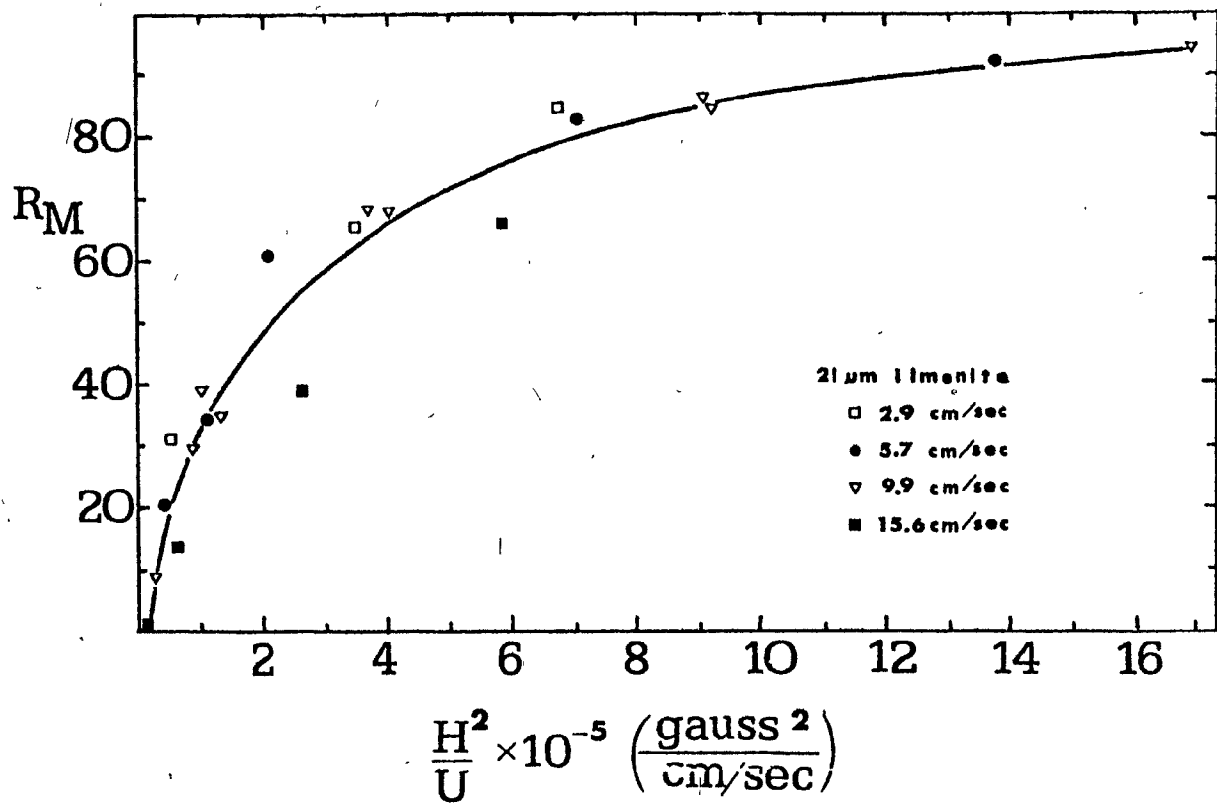


FIGURE 36(a)

$R_M$  vs  $H^2/U$  for data of Fig. 35.

FIGURE 36(b)

$R_M$  vs  $\log H^2/U$  for data of Fig. 35.



### 3.2.4 Effect of Viscosity

The influence of viscosity was studied through duplicate tests at two water temperatures. Table 13 summarizes the conditions and results of two series of such tests. Although there was at least a doubling of viscosity in both sets of tests, the differences in  $R_T$  were minimal, and were within the range of reproducibility of a single test.  $R_T$  actually increased (although only slightly) with increasing viscosity, which is opposite to that which would be expected when considering the force balance model.

### 3.2.5 Effect of Matrix Loading

Matrix loading was varied from 0.083 to 1.0 (equivalent to a feed weight varying from 5 gms to 60 gms) in tests using 11, 21 and 30  $\mu\text{m}$  ilmenite at 9.9 cm/sec and 1 kG. The results are shown in Figure 37. As  $L_m$  increased,  $R_M$  decreased, and the extent to which this occurred was seen to depend on  $d$ ; as  $d$  increased, the slope of the plot of  $R_M$  vs  $L_m$  increased. Figure 38 was derived from the same data and indicates that  $R_M$  is approximately proportional to  $\log \left[ \frac{HM_w d^2}{L_m} \right]$ .

### 3.2.6 Sphalerite and Chalcopyrite Recovery

The results of several tests with sphalerite and chalcopyrite under various conditions of  $d$ ,  $U$ , and  $H$  are shown in Figure 39. The data from the same tests, plus others, has been plotted in Figure 40 in the form of  $R_M$  vs  $\log \left[ \frac{HM_w d^2}{U} \right]$ . As can be seen, an approximately linear relationship resulted. It is noteworthy that both the sphalerite and chalcopyrite fell approximately along the same line in Figure 40, while having a 30% difference in their respective volume susceptibility.

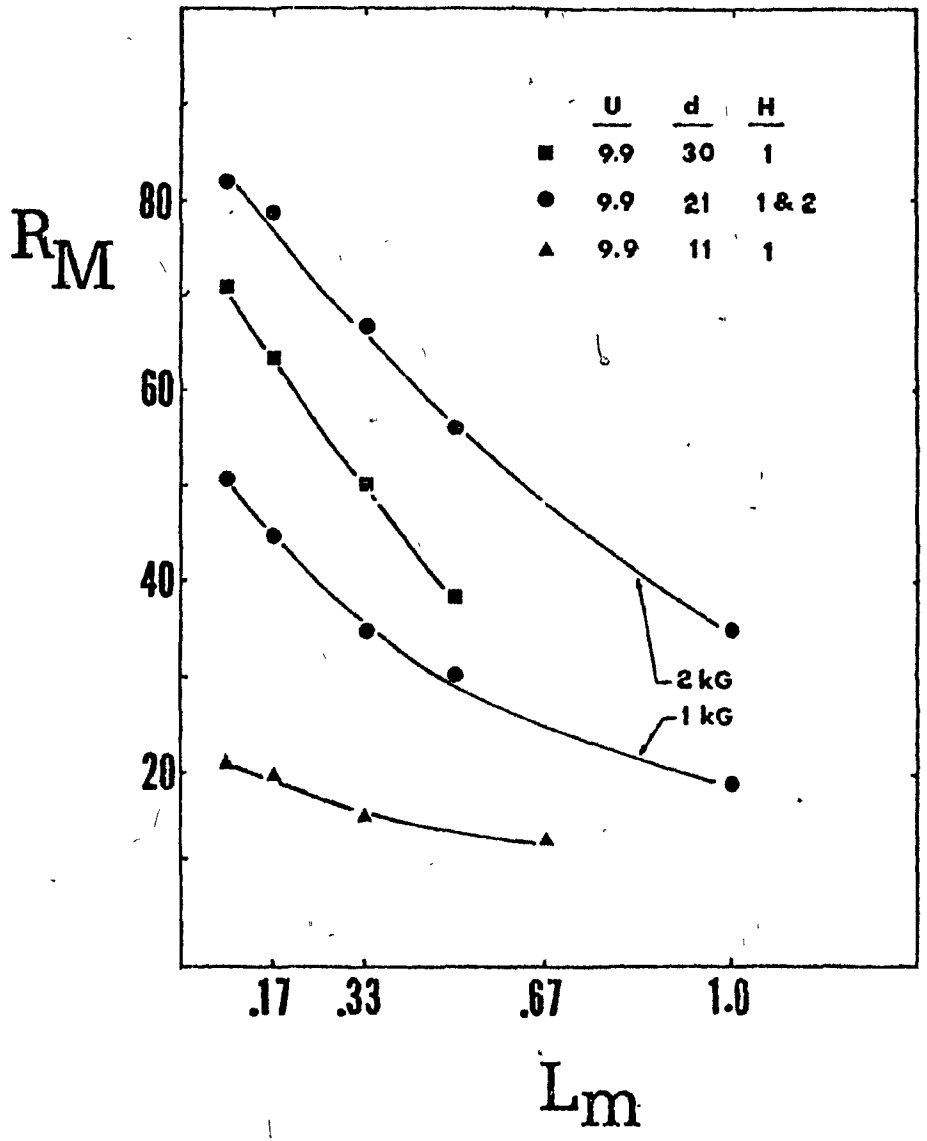
TABLE 13

Magnetic Recovery vs Viscosity - Constant Head System

Conditions	T (°C)	$\eta$ (cp)	$R_T$ (%)
A. H = 0.9 kg k = $5.6 \times 10^{-4}$ d = 35 $\mu$ m U = 9.9 cm/sec $L_m = 1/3$	4.5	1.53	49.3
	4.5	1.53	52.3
	32.0	0.76	49.2
	32.0	0.76	46.3
			50.8
			47.8
B. H = 4.2 kg k = $5.6 \times 10^{-4}$ d = 21 $\mu$ m U = 9.9 cm/sec $L_m = 1/3$	10.0	1.31	94.5
	10.0	1.31	93.7
	53.0	0.52	92.0
	49.0	0.55	94.2
			94.1
			93.1

FIGURE 37.

$R_M$  vs  $L_m$  for ilmenite at 9.9 cm/sec. Constant head system.



80

60

40

20

.17

.33

.67

1.0

O

FIGURE 38

$R_M$  vs  $\log \frac{H^2 d^2}{L_m}$  for the data of Fig. 37.

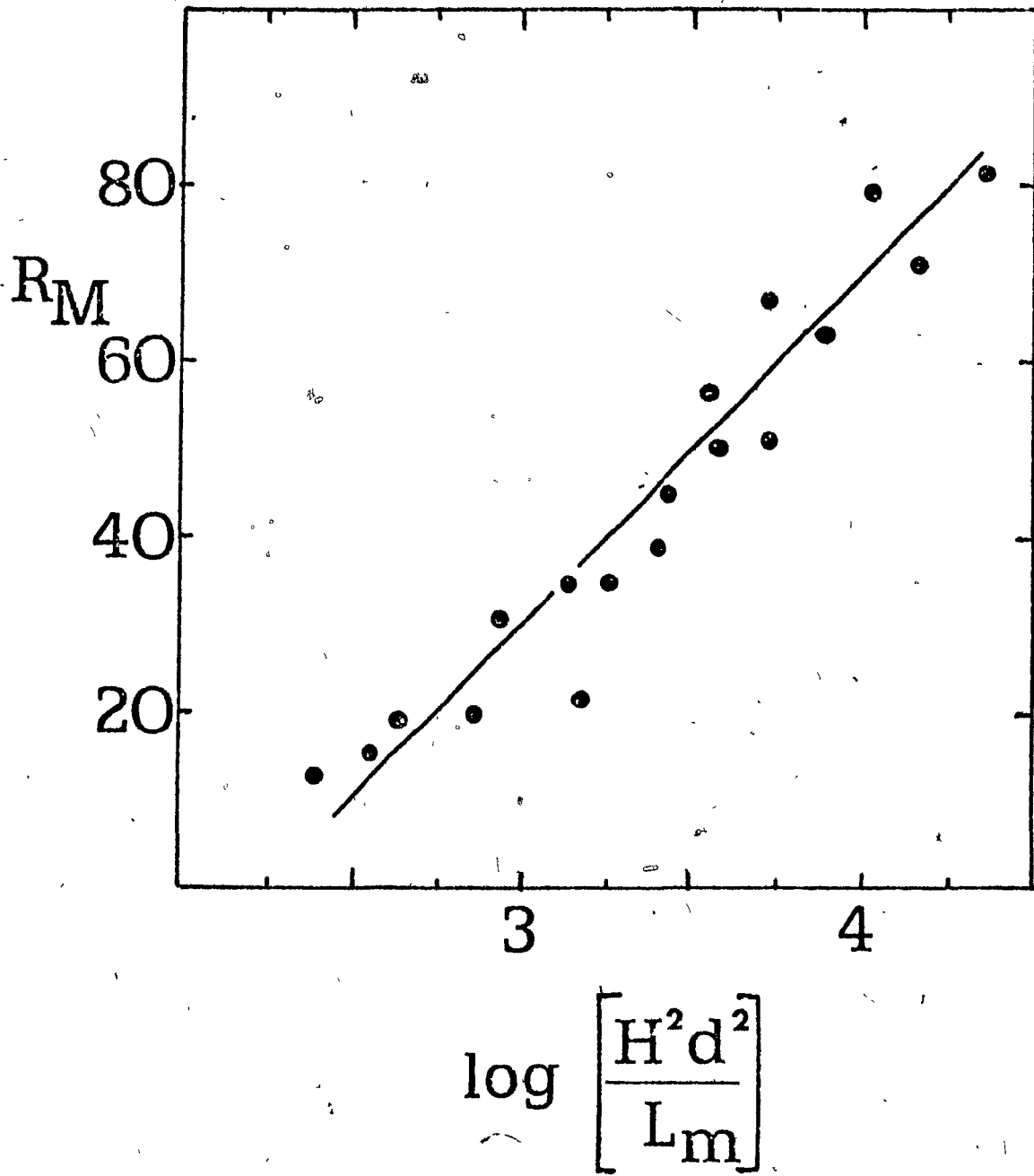


## FIGURE 39

$R_M$  vs H for three particle sizes of sphalerite and  
chalcopyrite at three velocities. Constant head system.

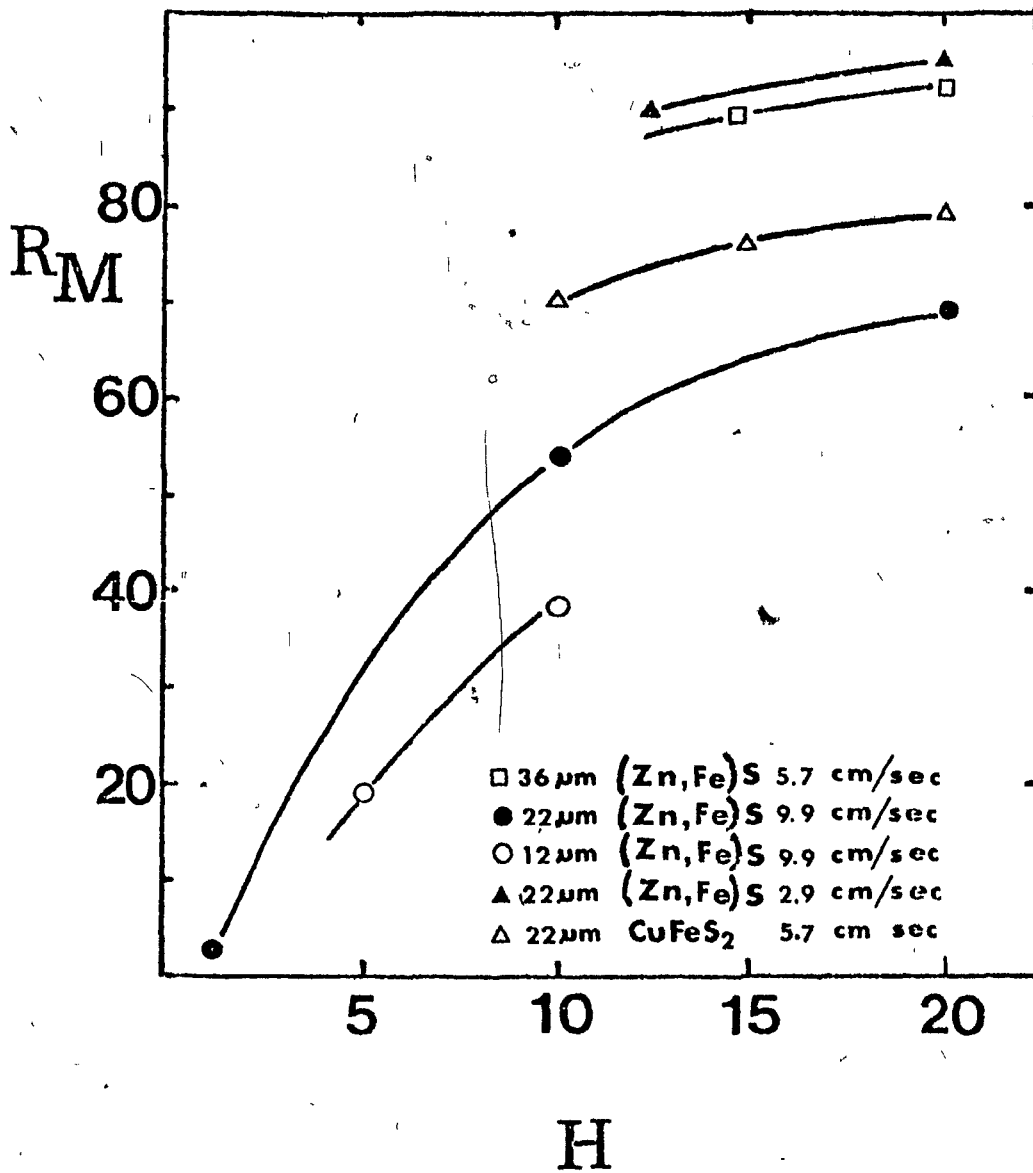
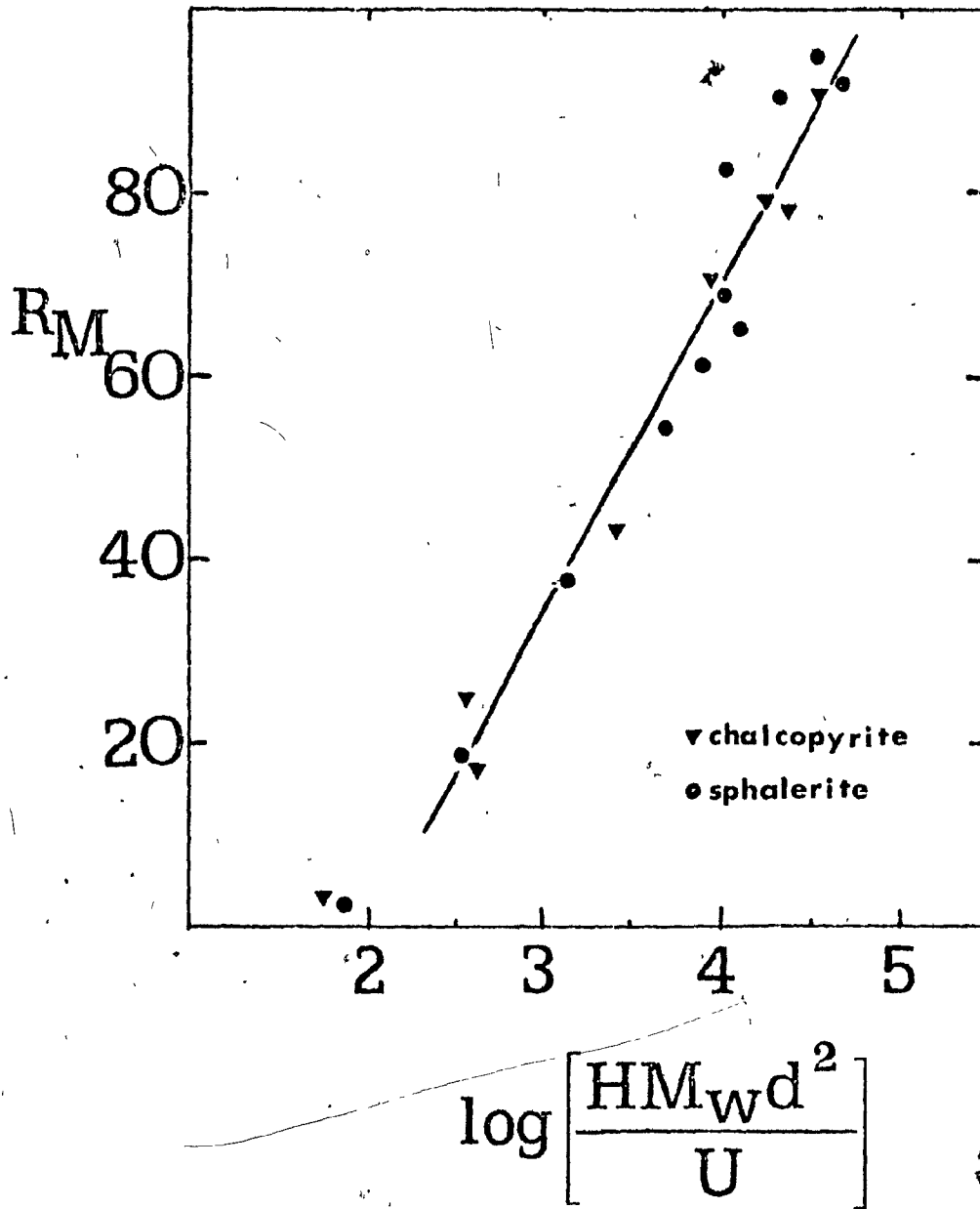


FIGURE 40

$R_M$  vs  $\log \frac{HM_w d^2}{U}$  for sphalerite and chalcopyrite data  
(tests 74 to 96, constant head system, Appendix 3).



### 3.2.7 Effect of Matrix Length

Matrix length tests were performed using the permanent magnet. The feed for each test was 10 gms of 22  $\mu\text{m}$  hematite at 3.0 cm/sec. Seven matrix segments, each consisting of three pieces of expanded metal lath, tied loosely together with fine copper wire, were employed. The first test was run with the matrix consisting of one segment, the second test with two segments, the third with three segments, etc.

Zero field runs were also performed for each matrix length. The results are shown in Table 14 for  $n$  between 1 and 7.

In an attempt to confirm the assumption that  $R_{M1}$  is independent of  $n$ , that was made in developing Eqs. (19) and (22),  $\log(1 - R_{Mn})$  vs  $n$  was plotted, Figure 41, as suggested in Section 1.2.5.  $R_{M1}$  was measured to be 0.094 and  $\log(1 - R_{M1})$  was -0.043. The slope of  $\log(1 - R_{Mn})$  vs  $n$  was -0.048. Since the slope was approximately equal to  $\log(1 - R_{M1})$ , the assumption that  $R_{M1}$  is independent of  $n$  appears, in this case, to be satisfactory.

### 3.3 An Empirical Model of Capture - Constant Head System

Given the extensive data and range of conditions tested, an empirical model of particle capture by HGMS could be developed. This was achieved using a step-wise linear regression technique. The variables employed were  $H$ ,  $k$ ,  $d$ ,  $U$ , and  $L_m$ , and the dependent variable was  $R_M$ . As suggested by the preceding results, the log of each independent variable was used. The  $HM_w$  exponent was set to 1 as suggested by the force balance model. The regression method and data is given in Appendix 4. For the 73 tests covering the following range of conditions:  $0.4 \leq H \leq 20$  kG;  $0.25 \times 10^{-4} \leq k \leq 8.0 \times 10^{-4}$  emu/cm<sup>3</sup>-0e;  $8.5 \leq d \leq 36$   $\mu\text{m}$ ;  $2.9 \leq U \leq 15.6$  cm/sec;  $0.083 \leq L_m \leq 1.0$ ;  $10 \leq R_M \leq 90\%$ , the following regression equation:

TABLE 14

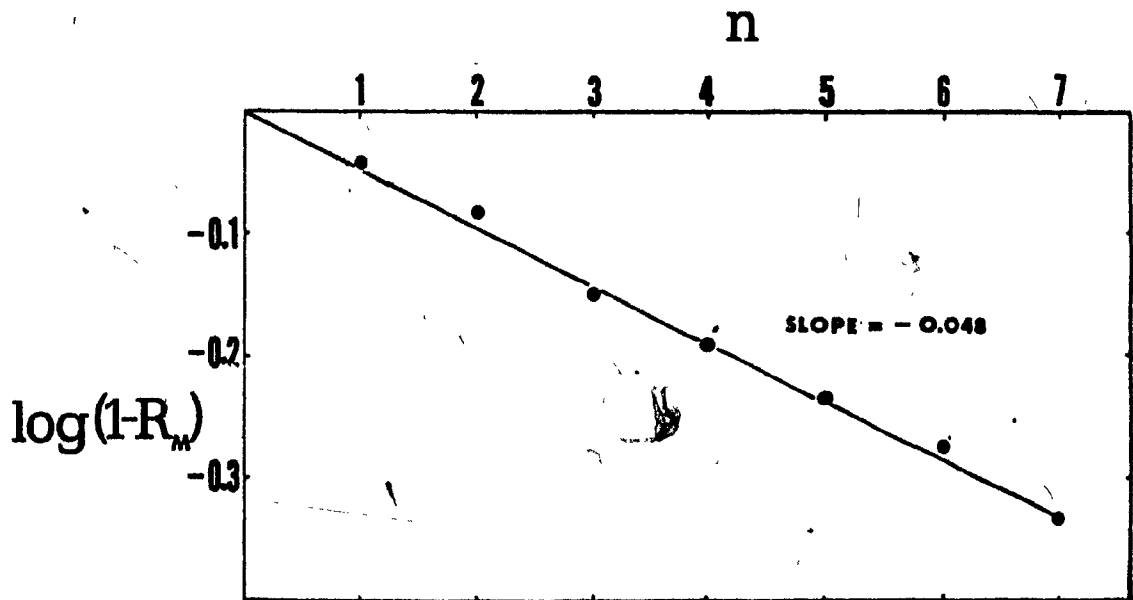
Matrix Length Tests

Conditions:    Sample:    Hematite  
                   Weight:    10 gms  
                   Size:        22  $\mu$ m  
                   H:            0.9 kg  
                   U:            3.0 cm/sec  
                   each n:     4.5 gms of expanded metal

n	matrix Wt. (gms)	$R_T$ (%)	$R_P$ (%)	$R_M$ measured (%)	$\log(1-R_{Mn})$
1	4.5	23.2	13.8	9.4	-0.043
2	9.0	31.9	14.3	17.6	-0.084
3	13.5	44.0	14.8	29.2	-0.151
4	18.0	54.8	19.1	35.7	-0.192
5	22.5	61.4	19.8	41.6	-0.235
6	27.0	67.2	20.4	46.8	-0.274
7	31.5	74.4	21.0	53.4	-0.332

## FIGURE 41

Log  $(1-R_{Mn})$  vs  $n$  for matrix length tests performed on  
the permanent magnet with 22  $\mu\text{m}$  hematite at 3 cm/sec.,



$$R_M = -60.6 + 34.8 \log \left[ \frac{H M_w k^{1.2} d^{2.5}}{U^{1.8} L_m^{0.8}} \right] \quad (27)$$

gave a standard error of estimate of 7.0. The fit is shown in Figure 42, which also includes points with  $10 \leq R_M \leq 90\%$  that were not included in the regression.

### 3.4 Effect of Parameters on HGMS Particle Capture - Drainage System

Test data and results for all drainage tests is given in Appendix 3.

Unless otherwise indicated, all of the following results are for a feed weight of 20 gm, i.e.  $L_m = 0.67$ .

#### 3.4.1 Zero Field Tests

Zero field runs were performed with ilmenite and sphalerite. The effects of  $d$  and  $U$  upon  $R_p$  are shown in Figure 43. Figure 44 shows the effect of  $L_m$  upon  $R_p$  for 21  $\mu\text{m}$  ilmenite at 10 cm/sec.  $R_p$  increased slightly with decreasing  $L_m$  for the range of  $L_m$  tested (0.33 to 2.0).

#### 3.4.2 Effect of Particle Size

The effect of particle size was studied using all four uni-mineral samples, although extensive work was only done with hematite.

Figure 45 is a plot of  $R_M$  vs  $H$  for various sizes of hematite at 10 cm/sec. A family of curves is evident, which suggests that recovery varied as the product  $Hd$ . This is plotted in Figure 46 (a). Figure 46 (b) shows that  $R_M$  vs  $\log(Hd)$  is approximately linear.

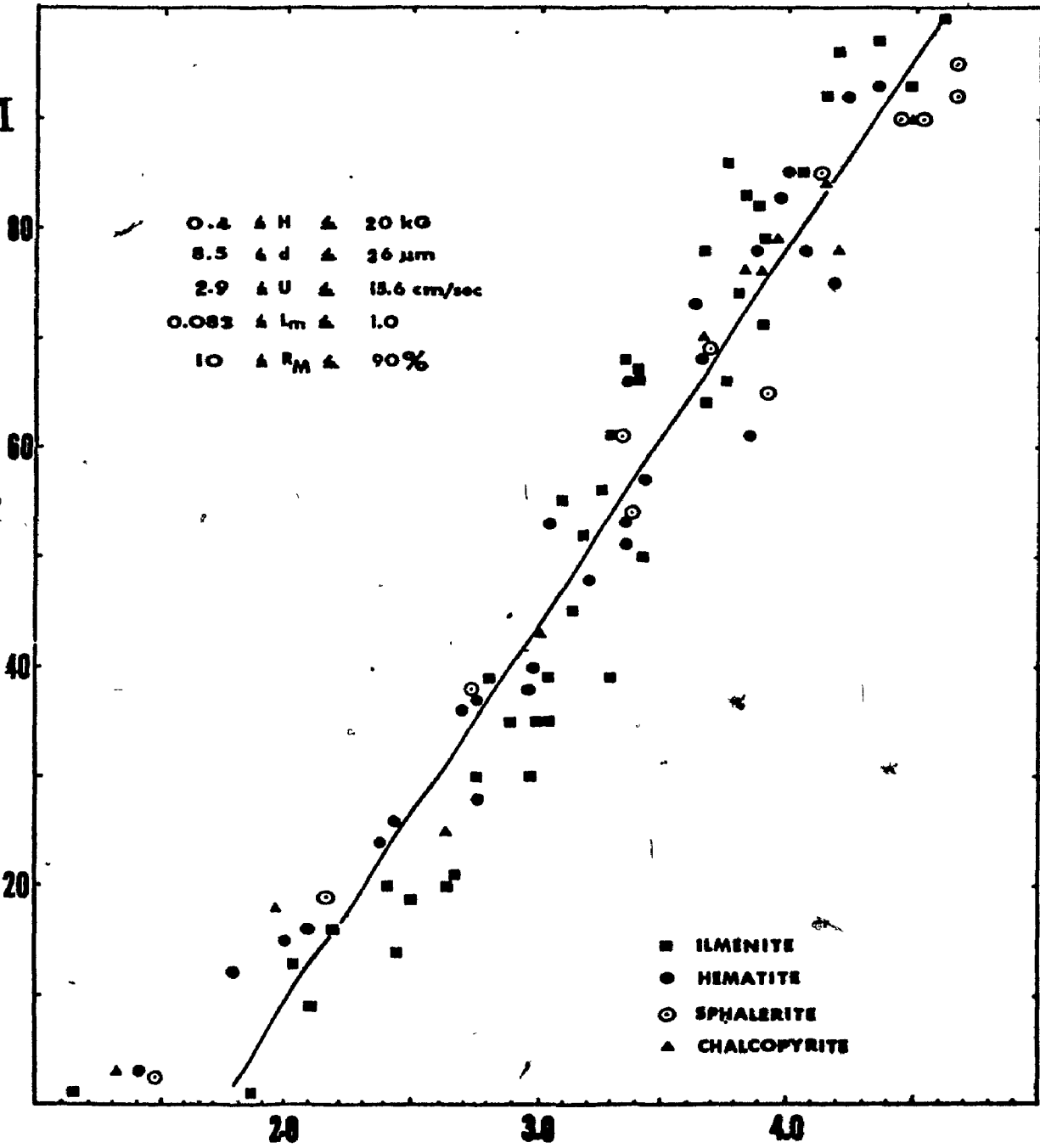
#### 3.4.3 Effect of Velocity

$R_M$  as a function of field strength is shown in Figure 47 for 21  $\mu\text{m}$  ilmenite at five different velocities. Quoted  $U$  is that which was measured during the first 500  $\text{cm}^3$  of flow. The decrease in  $R_M$  with increasing  $U$ , as predicted by Eq. (17), was substantiated. A family

## FIGURE 42

Plotted regression results (Eq 27) for constant head system.

$R_M$



$$\log\left(\frac{HM_wk^{L225}}{U^{L20.8} L_m}\right)$$

## FIGURE 43

$R_p$  vs  $d$  for ilmenite and sphalerite at several velocities.  
Drainage system.

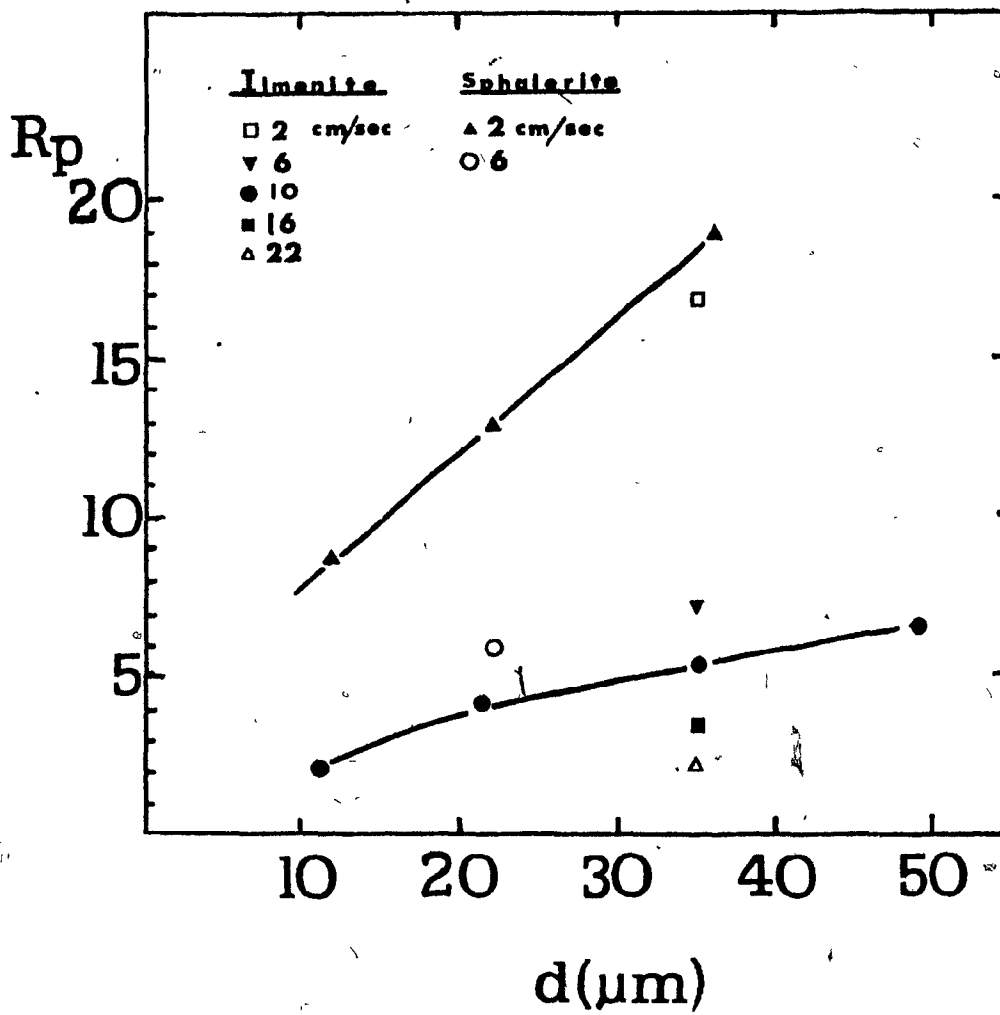
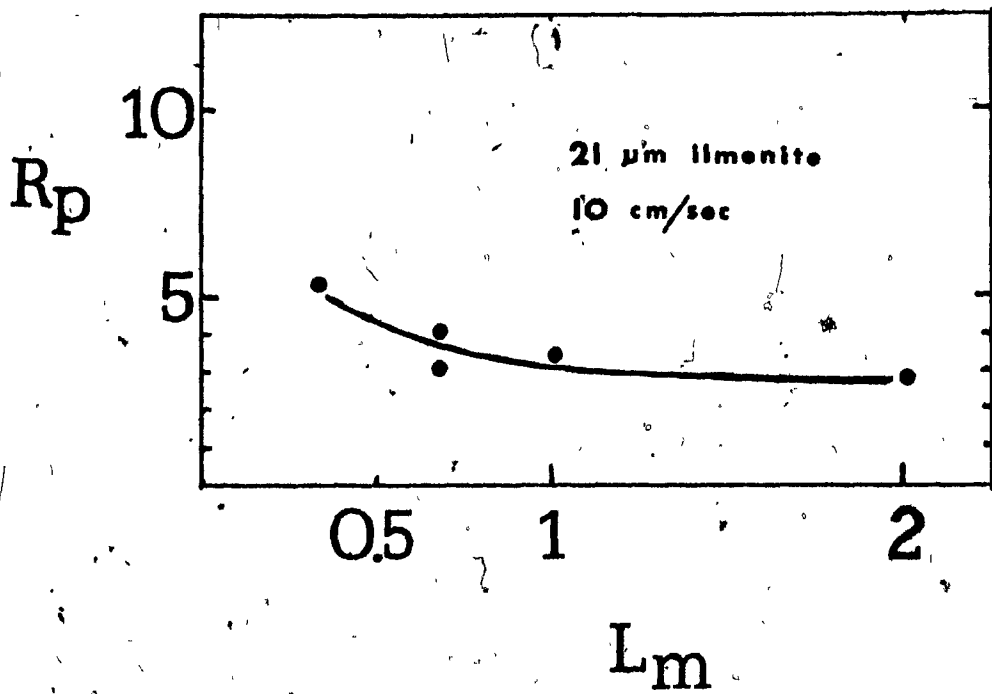


FIGURE 44

$R_p$  vs  $L_m$  for 21  $\mu$ m ilmenite at 10 cm/sec. Drainage system.



## FIGURE 45

$R_M$  vs H for 5 particle sizes of hematite at 10 cm/sec.  
Drainage system.

### EFFECT OF PARTICLE SIZE

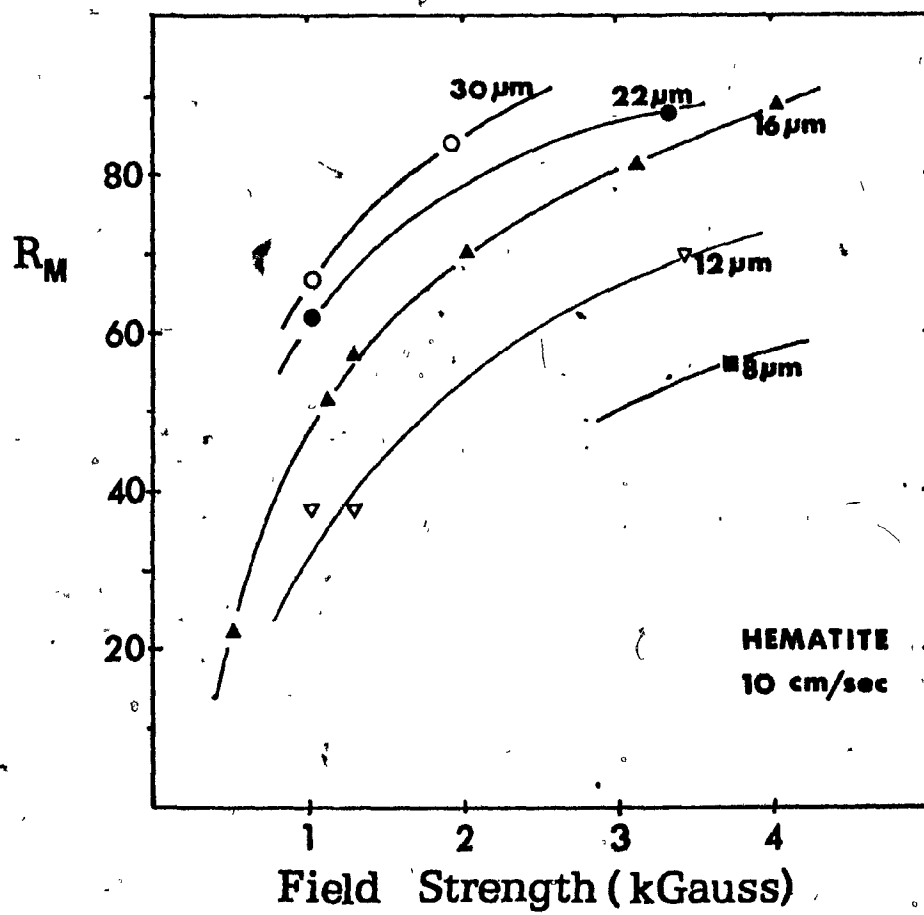


## FIGURE 46

(a)  $R_M$  vs  $H_d$  for the data of Fig. 45.

(b)  $R_M$  vs  $\log(H_d)$  for the data of Fig. 45.

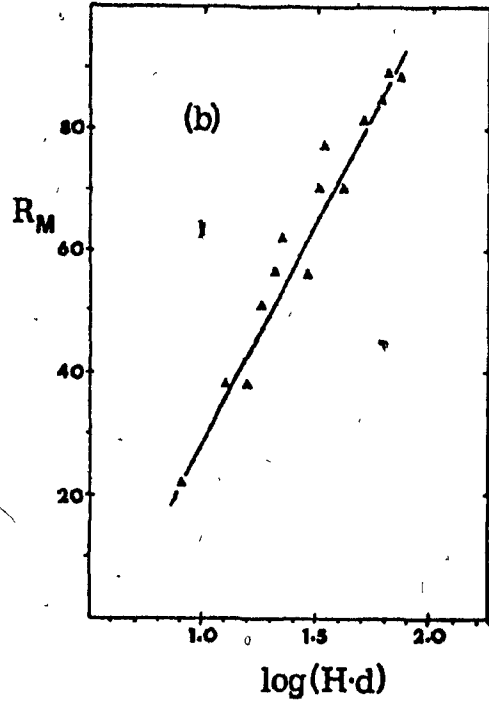
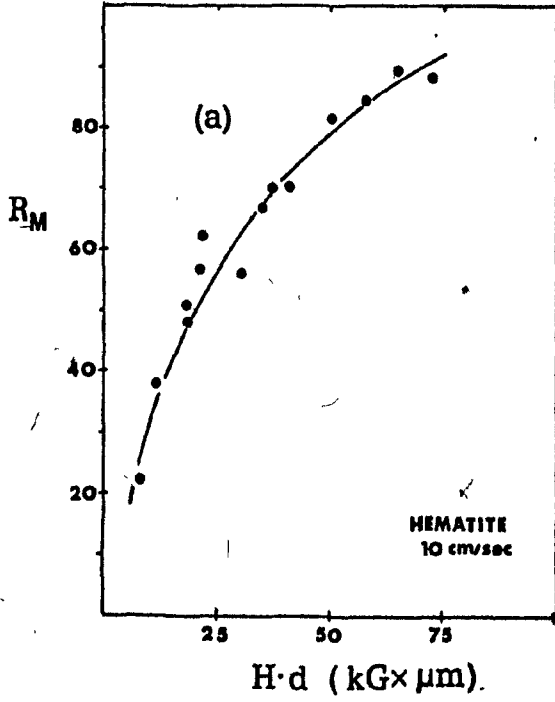
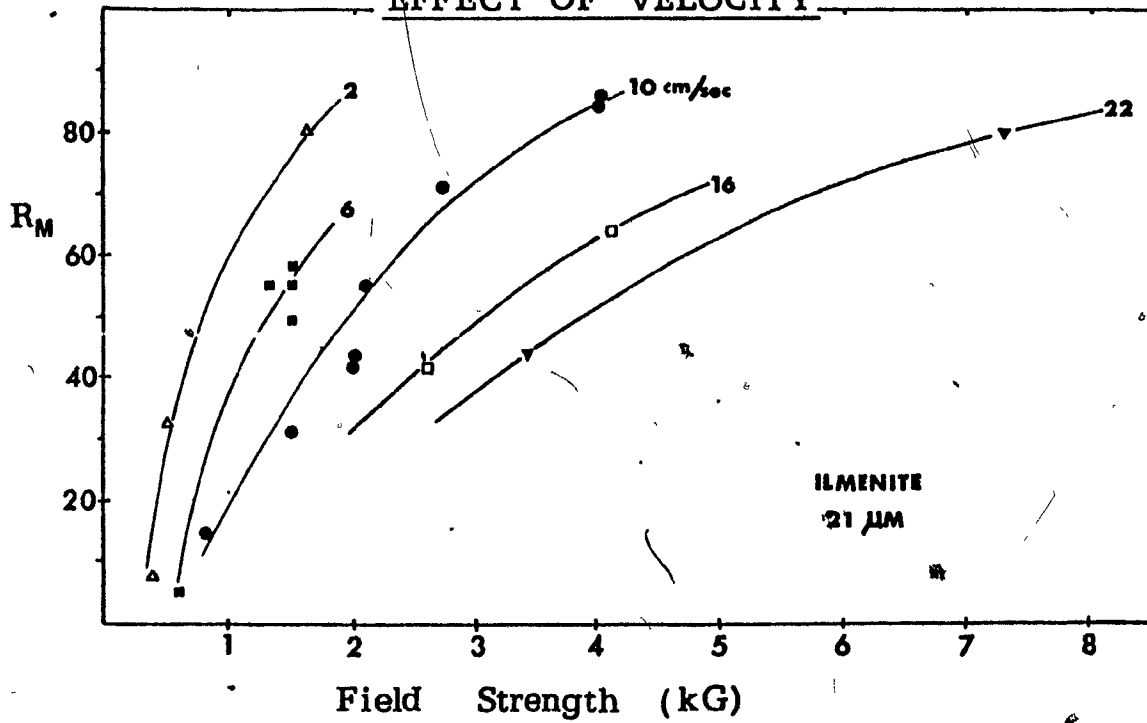


FIGURE 47

$R_M$  vs H for 21  $\mu\text{m}$  ilmenite at 5 velocities. Drainage system.

EFFECT OF VELOCITY



of curves is again evident and Figure 48 (a) shows  $R_M$  as a function of  $\frac{H}{U}$ . Figure 48 (b) indicates that  $R_M$  is apparently proportional to  $\log \frac{H}{U}$  for  $U > 2$  cm/sec. The points derived from tests at 2 cm/sec fell considerably below the others. The effect of  $U$  was also studied at other  $d$  and with the other minerals, although not extensively.

#### 3.4.4 Effect of Viscosity

Only runs using the permanent magnet were made. The results of duplicate tests at water temperatures of 35°C, 22°C and 5°C are given in Table 15. They reveal the correct sign of the dependence that the force balance model dictates, but not the magnitude that would be expected from the doubling of the viscosity over this temperature range.

#### 3.4.5 Effect of Matrix Loading

Experiments were performed with 21  $\mu\text{m}$  ilmenite at 10 cm/sec under varying conditions of field strength and feed weight, with  $L_m$  varying between 0.17 and 2.0. The results are plotted in Figure 49 (a).

Figure 49 (b) was derived from the same data and indicates that  $R_M$  is approximately proportional to  $\log \frac{H^2}{L_m}$ .

#### 3.4.6 Sphalerite and Chalcopyrite Recovery

Figure 50 shows the results of tests with 22  $\mu\text{m}$  sphalerite and chalcopyrite at 2 and 4 cm/sec. The recovery of chalcopyrite at 20 kG and 4 cm/sec was considerably higher than would be expected by the shape of the curves.

## FIGURE 48

(a)  $R_M$  vs  $H/U$  for the data of Fig. 47.

(b)  $R_M$  vs  $\log(H/U)$  for the data of Fig. 47.

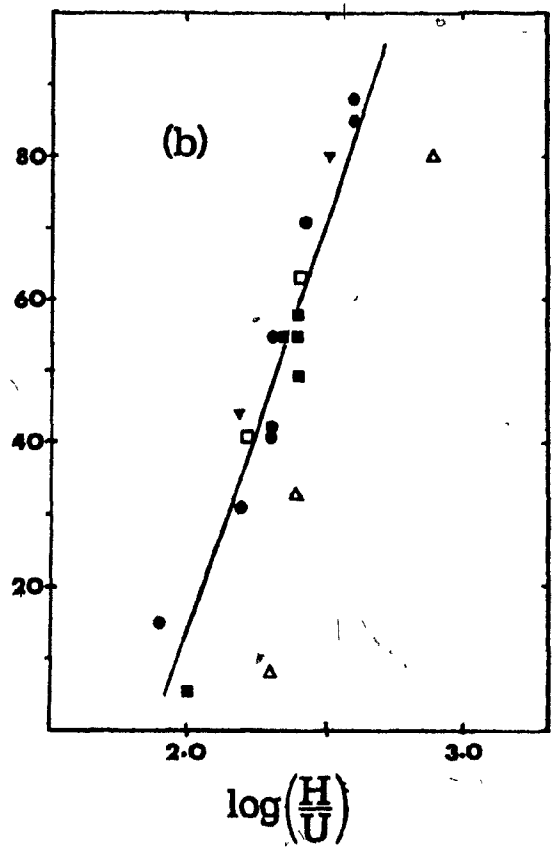
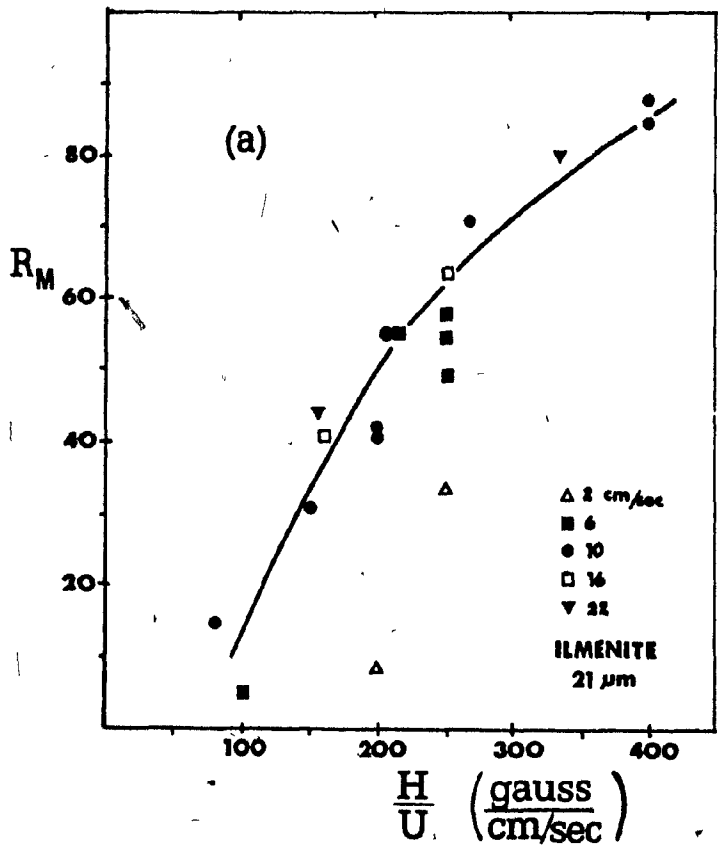


TABLE 15 - MAGNETIC RECOVERY vs VISCOSITY-DRAINAGE SYSTEM

Conditions: H = 1 kG (permanent magnet)

d = 22 um (hematite)

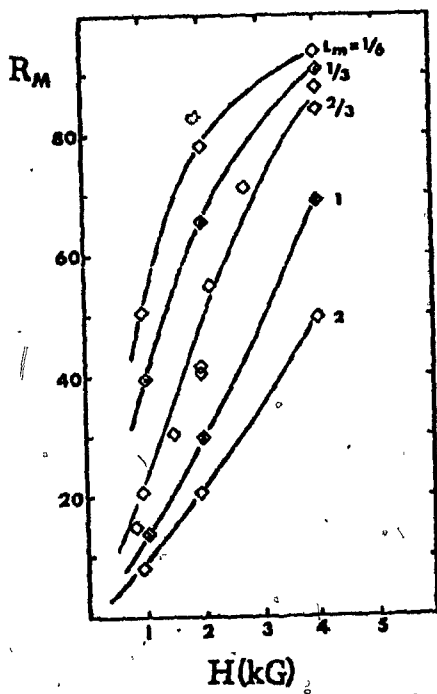
U = 8 cm/sec

TEMPERATURE (°C)	VISCOSITY (cp)	MAGNETIC RECOVERY (%)
5	1.5	37
22	0.95	39
35	0.72	43

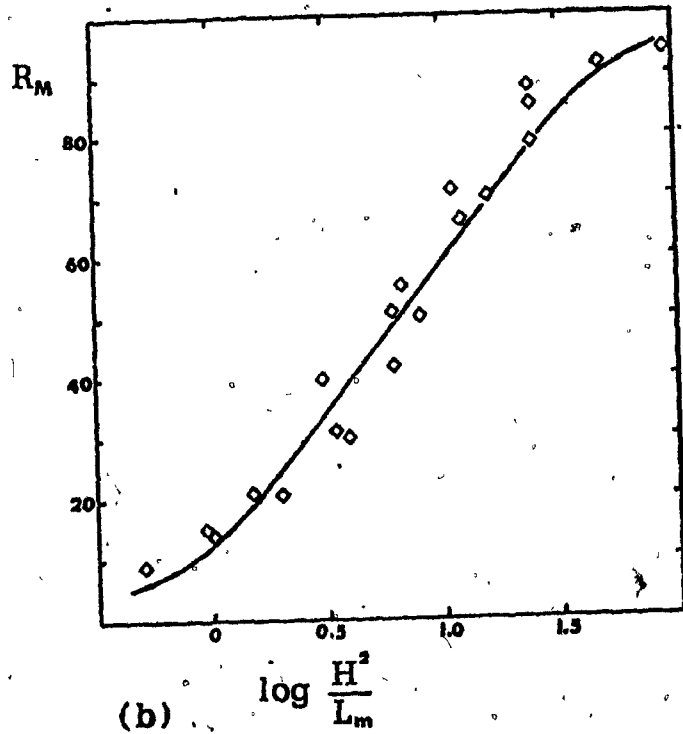
FIGURE 49

(a)  $R_M$  vs  $H$  for 21  $\mu\text{m}$  ilmenite at 10 cm/sec and five matrix loadings. Drainage system.

(b)  $R_M$  vs  $\log(H^2/L_m)$  for the same data.



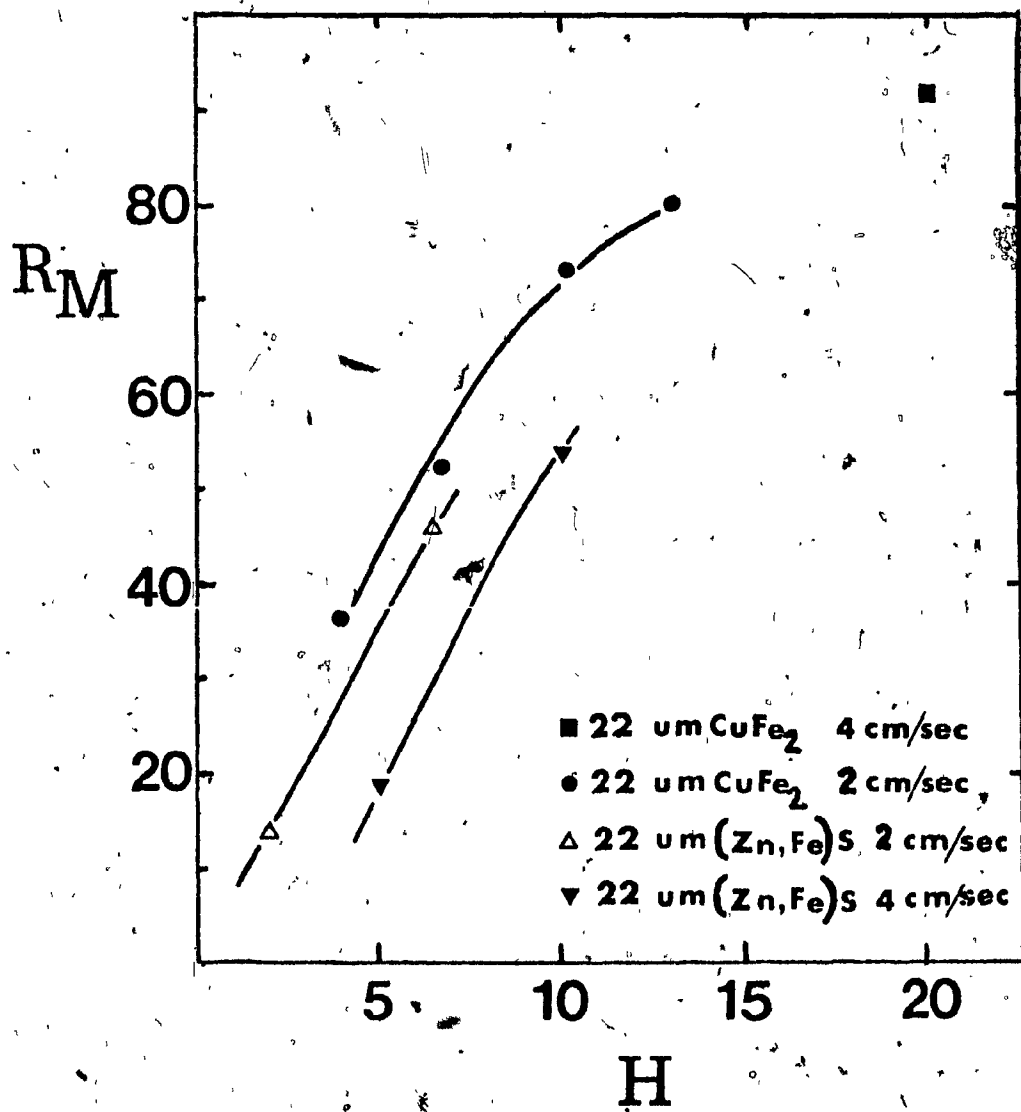
(a)



(b)

## FIGURE 50

$R_M$  vs H for 22  $\mu\text{m}$  chalcopyrite and sphalerite at two velocities. Drainage system.



### 3.5 An Empirical Model of Capture - Drainage System

An empirical model was developed using the same step-wise linear regression technique employed to treat the constant head system results. The same variables were employed, and the log of each variable was used, with the  $HM_w$  exponent set to 1. The regression data is given in Appendix 4.

A satisfactory fit over the entire field strength range could not be achieved; at  $H > 15$  kG, the  $R_M$  for sphalerite and chalcopyrite was considerably higher than could be included without unacceptable distortion. For the 72 tests covering the following range of conditions:  $0.4 \leq H \leq 13$  kG;  $8.5 \leq d \leq 49$   $\mu$ m;  $2 \leq U \leq 22$  cm/sec;  $0.17 \leq L_m \leq 2.0$ ;  $0.25 \times 10^{-4} \leq k \leq 8.0 \times 10^{-4}$  emu/cm<sup>3</sup>-0e;  $9 \leq R_M \leq 95\%$ , the following regression equation:

$$R_M = -58.9 + 38.3 \log \left[ \frac{HM_w k^{1.8} d^{1.6}}{U^{1.3} L_m^{1.1}} \right] \quad (28)$$

gave a standard error of estimate 9.7. The fit is shown in Figure 51.

The considerable effect of  $k$  and the difficulty of including the term is illustrated by the regression fit obtained for just the 59 ilmenite and hematite tests:

$$R_M = -137.4 + 41.3 \log \left[ \frac{H^2 k^{3.9} d^{1.6}}{U^{1.3} L_m^{1.1}} \right] \quad (29)$$

The standard error of estimate was reduced to 6.5. The fit is given in Figure 52 along with the range of conditions. The dependence on  $k$  changed considerably but the dependence on the other parameters was unaltered.

## FIGURE 51

Plotted regression results (Eq. 28) of drainage system tests including all four minerals.

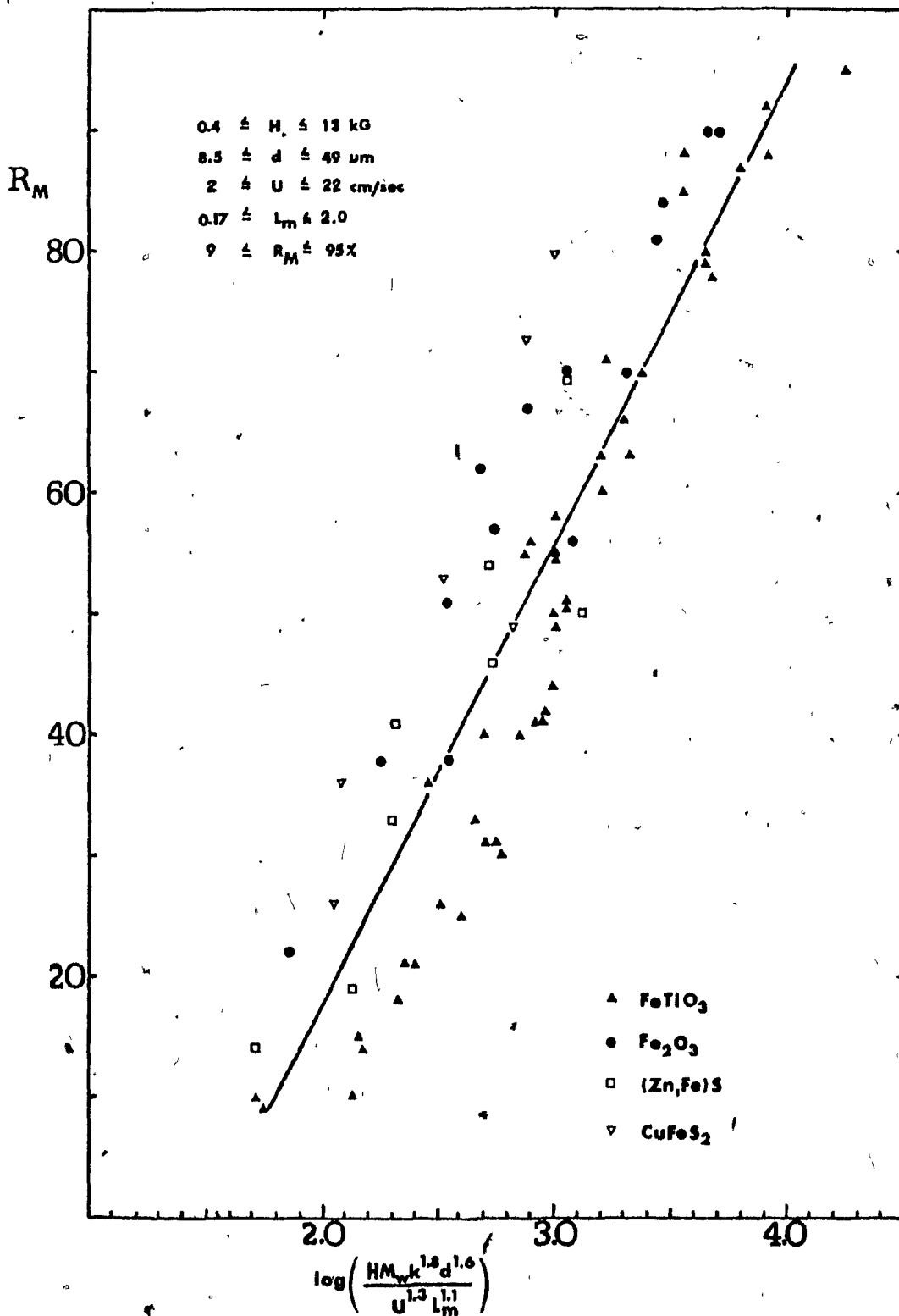
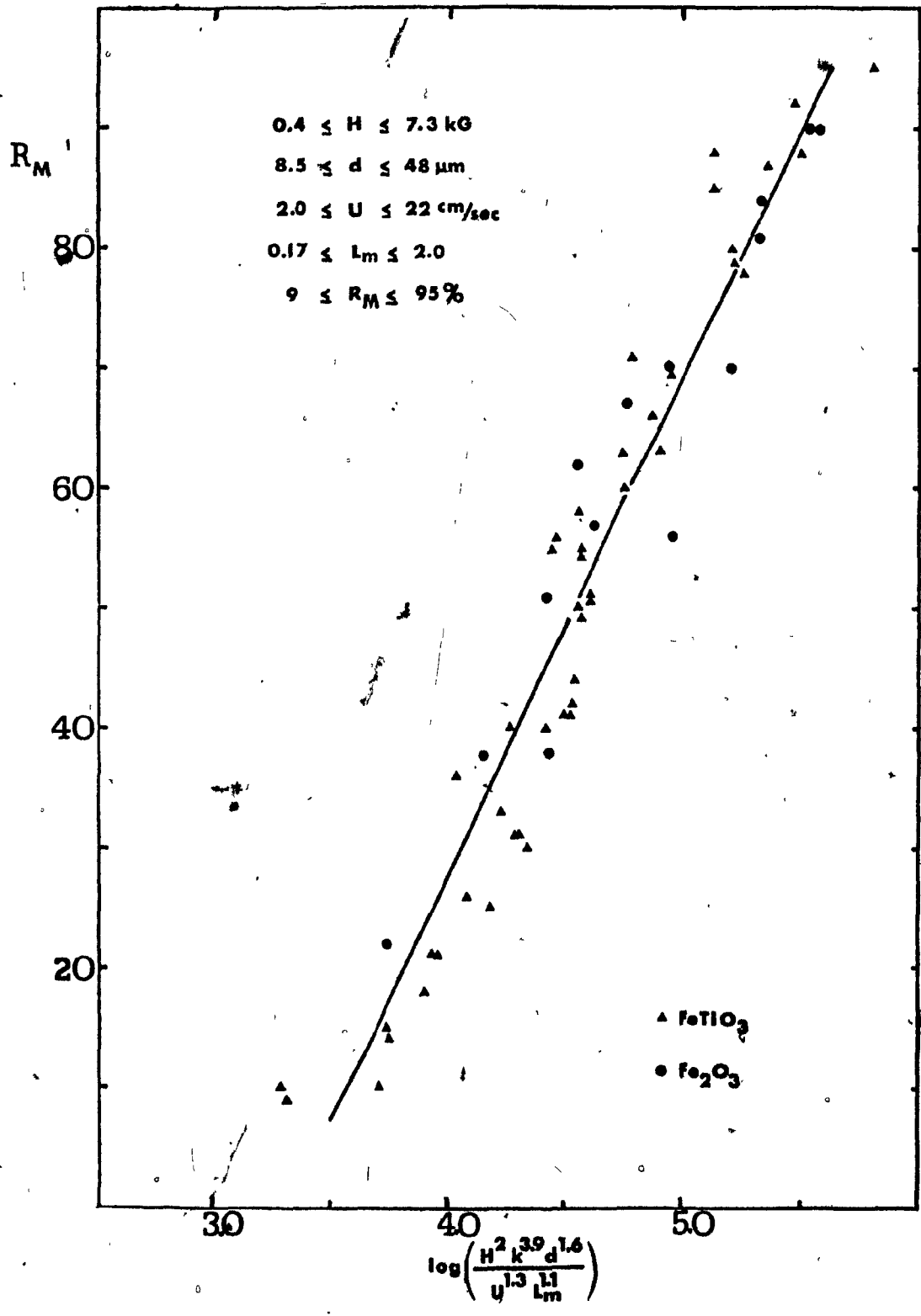


## FIGURE 52

Plotted regression results (Eq. 29) of drainage system  
ilmenite and hematite tests.



CHAPTER 4

EMPIRICAL MODEL  
PREDICTIONS

#### 4.1 Recovery of a Size Range of Hematite

Hematite cyclone underflow, with the distribution shown in Table 4, was used in a test with the constant head system and in three tests with the drainage system. Predictions were made by calculating  $R_M$  (with Eq. (27) or (29)) for each size interval, and summing the fractional recoveries of each interval. Thus

$$R_T = f_d \times (R_{Md} + R_{Pd}) \quad (30)$$

Predicted and measured results from the constant head test are given in Table 16.  $R_T$  was 13.5%. The results of tests with the drainage system are given in Table 17. Average  $R_T$  for the three tests was 6.6%. These results indicate that the summation procedure used is a reasonable method of handling a wide size distribution.

#### 4.2 Hematite - Silica Separations

Drainage system model predictions were evaluated for separation of  $16 \mu\text{m}$   $\text{Fe}_2\text{O}_3$  from  $30 \mu\text{m}$  silica. Consider the grade and recovery to mags of mineral a ( $\text{Fe}_2\text{O}_3$ ) in a synthetic mixture of minerals a and b (silica). Total recovery of a is given by:

$$R_{aT} = R_{aM} + R_{aP} \quad (31)$$

and grade of a to the mags is given by:

$$G_{aMags} = \frac{100 W_a R_{aT}}{W_a R_{aT} + W_b R_{bT}} \quad (32)$$

For a synthetic mixture there is no locking of a and b minerals so that  $R_{aM}$  or  $R_{bM}$  can be estimated from Eq. (28) or (29).  $R_{aP}$  and  $R_{bP}$  will be known. Thus,  $R_{aT}$  and  $G_{aMags}$  can be predicted. Six tests, with varying, feed % hematite, were performed. Results are given in Table 18. Figure 53

TABLE 16Predicted and Measured Recovery of a Size Range of HematiteConditions: Constant Head System - 59 gm matrix

$$k = 8.0 \times 10^{-4} \text{ emu/cm}^3 - \text{Oe}$$

$$U = 9.9 \text{ cm/sec}$$

$$L = 0.33$$

$$H^m = 3.0 \text{ kG}$$

$\frac{d_{ave}}{(\mu m)}$	$f_d$	$R_{Md}^*$	$R_{Pd}$	$R_{Td}$	$R_{fract}$
32	0.074	92.2	1.5	93.7	6.9
24.7	0.236	82.4	1.0	83.4	19.7
18.7	0.312	71.9	0.5	72.4	22.6
13.5	0.206	59.5	0.5	60.0	12.4
9.8	0.097	47.5	0.5	48.0	4.6
~ 5.0	0.075	22.0	0.5	22.5	1.7

67.9% =  $R_T$  predicted  
 81.4% =  $R_T$  measured  
 $\Delta R_T = 13.5\%$

\* using Eq. (27)

TABLE 17

Predicted and Measured Recovery of a Size Range of HematiteConditions: Drainage System

$$k = 8.0 \times 10^{-4} \text{ emu/cm}^3 - 10e$$

$$U = 10 \text{ cm/sec}$$

$$L_m = 0.67$$

I. H = 0.9 kG

$\frac{d}{(\mu\text{m})}$	$\frac{f_d}{}$	$\frac{R_{Md}^*}{}$	$\frac{R_{Pd}}{}$	$\frac{R_{Td}}{}$	$\frac{R_{\text{fract}}}{}$
32	0.074	57.9	5	62.9	4.7
24.7	0.236	50.5	4	54.5	12.9
18.7	0.312	42.5	3	45.5	14.2
13.5	0.206	33.2	2	35.2	7.2
9.8	0.097	24.0	1	25.1	2.4
~ 5.0	0.075	4.7	1	5.7	0.4

$$41.8\% = R_T \text{ predicted}$$

$$55.0\% = R_T \text{ measured}$$

$$\Delta R_T = 13.2\%$$

II. H = 3.0 KG

$\frac{d}{(\mu\text{m})}$	$\frac{f_d}{}$	$\frac{R_{Md}^*}{}$	$\frac{R_{Pd}}{}$	$\frac{R_{Td}}{}$	$\frac{R_{\text{fract}}}{}$
32	0.074	100	5	100	7.4
24.7	0.236	93.7	4	97.7	23.1
18.7	0.312	85.7	3	88.7	27.7
13.5	0.206	76.4	2	78.4	16.2
9.8	0.097	67.2	1	68.2	6.6
~ 5.0	0.075	47.9	1	48.9	3.7

$$84.7\% = R_T \text{ predicted}$$

$$84.0\% = R_T \text{ measured}$$

$$\Delta R_T = 0.7\%$$

III. H = 6.5 kG

$\frac{d}{(\mu\text{m})}$	$\frac{f_d}{}$	$\frac{R_{Md}^*}{}$	$\frac{R_{Pd}}{}$	$\frac{R_{Td}}{}$	$\frac{R_{\text{fract}}}{}$
32	0.074	100	5	100	7.4
24.7	0.236	100	4	100	23.6
18.7	0.312	100	3	100	31.2
13.5	0.206	100	2	100	20.6
9.8	0.097	94.9	1	95.9	9.3
~ 5.0	0.075	75.6	1	76.6	5.7

$$97.8\% = R_T \text{ predicted}$$

$$92.0\% = R_T \text{ measured}$$

$$\Delta R_T = 5.8\%$$

\* using Eq. (29)

TABLE 18

Predicted and Measured Fe<sub>2</sub>O<sub>3</sub> Recovery and Grade in Separations  
of Synthetic Fe<sub>2</sub>O<sub>3</sub> - SiO<sub>2</sub> Mixtures

$$R_{\text{Silica M}} = 0$$

$$R_{\text{Silica P}} = 3\%$$

$$R_{\text{Fe}_2\text{O}_3 \text{ P}} = 3.5\%$$

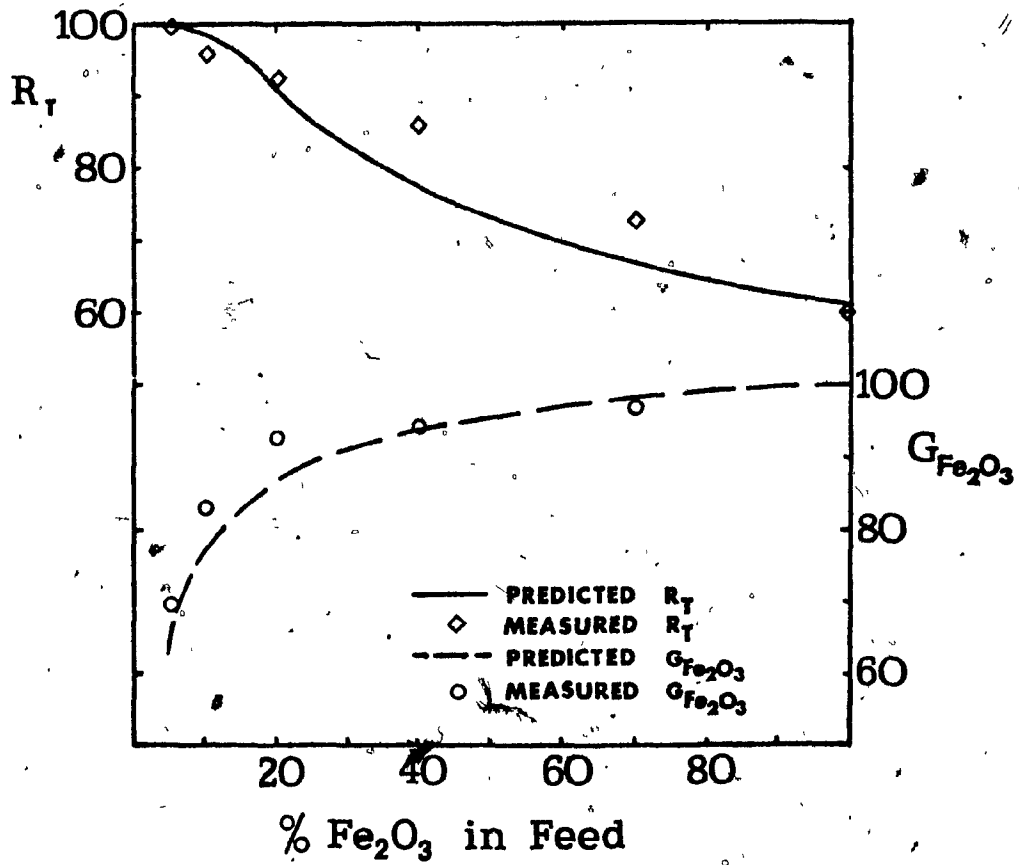
Conditions:  $k = 8.0 \times 10^{-4} \text{ emu/cm}^3 - 0e$   
 $H = 1.5 \text{ kG}$   
 $d = 16 \text{ } \mu\text{m}$   
 $U = 10 \text{ cm/sec}$   
 Drainage System

Test#	Feed % Fe <sub>2</sub> O <sub>3</sub>	L <sub>m</sub>	R <sub>Fe<sub>2</sub>O<sub>3</sub> T</sub> (%)		F <sub>Fe<sub>2</sub>O<sub>3</sub> Mags</sub> (%)	
			Predicted*	Measured	Predicted	Measured
1	100	.67	59	60	-	-
2	70	.47	67	73	98	97
3	40	.27	78	86	95	94
4	20	.13	91	92	88	94
5	10	.067	100	96	79	83
6	5	.033	100	99	64	70

\* using Eq. (29)

## FIGURE 53

Predicted and measured grades and recoveries for  $\text{Fe}_2\text{O}_3$  from synthetic  $\text{Fe}_2\text{O}_3$ - $\text{SiO}_2$  mixtures as a function of feed %  $\text{Fe}_2\text{O}_3$ .



is a plot of  $R_{Fe_2O_3T}$  and  $G_{Fe_2O_3}$  vs feed %  $Fe_2O_3$ .

The total feed weight was maintained at 20 gms, but  $L_m$  was based on the weight of hematite in the feed. Products were analyzed for hematite using the Frantz. Recovery and grade correlations were reasonable, indicating that basing  $L_m$  upon the weight of magnetically recoverable material, and not the total feed weight, was correct.

#### 4.3 Prediction of Mineral Separation - A Methodology

To make a reasonable estimate of the metallurgy expected from the subsection of a given material to HGMS it is essential to be able to describe the susceptibility and particle size of the material. The empirical models of capture were developed from data from tests employing samples that could, with reasonable accuracy, be described by a single  $k$  value and a single  $d$  value. Real samples generally have wide ranges of  $k$  and  $d$  and, practically, can not be described by single values. Therefore the sample must be split into several  $k$  and  $d$  values, and the weight fraction and the mineral distribution must be known for each size interval at each susceptibility value. It should be stressed at this point that the models were developed within specific parameter limits, and that results from its use beyond these limits should be treated with caution.

The splitting of the sample into several particle sizes and calculation of  $R_M$  for each size has already been described. A summation of the fractional recoveries to yield the total predicted  $R_M$  yielded reasonable results.

A similar procedure was applied to adjust for a wide range in susceptibility. However, unlike particle size distribution, which the cyclosizer clearly defines into several intervals, the susceptibility distribution, as derived from the magnetic response curve from the Frantz, is a smooth function and must be arbitrarily split into several intervals. Using the magnetic

response curve; a sample is mathematically split into several weight fractions. Each fraction will have an upper and lower current at which it has been magnetically recovered on the Frantz. The average of the two current values is then used as the  $I_{50\%}$  which describes the susceptibility of that particular weight fraction of the sample (using Eq. (24)).

Alternatively, the sample can be mathematically split into several current fractions, and the weight fraction of each current interval determined from the difference in the two weight percent extremes as measured from the curve.

The sample has thus been split into several size intervals and each size interval is described by several susceptibility values. The weight fraction of the sample in each  $k$  and  $d$  interval is known. As well, the distribution of a certain mineral or element, from chemical analysis of cyclosizer and/or Frantz products, might be known. The only other parameter that needs to be quantified before the empirical model can be applied to each  $k$  and  $d$  interval is  $L_m$ . This value is difficult to specify if a wide susceptibility range is present. As a first approximation, the expected magnetic weight recovery can be used to determine  $L_m$ . If the predicted weight recovery differs greatly from the  $L_m$  employed to determine it, then  $L_m$  should be adjusted and  $R_M$  re-calculated.

The prediction technique, then, involves calculating  $R_M$  for each  $d$  and  $k$  interval, determining the fractional recovery for each interval by multiplying  $R_M$  by the interval weight fraction, and then summing the fractional recoveries. With sufficient information very complex minerals can thus be handled. The basic information required to predict weight recoveries using the empirical model are the size distribution of the sample and its magnetic response curve. Assays from fractions removed on the Frantz at specific current levels and assays of the individual size intervals are necessary if predicting elemental or mineral recoveries.

#### 4.3.1 Predicted and Measured Metallurgy of Tin Concentrate Separations

The cyclone U/F, -325 m tin concentrate was employed to test the methodology and use of the empirical model developed with the constant head system. The size distribution of the sample was given in Table 8 and the response curves are shown in Figure 25. The four size intervals were also assayed for iron, which was assumed to be in the form of pyrrhotite. Pyrrhotite assays and distribution are also given in Table 8. The final sample information available is the weight and pyrrhotite distribution to the two products resulting from a separation of the sample on the Frantz at 0.6 Amp, given in Table 8.

Appendix 5 gives the prediction calculations for each test. Material magnetically recovered on the Frantz up to 0.8 Amp. (at which point the response curve had reached a plateau) was mathematically divided into three equal weight fractions, and the representative susceptibility of each fraction determined as per the method described in Section 4.3. Table 12 gives the determined k values as well as the  $I_{50\%}$  and specific gravity used to derive them.

The empirical model was then applied to calculate the individual  $R_M$  and  $R_{Fe_7S_8M}$  was determined by summing the fractional recoveries. Determination of total weight recovery was made difficult by the interlocking of pyrrhotite and cassiterite. The separation on the Frantz at 0.6 Amp. was used to solve this. In the Frantz separation  $Fe_7S_8$  recovery was 94.4% and total weight recovery to mags was 13.5%. Units of weight recovery per unit of pyrrhotite recovery (13.5/94.4) was used to estimate weight recovery on the HGMS, as expressed by:

$$R_T = \left[ \frac{13.5}{94.4} \times R_{Fe_7S_8M} \right] + R_P \quad (33)$$

where  $R_p$ , the estimated total physical entrainment, was 2%.

The sample was assumed to consist of only  $Fe_7S_8$  and  $SnO_2$  (although a small amount of impurities may have been present, eg PbS). The weight loss of  $SnO_2$  to the mags was therefore estimated from:

$$R_{SnO_2T} = R_T - (R_{Fe_7S_8M} \times 8.57)/100 \quad (34)$$

Grade of  $Fe_7S_8$  in the mags was estimated using Eq. (32), and grade of  $Fe_7S_8$  in the non-mags using,

$$G_{N-M} = \frac{100 W_a (100 - R_{aT})}{W_a (100 - R_{aT}) + W_b (100 - R_{bT})} \quad (35)$$

where a corresponds to  $Fe_7S_8$  and b corresponds to  $SnO_2$ .

Predicted and measured weight recovery, pyrrhotite recovery, and %  $Fe_7S_8$  for the five tests are summarized in Table 19. Predicted pyrrhotite recovery and weight recovery were slightly lower than the measured values in each case except one. Generally, however, agreement of predicted with measured metallurgy was good.

#### 4.3.2 Predicted and Measured Metallurgy of Copper Concentrate Separation

The cyclone U/F copper concentrate, containing chalcopyrite, pyrrhotite and pyrite was tested with the constant head system. The aim of such a separation is to concentrate the chalcopyrite by magnetically removing the pyrrhotite. The prediction technique described in Section 4.3.1 is not feasible in this case. Major complications are (1) Fe is contained in all three main minerals, so that Fe assays alone would not describe the mineral occurrence (extensive mineralogical preparation and mineral point counting would be required), and (2) a large degree of mineral interlocking is present.

TABLE 19

Predicted and Measured Metallurgy of Tin Concentrate Separations

Test	Product	$R_T$ (%)		% $Fe_7S_8$		$R_{Fe_7S_8 T}$	
		Predicted*	Measured	Predicted*	Measured	Predicted*	Measured
#1 H = 3.9 U = 15.6 $L_m = .04$	Mags	15.0	20.0	53.9	41.5	91.1	89.3
	Non-Mags	85.0	80.0	0.89	1.25	8.9	10.7
#2 H = 2.0 U = 15.6 $L_m = .04$	Mags	13.0	17.2	53.0	45.5	78.4	82.1
	Non-Mags	87.0	82.8	2.12	1.93	21.6	17.9
#3 H = 1.2 U = 15.6 $L_m = .04$	Mags	11.0	13.8	51.8	49.2	64.7	74.5
	Non-Mags	89.0	86.2	3.38	2.70	35.3	25.5
#4 H = 2.0 U = 15.6 $L_m = 0.08$	Mags	12.3	16.3	52.2	49.5	72.9	85.0
	Non-Mags	87.7	83.7	2.63	1.71	27.1	15.0
#5 H = 2.1 U = 22 $L_m = .04$	Mags	12.3	13.3	52.2	54.8	72.9	80.5
	Non-Mags	87.7	86.7	2.63	2.04	27.1	19.5

\* See Appendix 5

However, data from the Frantz Isodynamic Separator can be used to initially approximate expected metallurgy of separations on the HGMS. Referring to the magnetic response curves of the sample (Figure 27), and realizing that  $\text{Fe}_7\text{S}_8$  is much more susceptible than  $\text{CuFeS}_2$  and  $\text{FeS}_2$ , it can be seen that virtually all of the pyrrhotite will be removed if 20 to 30% of the sample is magnetically recovered. Some copper will naturally be removed due to particle locking. An indication of the expected metallurgy is given by the separation on the Frantz of #2 cyclone material at 0.4 Amp., shown in Table 9. (There appears to be little size effect in the magnetic response of the sample, so #2 cone material is used to approximate the whole sample). This metallurgy could be used as an initial approximation to the metallurgy from HGMS that produced a 20 to 30% weight recovery.

The size distribution of the copper concentrate cyclone U/F is given in Figure 26, and the magnetic response curves of the first three cyclosizer intervals are shown in Figure 27. Appendix 5 gives the calculations for each test. An average response curve of the #2 and #3 cyclosizer cones (which represents 53% of the sample) was used in splitting the susceptibility into four k values. The weight fraction of the sample apportioned to each susceptibility interval was determined as per the method described in Section 4.3.

Table 20 gives the predicted and measured weight recoveries for the four tests, as well as the Cu and Fe assays and distributions in the mags product. Predicted weight recoveries were reasonably accurate, although they were all slightly higher than the actual weight recoveries.

TABLE 20Copper Concentrate Separation Results

Test #	H (kG)	U ( $\frac{cm}{sec}$ )	$R_T$		% Cu in Mags	Cu Rec to Mags (%)	% Fe in Mags	Fe Rec to Mags (%)
			Predicted*	Measured				
1	2.1	22	23	19	7.7	7.4	43.6	34.1
2	1.1	15.6	19	17	9.0	7.3	46.2	31.3
3	2.1	15.6	28	23	9.5	11.5	43.6	38.8
4	4.0	15.6	35	28	12.2	17.1	38.4	43.6

\* See Appendix 5

Tests 1, 2 and 3 had weight recoveries between 17 and 23%, and their copper assays and distribution were approximated, as expected by the separation on the Frantz of #2 cyclone material at 0.4 Amp.

#### 4.4 Predictions Using Shorter Matrix

Several tests using ilmenite and hematite, including hematite cyclone U/F were performed with the constant head system using the shorter expanded metal matrix described in Table 2. To predict the recovery in each case,  $R_M$  for the longer matrix was first estimated using Eq. (27).  $R_M$  for the shorter matrix was then estimated using Eq. (22), where  $x$  was equal to 59 gms and  $y = 32$  gms.  $R_M$  for the long matrix was, therefore, denoted by  $R_{59}$ , and for the short matrix by  $R_{32}$ .

Table 21 gives the conditions of each test employing the closely sized samples, and predicted and measured  $R_T$ . The average difference between predicted and measured recoveries was 5%. Table 22 gives the predicted and measured  $R_T$  for the test employing the hematite cyclone U/F.  $R_{32}$  was determined for each  $d$  interval, and  $R_T$  from the summation of the fractional recoveries.  $R_T$  was 5.3%. Considering that the predicted recoveries involved a prediction using the empirical model plus a prediction of the effect of matrix length, the results are reasonable.

TABLE 21

Predicted and Measured Recovery Using Short Matrix

Test #	Test Conditions					$R_{59}^*$	$R_{32}^{\square}$	$R_p$	$R_T$	$R_T$	$\Delta R_T$
	$k$	H	d	U	$L_m$	Predicted (%)	Predicted (%)	(%)	Predicted (%)	Measured (%)	
	$(\frac{\text{emu}}{3} \times 10^4)$	(kG)	( $\mu\text{m}$ )	( $\frac{\text{cm}}{\text{sec}}$ )							
1	5.6	3.3	21	9.9	.33	72.2	49.8	1	51	48	3
2	5.6	1.8	21	9.9	.33	53.5	34.0	1	35	26	9
3	5.6	1.1	21	9.9	.33	39.5	23.7	1	25	16	9
4	8.0	3.3	22	9.9	.33	80.4	58.5	1	60	57	3
5	8.0	1.1	22	2.9	.33	81.1	59.2	5	64	63	1

\* Using Eq. (27)

 $\square$  Using Eq. (22);  $R_y = 1 - (1 - R_{59})^{y/59}$ , where  $y = 32$

TABLE 22

Predicted and Measured  $R_T$  Using Short Matrix  
and Hematite Cyclone U/F

Conditions: constant head system - 32 gm matrix

$$k = 8.0 \times 10^{-4} \text{ emu/cm}^3 - \text{Oe}$$

$$U = 9.9 \text{ cm/sec}$$

$$L = 0.33$$

$$H^m = 3.3 \text{ kG}$$

$d_{\text{ave}}$ ( $\mu\text{m}$ )	$f_d$	$R_{59}^*$	$R_{32}^{\square}$	$R_{p_d}$	$R_{T_d}$	$R_{\text{fract}}$
32	0.074	94.6	79.5	1.0	80.5	6.0
24.7	0.236	84.8	64.0	0.5	64.5	15.2
18.7	0.312	74.3	52.1	0.5	52.6	16.4
13.5	0.206	61.9	40.8	0.5	41.3	8.5
9.8	0.097	49.9	31.3	0.5	31.8	3.1
~ 5.0	0.075	24.4	14.1	0.5	14.6	1.1

50.3 =  $R_T$  predicted  
55.6 =  $R_T$  measured  
 $\Delta R_T = 5.3\%$

\* Using Eq. (27)

$\square$  Using  $R_y = 1 - (1 - R_{59})^{y/59}$ , where  $y = 32$

CHAPTER 5

DISCUSSION

### 5.1 Susceptibility Measurements

The use of the Frantz Isodynamic Separator as a susceptibility measurement device was attempted because it is easily accessible to personnel in the mining industry. With the Frantz, magnetic susceptibility can be quickly and easily measured. An added, and important, benefit is that the range of susceptibility within a single sample can be determined in the form of a magnetic response curve, a feature of which conventional measurement devices (eg. magnetometers) are incapable. At the same time, sample fractions can be separated and removed at various levels of magnetic susceptibility and assayed, which then permits metallurgy to be introduced. However, the validity and accuracy of the susceptibility measurements made with the Frantz are debatable.

Measured susceptibility of all four uni-mineral samples was found to vary considerably with the side slope employed. In each case there was a large decrease in measured susceptibility as the applied field strength at which the measurement was made increased. Paramagnetic material will saturate at high enough strengths, and when approaching saturation  $k$  will decrease with  $H$ . However, at room temperature, the field strength required before a noticeable susceptibility decrease occurs is extremely high ( $> 10^5$  gauss). Minerals present a problem, though, as minute amounts of ferromagnetic minerals within the crystal structure of the paramagnetic mineral can greatly affect the magnetization. It is doubtful that this occurs to such a large degree with all four uni-mineral samples. Two explanations seem possible: (1) the susceptibilities of the minerals do change with field strengths by the amounts indicated, or (2) the susceptibilities do not vary to such an

extent and the effect is an artifact of the measuring technique. The author feels that the latter is more likely, suggesting that the technique of susceptibility measurement with the Frantz should be investigated.

Table 11 indicates that  $k$  can vary with  $d$ . A noticeable, but not large, size effect was observed with the hematite sample but not with the sphalerite. This suggests that the phenomenon was probably a feature of the hematite itself and not due to the measurement technique, otherwise equal effects on both samples would be expected. The type of grinding media employed in preparing the hematite may have been influential. Extensive examination of the size effect was not performed, although such a study might be beneficial.

In light of the above discussion it was decided that, for the sake of consistency, all susceptibility measurements would be made at a side slope of  $20^\circ$  and with a particle size of 25 to 40  $\mu\text{m}$ .

## 5.2 Force Balance Model of Capture

As an initial description of particle capture in a high gradient magnetic separator the force balance model is marginally adequate. It fails to predict the log dependence and does not account for matrix loading. Quantitatively, the effects of velocity, viscosity, and particle size are underestimated. However, the model's uncomplicated approach serves as a good qualitative introduction to the forces involved in magnetic capture of particles.

In comparing the results of the empirical models with the force balance model of Eq. (17), it must be remembered that the force balance model was developed under the conditions of several simplifying assumptions. Firstly, the actual matrices were not circular in cross section, as was assumed in the force balance model. Both matrices, especially the steel wool, exhibited the sharp edges at which localized, higher than average

radient would be created. Therefore, classification of the field gradient by a single value was only an approximation of the real situation of a range of gradients.

The assumption of fluid flow in the Stokesian regime was not totally valid. At the higher velocities and with most of the particle sizes employed an intermediate flow regime would be present, thus affecting the  $d$  and  $U$  exponents of the drag force. The particle was also assumed to be moving with a velocity equal to the fluid velocity. This was obviously not the case as it moved towards the wire in a direction which was generally at an angle to the fluid flow. Derivation of the drag force also assumed the presence of spherical particles which, naturally, is not the case with an actual sample.

The drainage mode of operation introduced two further considerations - a non-constant velocity, and an added force, residing in the interfacial tension of the air-water boundary.

Finally, the force balance model was developed for the case of a single wire and a single particle, which may be confusingly over simplified.

An extensive comparison of the results from actual tests to the force balance model is, therefore, not a worthwhile exercise. The use of the force balance model should be confined to a general qualitative description of HGMS, in which it is reasonably successful.

### 5.3 Empirical Models of Capture

A model capable of predicting HGMS performance from readily obtainable test data would be invaluable as an initial guide to applicability of this separation technique. This was the main purpose in developing the empirical models of capture.

Empirical models of HGMS were developed for both the constant head and drainage modes of operation. In both cases the regression analysis set the  $HM_w$  exponent to 1. However, there were considerable differences in the respective exponents for  $k$ ,  $d$ , and  $U$ . These were a result of two major differences existing between the two systems of operation. First, one was operated at a constant velocity while the other was not, and second, an expanded metal matrix was employed in the constant head system and steel wool matrix in the drainage system. Observations during initial tests with the permanent magnet and a glass matrix canister indicated that when the column was allowed to drain, the accompanying interfacial tension at the air-water boundary tended to drag out particles from the matrix. This added force would preferentially remove physically entrained and weakly magnetically held particles, a useful advantage if attempting to produce a clean mags product. For this reason operation in the drainage mode was examined.

The major difference between the two matrix types employed was in their cross sectional area. The expanded metal matrix had an average equivalent diameter an order of magnitude greater than that of the steel wool, which meant that higher field gradients were created with the steel wool matrix. The cross section of the expanded metal was also very uniform in comparison to that of the steel wool.

Finally, the axis of the expanded metal wire was nearly always perpendicular to the direction of background magnetic field, while the orientation of the steel wool was random.

### 5.3.1 Form of the Models

The form of the empirical models and the values of the parameter exponents are worthy of discussion. A stepwise linear regression using the data from all the tests yields a relationship between the dependent and independent parameters. In each case, the five independent parameters from the results of about 80 tests were used. With such a large number of variables, a completely reliable regression would require several hundred sets of data. Interpretation of the exact values of the resulting parameter exponents is consequently difficult. The magnitude of the exponents should therefore be discussed only in relative terms.

A computational problem in the regression analysis was the handling of results from tests performed at  $H > 10$  kG. Above  $\sim 10$  kG the matrix has become magnetically saturated and the dependence of  $R_M$  on  $H$  is to the first power of  $H$ , while below 10 kG the dependence should be to the second power (as is assumed in the regression development). However, the simple technique applied to combine in a regression the results of tests above and below 10 kG, as described in Appendix 4, was satisfactory.

Results from tests studying the individual parameters showed a logarithmic dependence of  $R_M$  upon the parameters. This type of relationship is a consequence of feeding many particles to many layers of matrix wire (unlike the situation used to develop the force balance model), which thus introduces the consideration of probability of capture. Any one particle, as it travels through the matrix, may pass close to a wire several times. Since there are millions of particles and, perhaps, millions of capture sites, probability then becomes an important aspect of particle capture.

### 5.3.2 Parameter Effects

#### Field Strength

The parameter effects can be discussed while keeping in mind that their exponents are relative to the  $HM_W$  exponent of 1. As the  $HM_W$  exponent was set to 1, comment on the effect of H is difficult. However, the assumption of  $M_W$  reaching saturation at 10 kG appears to be satisfactory.

#### Particle Size

The effect of particle size was observed to be considerable in the constant head system and less so with the drainage system. This difference in its degree of influence was a result of the differences in matrices as well as the mode of operation. The expanded metal has a fairly constant cross section and consequently produced a relatively narrow range of gradients plus an average diameter that was at least an order of magnitude greater than the particle diameters. Thus a matched system, which would lessen the influence of d upon  $R_M$  (comparing Eqs. (14) and (15)) could not be assumed. However, the steel wool matrix had a wider range of matrix size, giving a wider range of gradients, plus an average matrix diameter which was better matched to the particle size. The result is that closer to optimum gradients would be available for more than a single particle size with the steel wool matrix. An uncertainty in this explanation lies in not knowing what role the particle size plays in the drag produced by the interfacial tension when the water level passes through the matrix in the drainage system.

When a range of particle sizes is fed to an HGMS, a question is whether or not the larger sizes are preferentially recovered in the first segments of the matrix to an extent larger than would be expected from

the empirical model. The results from testing the hematite U/F show that if that is the case, then its effect is not very large. Using the sample size distribution, a simple fractional recovery summation procedure produced good results.

### Susceptibility

Handling of susceptibility in the regression analysis was difficult, although results with the constant head system were good. The drainage system did not give a value for the  $k$  exponent near unity, which the force balance model would predict. The drainage model was also incapable of handling results from tests with field strengths greater than  $\sim 15$  kG. The cause of these problems was not found, although they were probably derived from the drainage mode of operation.

### Velocity and Viscosity

With the constant head system, the effect of velocity was considerably greater than the force balance model would predict. With both systems, viscosity was found to have little or no effect between temperatures of  $5^{\circ}$  and  $40^{\circ}\text{C}$ . Both of these parameter effects indicate, then, that the limiting of the competing force to that of hydrodynamic drag is an over-simplification. In a theoretical analysis of particle capture, other forces should be considered.

### Feed Weight and Matrix Length

Matrix loading, as defined as the ratio of feed weight to matrix weight, can be altered by a feed weight change or a matrix length change. The effects of feed weight and matrix length can therefore be discussed together.

Results from Section 3.2.7 showed that the fractional recovery of a

sample in each segment of a matrix of  $n$  segments was constant. Since the feed to each successive segment decreased, this implied that the fractional recovery was constant for decreasing feed weights. This appears to contradict the matrix loading results, where  $R_M$  increased with decreasing  $L_m$ . Figure (37); however, shows that the recovery of ilmenite increased only slightly with decreasing  $L_m$  when the conditions were set for a recovery of less than 20%. When the conditions were set for higher recoveries there was a considerable effect of feed weight upon recovery. The matrix length tests employed low recoveries, so that the apparent proof of a constant  $R_M$  with  $n$  may be an artifact of choosing low recoveries. When dealing with  $R > 20\%$ , the matrix length correction (Eq. (19)) may possibly be incorrect.

The non-uniformity of the sample may also influence interpretation of the matrix length results. In the tests studying the effect of matrix length (as in the other tests) the hematite sample employed had a narrow particle size and susceptibility range, but, none the less, a finite range. The expected increase of  $R_M$  of each segment as the feed to each segment decreased, may have been counter-balanced by a selective capture in the first matrix segments of the more susceptible and larger particles of the sample. An analogy is the presence in a flotation feed of minerals of the same sulfide that exhibit different rates of flotation. This effect of sample non-uniformity may have been small, but since the individual segment recoveries were only  $\sim 10\%$  (where a 10 to 20% change in recovery is difficult to notice), the effect may have been sufficient to counter-balance the increase of  $R_M$  with decreasing feed weight.

Therefore, a combination of low recoveries in the matrix length tests, and sample non-uniformity, may have caused the apparent proof of

constant  $R_M$  with  $n$ . Results of predicting the effect of matrix length

through the use of Eq. (22) are further discussed in Section 4.4

Two variables that were not investigated were matrix packing density and slurry density. It has been assumed that, within limits, their effects upon  $R_M$  would be negligible. However, both the steel wool packing density and the slurry density employed were very low, so that if tests were performed at much higher densities, their effects should first be examined.

### 5.3.3 Precision of Separation

Precision of separation is an important consideration in any mineral separation technique. An interesting observation from the empirical models of the two systems of operation is that, with respect to susceptibility, separation with the drainage system is more precise than with the constant head system, but with respect to particle size, the constant head system is more precise. As an illustration assume that a feed with a single particle size and containing two paramagnetic minerals is fed to an HGMS under set conditions of  $H$ ,  $U$ , and  $F_m$ . One mineral with susceptibility  $k_1$ , is 90% recovered and the other mineral, with susceptibility  $k_2$ , is 10% recovered. In the drainage system of operation the ratio of  $k_1$  to  $k_2$  would be 14.3, while in the constant head system it would be 83. Appendix 6 gives the calculations of the figures. Thus, in the constant head system,  $k_1$  would have to be 83 times greater than  $k_2$  to produce the separation (90%-10%), while in the drainage system,  $k_1$  would only have to be 14.3 times greater than  $k_2$ . The drainage mode of operation is more precise a separation with respect to  $k$  than is the constant head system.

To illustrate the precision of separation with respect to particle size assume that a feed with a single, narrow susceptibility range, but containing two particle sizes, is fed to an HGMS. The particles with size  $d_1$  are 90% recovered and the particles with size  $d_2$  are 10% recovered. Then, in the constant head system the ratio of  $d_1$  to  $d_2$  is 8.3, while in the drainage system the ratio of  $d_1$  to  $d_2$  is 20. The constant head system is more precise with respect to particle size than is the drainage system.

In any one sample the combined effects of susceptibility and particle size would have to be considered. If a precise separation with respect to susceptibility is desired, which is the usual case in magnetic separation operation, then a relatively narrow particle size will be required. If a wide range of  $d$  is present, and the operating parameters are adjusted for a high recovery of the smallest particle size of the more susceptible material, then the larger particles of the less susceptible material may also have a high recovery. The combination of particle size ranges and susceptibility ranges are, therefore, the limiting factors in precision of separation.

#### 5.4 Matrix Length and the Empirical Model

The empirical model of capture accounted for the effect of matrix loading, as expressed by feed weight. The model, in conjunction with Eq. (22), was also capable of predicting the recovery of a sample when a matrix was employed that had a length different from that used to develop it. The empirical model would first be used to determine the recovery with the matrix length for which the model was developed, at the same time accounting for the effect of feed weight. Having handled the matrix loading effect, the matrix length effect could then be determined with the use of Eq. (22). In this manner, the two effects were computationally separated. The validity of the technique was tested

under several conditions with the shorter expanded metal matrix. The results (Section 4.4) show that the average difference between predicted and measured  $R_T$  for the six tests was only ~5%. This method was therefore capable of handling the effects of matrix length and matrix loading, although the assumption of constant fractional recovery with varying feed weight that was made in developing Eq. (22) does not appear to be totally correct. A firmer understanding of the concept of matrix loading and its effect upon magnetic recovery would be beneficial.

The results clearly show that the effects of doubling the matrix loading through either a doubling of the feed weight, or a halving of the matrix length are not equivalent. As an illustration, assume an  $R_M = 70\%$  has been obtained using the longer expanded metal matrix. If the feed weight was doubled, Eq. (27) shows that an  $R_M = 62\%$  would be expected. If the matrix length was halved, Eq. (22) indicates that an  $R_M = 45\%$  would result. Experimentation confirms these results. The effect of matrix length on  $R_M$  was considerably greater than the effect of feed weight.

### 5.5 Separation Predictions and the Use of the Frantz Isodynamic Separator

The purpose in developing an empirical model of capture was to permit initial predictions of recovery and grade that could be expected from high gradient magnetic separation. Knowing the size distribution of a sample and the magnetic response curve for selected size intervals, the magnetic recovery could be predicted for any set of operating conditions. Applications of the model to pyrrhotite removal from tin and copper concentrates demonstrated the methodology.

The methodology of mineral separation prediction produced results reasonably close to the measured values, even though several assumptions were required.

A single response curve was used to describe the whole sample, while each size interval may have had (and generally does have) a unique response curve. Response curves for each size interval can be obtained and used, which would provide further accuracy of prediction.

Another problem is the choice of the value of  $L_m$ . Results from separations of the mixtures of  $Fe_2O_3$  and  $SiO_2$  (Figure 53) showed that  $L_m$  can be described by the amount of magnetically recoverable material. However, the susceptibility difference between  $Fe_2O_3$  and  $SiO_2$  is great. If a range of susceptibility is present in the sample, as with the copper and tin concentrates, then the choice of  $L_m$  becomes more subjective, and has to be set to the expected weight recovery. Test 5 of the copper concentrate separations showed, though, that the effect of marginal change in  $L_m$  will not greatly affect the predicted  $L_m$ .

A final source of error in the model applications was that the model limits of particle size and susceptibility were slightly extended.

The Frantz Isodynamic Separator was found to be a very useful device in predicting separation metallurgy from HGMS. Its use in describing the range of magnetic susceptibility of a sample has already been discussed. The metallurgy from a Frantz Separation can be an initial estimate of metallurgy from a high gradient separation that produces an approximately similar weight recovery as that on the Frantz, provided the effects of  $k$  and  $d$  ranges and physical entrainment have been accounted for.

A limitation in the use of the Frantz is particle size. Generally, the Frantz is incapable of handling particles less than  $\sim 20 \mu m$ . The response curves of these sizes would have to be approximated by the coarser fractions.

In summary, the methodology of prediction that has been developed is capable, with sufficient information, of handling very complex mineral samples. A sample with a wide susceptibility range and a wide size distribution can be broken down into manageable intervals of  $k$  and  $d$ , to which the empirical model of particle capture can then be applied. The model and the methodology of prediction should find many applications in the field of mineral processing.

CHAPTER 6

CONCLUSIONS

AND

FUTURE WORK

## 6.1 Conclusions

1. Qualitatively, the force balance model is marginally successful as a description of particle capture in a high gradient magnetic separator. Quantitatively, the force balance model fails.
2. Magnetic recovery in a high gradient magnetic separator is a function of the log of the process variables.
3. Field strength, particle susceptibility, particle size, fluid velocity, matrix loading and matrix length all play an important role in magnetic capture. Fluid viscosity appears to have little effect between water temperatures of 5° and 40°C.
4. The susceptibility of a paramagnetic particle when measured with the Frantz Isodynamic Separator will vary with side slope of the Frantz, inferring that measurements with the Frantz may be invalid.
5. The magnetic response of material, i.e. its susceptibility distribution, can be easily and quickly determined with the Frantz. Such sample information is essential for analysing the potential of a sample for high gradient separation.
6. In a constant head system of operation using an expanded metal matrix, the magnetic recovery of a paramagnetic mineral can, within the range of conditions quoted, be predicted by:

$$R_M = - 60.6 + 34.8 \log \left[ \frac{HM_w k^{1.2} d^{2.5}}{U^{1.8} L_m^{0.8}} \right]$$

7. In a drainage mode of operation using a steel wool matrix, magnetic recovery can, within the range of conditions quoted, be predicted for minerals of volume susceptibility between  $5$  and  $8 \times 10^{-4}$  emu/cm<sup>3</sup> - 0e by:

$$R_M = - 137.4 + 41.3 \log \left[ \frac{HM_w k^{3.9} d^{1.6}}{U^{1.3} L_m^{1.1}} \right]$$

The accuracy of an equation of this type becomes considerably poorer for a wider range in k.

8. If  $R_{Mx}$  represents the magnetic recovery of a mineral using the matrix length for which the model was developed, then  $R_{My}$ , the recovery at a different matrix length, can be predicted by:

$$R_{My} = (1 - R_{Mx})^{y/x}$$

where  $y/x$  is the ratio of the two matrix lengths (or weights).

Although the experimental applications of this equation are successful, its theoretical development is apparently unsound.

9. Matrix loading can be altered by altering either the feed weight or the matrix length. A doubling of the feed weight in order to double the matrix loading will not produce the same effect upon  $R_M$  as a halving of the matrix length.
10. The precision of a separation by high gradient magnetic separation will be a function of the range of particle size and susceptibility present within the sample. The constant head system is more precise a separation with respect to particle size than the drainage system is, while the drainage system is more precise with respect to susceptibility.

11. Through a simple summation procedure, a wide particle size distribution can be handled by the empirical models. The size distribution is split into several intervals and  $R_M$  calculated for each  $d$ . The product of the weight distribution to each size interval and its respective  $R_M$  yields a fractional recovery for each interval. Hence, the total recovery is the sum of the fractional recoveries.
12. The developed methodology of predicting HGMS performance is capable of handling very complex mineral samples. The important information necessary for its application are the particle size distribution and the susceptibility distribution, in the form of a magnetic response curve obtained from the Frantz. Assays of elements or minerals as distributed in the particle size and susceptibility intervals will generally be necessary for prediction of elemental or mineral recoveries.
13. The metallurgy from a separation on the Frantz Isodynamic Separator can be an initial estimate of metallurgy from an HGMS that produces an approximately similar weight recovery as that on the Frantz. To make such an estimate the effects of wide  $k$  and  $d$  ranges, and physical entrainment should be accounted for.

## 6.2 Claims for Original Research

1. Paramagnetic minerals were prepared to very narrow particle size and susceptibility ranges, and the effects of d and k were examined.
2. Empirical models of particle capture in a high gradient magnetic separator were developed for two systems of operation. Parameters included in the models were field strength, susceptibility, particle size, velocity, and feed weight. The effect of matrix length was also experimentally determined.
3. A methodology of predicting high gradient magnetic separation performance was developed and demonstrated.

### 6.3 Suggestions for Future Work

1. Susceptibility of the uni-mineral samples should be determined with a conventional measurement technique to verify and calibrate the measurements made on the Frantz.
2. The effect of particle size and grinding media upon particle susceptibility as measured on the Frantz should be studied.
3. The empirical models should be developed to wider ranges of  $d$ ,  $k$  and  $U$ .
4. The feed weight and matrix length affects require further examination.
5. An empirical model for the constant head system employing the steel wool matrix should be developed to compare the effects of the two matrices. This would also enable a direct comparison of the drainage and constant head systems of operation.
6. Application of the model to various ores, concentrates and tailings could determine the potential of high gradient magnetic separation and its range of feasible applications.

APPENDIX 1Effect of Matrix Length

Conditions - the matrix is divided into n layers, each of similar weight and length.

- fractional recovery of feed to first layer =  $R_{M1}$

Assumption - fractional recovery to layer n is  $R_{M1}$  of feed to that layer.

1. Fractional recovery to first layer =  $R_{M1}$

Fraction of feed remaining =  $1 - R_{M1}$

2. Fractional recovery to second layer =  $R_{M1} (1 - R_{M1})$

Fraction of feed remaining =  $(1 - R_{M1}) - R_{M1} (1 - R_{M1})$   
 $= (1 - R_{M1})^2$

and, total recovery with 2 layers =  $1 - (1 - R_{M1})^2$

3. Fractional recovery to third layer =  $R_{M1} (1 - R_{M1})^2$

Fraction of feed remaining =  $(1 - R_{M1})^2 - R_{M1} (1 - R_{M1})^2$   
 $= (1 - R_{M1})^3$

Thus, total recovery with n layers is,

$$R_{Mn} = 1 - (1 - R_{M1})^n$$

Now, let  $n = x$ , where x is the matrix weight for n layers.

$$R_{Mx} = 1 - (1 - R_{M1})^x$$

$$1 - R_{Mx} = (1 - R_{M1})^x$$

$$R_{M1} = 1 - (1 - R_{Mx})^{1/x}$$

$R_{My}$  for a matrix of weight  $y$  is given by:

$$R_{My} = 1 - (1 - R_{M1})^y.$$

Thus,

$$R_{My} = 1 - (1 - 1 + (1 - R_{Mx})^{1/x})^y$$

$$R_{My} = 1 - (1 - R_{Mx})^{y/x}.$$

APPENDIX 2

Cross-Sectional diagram of helium dewar



APPENDIX 3

TABLE 3-1

Data from Constant Head System Tests

TABLE 3-2

Data from Drainage System Tests

CONSTANT HEAD SYSTEM

<u>Test#</u>	$k \times 10^4$ $\left(\frac{\text{emu}}{\text{cm}^2 \cdot \text{Oe}}\right)$	<u>H</u> (kG)	<u>d</u> ( $\mu\text{m}$ )	<u>U</u> $\left(\frac{\text{cm}}{\text{sec}}\right)$	<u>L</u> <u>m</u>	<u>R<sub>M</sub></u> (%)
1.000	3.000	1.000	30.000	9.900	0.330	66.000
2.000	3.000	1.000	22.000	9.900	0.330	52.000
3.000	3.000	1.000	16.000	9.900	0.330	36.000
4.000	3.000	1.000	12.000	9.900	0.330	24.000
5.000	3.000	1.000	8.500	9.900	0.330	15.000
6.000	3.000	0.500	30.000	9.900	0.330	37.000
7.000	3.000	0.500	22.000	9.900	0.330	26.000
8.000	3.000	0.500	16.000	9.900	0.330	16.000
9.000	3.000	0.500	12.000	9.900	0.330	12.000
10.000	3.000	2.000	30.000	9.900	0.330	83.000
11.000	3.000	2.000	22.000	9.900	0.330	73.000
12.000	3.000	2.000	12.000	9.900	0.330	40.000
13.000	3.000	3.100	30.000	9.900	0.330	93.000
14.000	3.000	3.100	22.000	9.900	0.330	85.000
15.000	3.000	3.000	16.000	9.900	0.330	68.000
16.000	3.000	3.100	12.000	9.900	0.330	53.000
17.000	3.000	3.000	8.500	9.900	0.330	38.000
18.000	3.000	4.000	22.000	9.900	0.330	92.000
19.000	3.000	3.000	12.000	9.900	0.330	75.000
20.000	3.000	3.000	8.500	9.900	0.330	61.000
21.000	3.000	3.000	16.000	9.900	0.330	94.000
22.000	3.000	1.100	30.000	5.700	0.330	78.000
23.000	3.000	1.400	16.000	5.700	0.330	48.000
24.000	3.000	3.000	30.000	5.700	0.330	98.000
25.000	3.000	3.000	16.000	5.700	0.330	78.000
26.000	3.000	1.100	22.000	15.600	0.330	28.000
27.000	3.000	5.100	12.000	15.600	0.330	57.000
28.000	5.000	1.800	21.000	2.900	0.330	66.000
29.000	5.000	0.400	21.000	2.900	0.330	30.000
30.000	5.000	1.400	21.000	2.900	0.330	85.000
31.000	5.000	2.000	21.000	5.700	0.330	83.000
32.000	5.000	0.300	21.000	5.700	0.330	35.000
33.000	5.000	0.500	21.000	5.700	0.330	20.000
34.000	5.000	1.100	21.000	5.700	0.330	61.000
35.000	5.000	2.800	21.000	5.700	0.330	92.000
36.000	5.000	3.000	21.000	9.900	0.330	86.000
37.000	5.000	3.000	21.000	9.900	0.330	85.000
38.000	5.000	1.900	21.000	9.900	0.330	68.000
39.000	5.000	2.000	21.000	9.900	0.330	67.000
40.000	5.000	0.500	21.000	9.900	0.330	9.000

TABLE 3-1 (cont'd)

<u>Test#</u>	<u>k</u>	<u>H</u>	<u>d</u>	<u>U</u>	<u>L<sub>m</sub></u>	<u>R<sub>M</sub></u>
41.000	5.000	1.000	21.000	9.900	0.330	39.000
42.000	5.000	1.100	21.000	9.900	0.330	35.000
43.000	5.000	0.900	21.000	9.900	0.330	30.000
44.000	5.000	4.200	21.000	9.900	0.330	94.000
45.000	5.000	5.000	21.000	9.900	0.330	96.000
46.000	5.000	6.000	21.000	9.900	0.330	97.000
47.000	5.000	8.000	21.000	9.900	0.330	99.000
48.000	5.000	0.500	21.000	15.000	0.330	1.000
49.000	5.000	1.000	21.000	15.000	0.330	14.000
50.000	5.000	2.000	21.000	15.000	0.330	39.000
51.000	5.000	3.000	21.000	15.000	0.330	66.000
52.000	5.000	1.900	11.000	5.700	0.330	55.000
53.000	5.600	1.000	35.000	5.700	0.330	79.000
54.000	5.600	1.100	21.000	5.700	0.083	74.000
55.000	5.600	1.100	21.000	5.700	0.500	52.000
56.000	5.600	1.100	21.000	9.900	0.500	30.000
57.000	5.600	1.100	21.000	9.900	1.000	19.000
58.000	5.000	1.100	21.000	9.900	0.167	45.000
59.000	5.600	1.100	21.000	9.900	0.082	51.000
60.000	5.600	1.100	35.000	9.900	0.500	37.000
61.000	5.600	1.100	35.000	9.900	0.082	71.000
62.000	5.600	1.100	35.000	9.900	0.330	50.000
63.000	5.000	2.000	21.000	9.900	0.500	56.000
64.000	5.600	2.000	21.000	9.900	0.167	73.000
65.000	5.600	2.000	21.000	9.900	0.083	33.000
66.000	5.000	2.000	21.000	9.900	1.000	35.000
67.000	5.600	1.100	35.000	9.900	0.167	64.000
68.000	5.000	1.100	11.000	9.900	0.083	21.000
69.000	5.600	1.100	11.000	9.900	0.500	13.000
70.000	5.600	1.100	11.000	9.900	0.167	20.000
71.000	5.600	1.100	11.000	9.900	0.330	16.000
72.000	5.000	0.500	11.000	15.000	0.330	1.000
73.000	8.000	0.500	12.000	15.000	0.330	3.000
74.000	0.340	1.100	22.000	9.900	0.330	2.500
75.000	0.340	10.000	36.000	9.900	0.330	65.000
76.000	0.340	10.000	22.000	9.900	0.330	54.000

TABLE 3-1 (cont'd)

<u>Test#</u>	<u>k</u>	<u>H</u>	<u>d</u>	<u>U</u>	<u>L<sub>m</sub></u>	<u>R<sub>M</sub></u>
77.000	0.340	10.000	12.000	9.900	0.330	38.000
78.000	0.340	20.000	22.000	9.900	0.330	69.000
79.000	0.340	14.700	36.000	5.700	0.380	90.000
80.000	0.340	14.800	12.000	5.700	0.230	61.000
81.000	0.340	12.500	22.000	2.900	0.220	90.000
82.000	0.340	20.000	36.000	5.700	0.220	92.000
83.000	0.240	20.000	22.000	2.900	0.330	95.000
84.000	0.340	5.000	12.000	9.900	0.330	19.000
85.000	0.340	7.800	22.000	2.900	0.330	33.000
86.000	0.250	15.000	22.000	5.700	0.330	76.000
87.000	0.250	20.000	22.000	5.700	0.330	70.000
88.000	0.250	10.000	22.000	5.700	0.330	70.000
89.000	0.250	10.000	36.000	5.700	0.330	73.000
90.000	0.250	10.000	12.000	5.700	0.330	42.000
91.000	0.250	20.000	22.000	2.900	0.330	90.000
92.000	0.250	10.000	22.000	5.700	0.083	84.000
93.000	0.250	10.000	22.000	5.700	0.167	76.000
94.000	0.250	1.100	22.000	9.900	0.330	3.000
95.000	0.250	5.000	12.000	9.900	0.330	25.000
96.000	0.250	5.000	12.000	9.900	0.330	18.000

TABLE 3-1 (cont'd)

ZERO FIELD TESTS

<u>Test#</u>	<u>k</u>	<u>H</u>	<u>d</u>	<u>U</u>	<u>L<sub>m</sub></u>	<u>R<sub>M</sub></u>
97.000	5.600	0.0	21.000	5.700	0.670	2.200
98.000	5.600	0.0	11.000	5.700	0.083	1.800
99.000	5.600	0.0	11.000	5.700	0.500	0.700
100.000	5.600	0.0	21.000	9.900	0.083	2.100
101.000	5.600	0.0	21.000	9.900	0.330	1.200
102.000	5.600	0.0	21.000	9.900	0.670	0.900
103.000	5.600	0.0	44.000	9.900	0.330	2.400
104.000	5.600	0.0	21.000	9.900	0.330	0.800
105.000	5.600	0.0	44.000	15.600	0.330	1.200
106.000	5.600	0.0	11.000	2.900	0.330	4.100
107.000	5.600	0.0	44.000	2.900	0.330	12.600
108.000	5.600	0.0	21.000	2.900	0.330	7.000
109.000	5.600	0.0	21.000	2.900	0.670	7.500
110.000	5.600	0.0	21.000	2.900	0.083	14.900
111.000	5.600	0.0	44.000	5.700	0.330	7.500
112.000	5.600	0.0	21.000	5.700	0.330	2.500
113.000	5.600	0.0	21.000	5.700	0.083	3.300
114.000	5.600	0.0	21.000	5.700	0.500	2.700
115.000	8.000	0.0	12.000	5.700	0.330	1.600
116.000	8.000	0.0	16.000	5.700	0.330	1.700
117.000	8.000	0.0	30.000	5.700	0.330	5.000
118.000	8.000	0.0	30.000	5.700	0.330	4.900
119.000	8.000	0.0	22.000	5.700	0.230	3.500
120.000	8.000	0.0	U/F*	9.900	0.330	4.600
121.000	0.030	0.0	45.000	5.700	0.330	2.500
122.000	0.030	0.0	12.000	5.700	0.330	0.200
123.000	0.030	0.0	45.000	5.700	0.330	2.700
124.000	0.030	0.0	32.000	9.900	0.167	0.700
125.000	0.030	0.0	32.000	9.900	0.083	1.300
126.000	0.030	0.0	32.000	9.900	0.330	1.000
127.000	0.030	0.0	32.000	9.900	0.670	0.600
128.000	0.030	0.0	42.000	9.900	0.330	2.200
129.000	0.030	0.0	42.000	9.900	0.330	2.400
130.000	0.030	0.0	23.000	9.900	0.330	0.500
131.000	0.030	0.0	17.000	9.900	0.330	0.100

\* cyclone underflow

TABLE 3-2DRAINAGE SYSTEM

<u>Test#</u>	<u>k</u>	<u>H</u>	<u>d</u>	<u>U</u>	<u>L<sub>M</sub></u>	<u>R<sub>M</sub></u>
1.000	8.000	0.500	16.000	10.000	0.670	22.000
2.000	8.000	1.100	16.000	10.000	0.670	51.000
3.000	8.000	2.000	16.000	10.000	0.670	70.000
4.000	3.000	3.100	16.000	10.000	0.670	81.000
5.000	8.000	4.000	16.000	10.000	0.670	90.000
6.000	8.000	1.000	22.000	10.000	0.670	62.000
7.000	8.000	3.300	22.000	10.000	0.670	90.000
8.000	8.000	1.000	30.000	10.000	0.670	67.000
9.000	8.000	1.900	30.000	10.000	0.670	84.000
10.000	8.000	1.000	12.000	10.000	0.670	38.000
11.000	8.000	3.400	12.000	10.000	0.670	70.000
12.000	8.000	3.400	8.500	10.000	0.670	56.000
13.000	8.000	1.300	16.000	10.000	0.670	57.000
14.000	8.000	1.300	12.000	10.000	0.670	38.000
15.000	5.600	0.400	21.000	2.000	0.670	8.000
16.000	5.600	0.500	21.000	2.000	0.670	33.000
17.000	5.600	1.600	21.000	2.000	0.670	78.000
18.000	5.600	1.500	21.000	6.000	0.670	55.000
19.000	5.600	1.500	21.000	6.000	0.670	49.000
20.000	5.600	1.500	21.000	6.000	0.670	58.000
21.000	5.600	1.300	21.000	6.000	0.670	55.000
22.000	5.600	0.600	21.000	6.000	0.670	5.000
23.000	5.600	1.000	21.000	6.000	2.000	10.000
24.000	5.600	1.000	21.000	6.000	1.000	36.000
25.000	5.600	1.000	21.000	6.000	0.330	50.000
26.000	5.600	0.800	21.000	10.000	0.670	15.000
27.000	5.600	1.500	21.000	10.000	0.670	31.000
28.000	5.600	2.100	21.000	10.000	0.670	55.000
29.000	5.600	2.700	21.000	10.000	0.670	71.000
30.000	5.600	4.000	21.000	10.000	0.670	88.000
31.000	5.600	1.000	21.000	10.000	0.670	21.000
32.000	5.600	2.000	21.000	10.000	0.670	42.000
33.000	5.600	2.000	21.000	10.000	0.670	41.000
34.000	5.600	4.000	21.000	10.000	0.670	85.000

TABLE 3-2 (cont'd)

Test#	k	H	d	U	$L_m$	$R_M$
35.000	5.600	0.800	49.000	10.000	0.670	21.000
36.000	5.600	0.800	44.000	10.000	0.670	25.000
37.000	5.600	0.800	11.000	10.000	0.670	10.000
38.000	5.600	3.100	49.000	10.000	0.670	88.000
39.000	5.600	3.100	44.000	10.000	0.670	87.000
40.000	5.600	4.400	11.000	10.000	0.670	60.000
41.000	5.600	4.400	11.000	10.000	0.670	63.000
42.000	5.600	2.000	11.000	10.000	0.670	26.000
43.000	5.600	2.000	11.000	10.000	0.330	40.000
44.000	5.600	2.000	11.000	10.000	1.000	18.000
45.000	5.600	0.900	21.000	10.000	2.000	9.000
46.000	5.600	1.900	21.000	10.000	2.000	21.000
47.000	5.600	4.000	21.000	10.000	2.000	50.000
48.000	5.600	4.000	21.000	10.000	1.000	70.000
49.000	5.600	2.000	21.000	10.000	1.000	30.000
50.000	5.600	1.000	21.000	10.000	1.000	14.000
51.000	5.600	4.000	21.000	10.000	0.330	92.000
52.000	5.600	2.000	21.000	10.000	0.330	66.000
53.000	5.600	1.000	21.000	10.000	0.330	40.000
54.000	5.600	1.000	21.000	10.000	0.167	51.000
55.000	5.600	4.000	21.000	10.000	0.167	94.000
56.000	5.600	2.000	21.000	10.000	0.167	79.000
57.000	5.600	2.600	21.000	16.000	0.670	41.000
58.000	5.600	4.100	21.000	16.000	0.670	62.000
59.000	5.600	3.400	21.000	22.000	0.670	44.000
60.000	5.600	7.300	21.000	22.000	0.670	80.000
61.000	0.250	6.700	22.000	2.000	0.670	53.000
62.000	0.250	13.000	22.000	2.000	0.670	80.000
63.000	0.250	4.000	22.000	2.000	0.670	36.000
64.000	0.250	10.000	22.000	2.000	0.670	72.000
65.000	0.250	10.000	12.000	4.000	0.670	26.000
66.000	0.250	10.000	36.000	4.000	0.670	49.000
67.000	0.250	20.000	22.000	4.000	0.670	92.000
68.000	0.250	20.000	22.000	6.000	0.670	78.000
69.000	0.250	20.000	22.000	6.000	0.670	84.000
70.000	0.250	20.000	12.000	6.000	0.670	54.000
71.000	0.250	20.000	22.000	10.000	0.670	68.000
72.000	0.250	20.000	36.000	10.000	0.670	70.000
73.000	0.340	2.000	22.000	2.000	0.670	14.000
74.000	0.340	6.500	22.000	2.000	0.670	46.000
75.000	0.340	6.500	36.000	2.000	0.670	50.000
76.000	0.340	6.500	12.000	2.000	0.670	41.000
77.000	0.340	10.000	22.000	4.000	0.670	54.000
78.000	0.340	10.000	12.000	4.000	0.670	32.000
79.000	0.340	10.000	36.000	4.000	0.670	70.000
80.000	0.340	5.000	22.000	4.000	0.670	19.000

TABLE 3-2(cont'd)ZERO FIELD TESTS

<u>Test#</u>	<u>k</u>	<u>H</u>	<u>d</u>	<u>U</u>	<u>L<sub>m</sub></u>	<u>R<sub>M</sub></u>
81.000	5.600	0.0	40.000	10.000	0.670	6.500
82.000	5.600	0.0	35.000	10.000	0.670	5.300
83.000	5.600	0.0	11.000	10.000	0.670	2.100
84.000	5.000	0.0	21.000	10.000	0.670	4.300
85.000	5.600	0.0	21.000	10.000	0.670	3.200
86.000	5.600	0.0	21.000	2.000	0.670	16.900
87.000	5.600	0.0	21.000	6.000	0.670	7.200
88.000	5.600	0.0	21.000	16.000	0.670	3.400
89.000	5.600	0.0	21.000	22.000	0.670	2.300
90.000	5.600	0.0	21.000	10.000	0.330	5.400
91.000	5.600	0.0	21.000	10.000	1.000	3.400
92.000	5.600	0.0	21.000	10.000	2.000	2.800
93.000	0.340	0.0	36.000	2.000	0.670	19.000
94.000	0.340	0.0	22.000	2.000	0.670	12.800
95.000	0.340	0.0	12.000	2.000	0.670	8.700
96.000	0.340	0.0	22.000	6.000	0.670	5.900

APPENDIX 4Step-wise Multiple Regression of DataI. Constant Head System

If  $H < 10\text{kG}$ , magnetic recovery may be expressed by:

$$R_M = A + B \log [H^a k^b d^c U^e L_m^f]$$

or

$$R_M = A + B [a \log H + b \log k + c \log d + e \log U + f \log L_m]$$

A step-wise regression was performed where the dependent variable was  $R_M$  and the independent variables were  $\log H$ ,  $\log k$ ,  $\log d$ ,  $\log U$  and  $\log L_m$ . The respective variable coefficients that were determined from the regression were therefore equal to  $aB$ ,  $bB$ ,  $cB$ ,  $eB$  and  $fB$ .

The data from 58 hematite and ilmenite tests is given in Table 4-1.

The range of conditions was:  $0.4 \leq H \leq 8.0 \text{ kG}$ ;  $5.6 \leq k \leq 8.0 \times 10^{-4} \text{ emu/cm}^3\text{-0e}$ ;

$8.5 \leq d \leq 40 \text{ } \mu\text{m}$ ;  $2.9 \leq U \leq 15.6 \text{ cm/sec}$ ;  $0.083 \leq L_m \leq 1.0$ ; and  $12\% \leq R_M \leq 86\%$ .

The resulting coefficients were:

$$H: aB = 72.04$$

$$k: bB = 56.45$$

$$d: cB = 91.78$$

$$U: eB = -64.05$$

$$L_m: fB = -30.34$$

$$A = -78.43$$

The value of  $a$  (the  $H$  exponent) was set to 2. Therefore,  $B = 36.02$

and

$$b = 1.6$$

$$c = 2.5$$

$$e = -1.8$$

$$f = -0.8$$

Thus,

$$R_M = -78.43 + 36.02 \log \left[ \frac{H^2 k^{1.6} d^{2.5}}{U^{1.8} L_m^{0.8}} \right]$$

Standard Error of Estimate = 7.53.

Inclusion of data from tests using  $H > 10$  kG in the same regression was difficult, because above  $\sim 10$  kG,  $M_w$  becomes saturated, so that the  $H$  exponent can no longer be set to 2. The  $k$  of chalcopyrite and sphalerite was considerably different from the  $k$  of hematite and ilmenite. A regression was therefore performed on the chalcopyrite and sphalerite data, using the results from the previous regression, to determine if the  $k$  exponent would vary to a great extent with the inclusion of  $\text{CuFeS}_2 - (\text{Zn, Fe})\text{S}$  data with the  $\text{Fe}_2\text{O}_3 - \text{FeTiO}_3$  data.

The independent variables were  $\log \left[ \frac{HM_w d^{2.5}}{U^{1.8} L_m^{0.8}} \right]$  and  $\log k$ . Data

from 13 chalcopyrite and sphalerite tests is shown in Table 4-2. The range of conditions was:  $10 \leq H \leq 20$  kG;  $0.25 \leq k \leq 0.34 \times 10^{-4}$  emu/cm<sup>3</sup>-0e;  $12 \leq d \leq 36$   $\mu\text{m}$ ;  $2.9 \leq U \leq 9.9$  cm/sec;  $L_m = 0.33$ ; and  $38 \leq R_M \leq 90\%$ . The result of the regression was:

$$R_M = -48.67 + 28.78 \log \left[ \frac{HM_w k^{0.8} d^{2.5}}{U^{1.8} L_m^{0.8}} \right]$$

Standard Error of Estimate was 5.00.

Thus,  $k$  exponents of 1.6 and 0.8 had been obtained for the two

regressions. A compromise of 1.2 was chosen and a linear regression was performed using all the data (above and below 10kG) with variable 1 =  $R_M$  and variable 2 =  $\log \left[ \frac{HM_w k^{1.2} d^{2.5}}{U^{1.8} L_m^{0.8}} \right]$ . The data is shown in

Table 4-3 for the 71 tests. The range of conditions was:  $0.4 \leq H \leq 20\text{kG}$ ;  $0.25 \leq k \leq 8.0 \times 10^{-4} \text{ emu/cm}^3\text{-0e}$ ;  $8.5 \leq d \leq 40 \mu\text{m}$ ;  $2.9 \leq U \leq 15.6 \text{ cm/sec}$ ;  $0.083 \leq L_m \leq 1.0$ ; and  $12 \leq R_M \leq 90\%$ . Resulting regression equation was:

$$R_M = -60.60 + 34.76 \log \left[ \frac{HM_w k^{1.2} d^{2.5}}{U^{1.8} L_m^{0.8}} \right]$$

with a Standard Error of Estimate of 6.95.

## II. Drainage System

A similar type of regression analysis was performed on the data obtained from the drainage system tests. The results from 61 hematite and ilmenite tests at  $H < 10\text{kG}$  were used in a step-wise regression. The data is given in Table 4-4. Range of conditions of the data was:  $0.4 \leq H \leq 7.3\text{kG}$ ;  $5.6 \leq k \leq 8.0 \times 10^{-4} \text{ emu/cm}^3\text{-0e}$ ;  $8.5 \leq d \leq 49 \mu\text{m}$ ;  $2 \leq U \leq 22 \text{ cm/sec}$ ;  $0.167 \leq L_m \leq 2.0$ ; and  $9 \leq R_M \leq 95\%$ .

The resulting coefficients were:

H:	aB	=	83.92
k:	bB	=	165.47
d:	cB	=	65.79
U:	eB	=	-53.26
$L_m$ :	fB	=	-45.13
	A	=	-140.81

The value of a (the H exponent) was set to 2. Therefore,  $B = 41.96$

$$b = 3.9$$

$$c = 1.6$$

$$e = -1.3$$

$$f = -1.1$$

Thus,

$$R_M = -140.81 + 41.96 \log \left[ \frac{H^2 k^{3.9} d^{1.6}}{U^{1.3} L_m^{1.1}} \right]$$

Standard Error of Estimate = 8.36.

Again, inclusion of data from tests using  $H > 10\text{kG}$  in the same regression was difficult. The results were used, therefore, to roughly determine if the k exponent would vary to a great extent with the inclusion of the  $\text{CuFeS}_2$  -  $(\text{Zn,Fe})\text{S}$  data. A step-wise regression was performed using data from the chalcopyrite, sphalerite and hematite tests and about half of the ilmenite tests.

The two independent variables were  $\log \left[ \frac{HM_w d^{1.6}}{U^{1.3} L_m^{1.1}} \right]$  and  $\log k$ .

Data from 49 tests, given in Table 4-5, had the following range of conditions:  $0.4 \leq H \leq 13 \text{ kG}$ ;  $0.25 \leq k \leq 8.0 \times 10^{-4} \text{ emu/cm}^3\text{-Oe}$ ;  $8.5 \leq d \leq 49 \text{ }\mu\text{m}$ ;  $2 \leq U \leq 22 \text{ cm/sec}$ ;  $L_m = 0.67$ ; and  $10 \leq R_M \leq 90\%$ . Tests with H greater than  $\sim 15\text{kG}$  could not be included with unacceptable distortion of the results. The resulting regression was:

$$R_M = -52.76 + 36.7 \log \left[ \frac{H^2 k^{1.8} d^{1.6}}{U^{1.3} L_m^{1.1}} \right]$$

Standard Error of Estimate = 11.32.

Thus the addition of chalcopyrite and sphalerite data changed the k exponent from 3.9 to 1.8 and increased the error of estimate from

8.4 to 11.3

Two linear regressions were therefore done - one on the regression results from all the data, and the second on the regression results from just the hematite and ilmenite data.

The variables used to develop an expression for all the data were

$R_M$  and  $\log \left[ \frac{HM_w k^{1.8} d^{1.6}}{U^{1.3} L_m^{1.1}} \right]$ . The data is shown in Table 4-6 for 71

tests. The range of conditions was:  $0.4 \leq H \leq 13$  kG;  $0.25 \leq k \leq 8.0 \times 10^{-4}$  emu/cm<sup>3</sup>-0e;  $8.5 \leq d \leq 49$   $\mu$ m;  $2 \leq U \leq 22$  cm/sec;  $0.167 \leq L_m \leq 2.0$ ; and  $9 \leq R_M \leq 95\%$ . Resulting regression equation was:

$$R_M = -58.9 + 38.3 \log \left[ \frac{HM_w k^{1.8} d^{1.6}}{U^{1.3} L_m^{1.1}} \right]$$

Standard Error of Estimate = 9.7.

The variables used to develop an expression for just the hematite

and ilmenite data were  $R_M$  and  $\log \left[ \frac{HM_w k^{3.9} d^{1.6}}{U^{1.3} L_m^{1.1}} \right]$ . The data for 59

hematite and ilmenite tests is shown in Table 4-7. The range of

conditions was:  $0.4 \leq H \leq 7.3$  kG;  $5.6 \leq k \leq 8.0 \times 10^{-4}$  emu/cm<sup>3</sup>-0e;

$8.5 \leq d \leq 49$   $\mu$ m;  $2 \leq U \leq 22$  cm/sec;  $0.167 \leq L_m \leq 2.0$ ; and  $9 \leq R_M \leq 95\%$ .

The resulting equation was:

$$R_M = -137.4 + 41.3 \log \left[ \frac{HM_w k^{3.9} d^{1.6}}{U^{1.3} L_m^{1.1}} \right]$$

Standard Error of Estimate = 6.5.

Table 4-1

Step-wise Regression Data - Hematite and Ilmenite-Constant Head System.

Table 4-2

Sphalerite and Chalcopyrite Data - Constant Head System

Table 4-3

Linear Regression - Constant Head System

Table 4-4

Step-wise Regression Data - Hematite and Ilmenite-Drainage System.

Table 4-5

Step-wise Regression - Data From All Four Samples-Drainage System.

Table 4-6

Linear Regression - All Data-Drainage System

Table 4-7

Linear Regression } Hematite and Ilmenite Data Only-Drainage System

TABLE 4-1

$R_M$	$\log H$	$\log k$	$\log d$	$\log U$	$\log L_m$
83.000	0.300	0.750	1.320	0.760	-0.490
35.000	-0.100	0.750	1.320	0.760	-0.490
55.000	0.280	0.750	1.040	0.760	-0.480
79.000	0.0	0.750	1.600	0.760	-0.480
66.000	0.0	0.750	1.320	0.460	-0.490
86.000	0.480	0.750	1.320	1.000	-0.480
68.000	0.280	0.750	1.320	1.000	-0.480
30.000	-0.400	0.750	1.320	0.460	-0.480
95.000	0.150	0.750	1.320	0.460	-0.480
20.000	-0.300	0.750	1.320	0.760	-0.460
39.000	0.0	0.750	1.320	1.000	-0.490
14.000	0.0	0.750	1.320	1.190	-0.490
39.000	0.390	0.750	1.320	1.190	-0.490
66.000	0.480	0.750	1.320	1.190	-0.490
61.000	0.040	0.750	1.320	0.760	-0.490
74.000	0.040	0.750	1.320	0.760	-1.080
52.000	0.040	0.750	1.320	0.760	-0.300
35.000	0.040	0.750	1.320	1.000	-0.480
30.000	0.040	0.750	1.320	1.000	-0.300
19.000	0.040	0.750	1.320	1.000	0.0
45.000	0.040	0.750	1.320	1.000	-0.790
50.000	0.040	0.750	1.540	1.000	-1.080
39.000	0.040	0.750	1.540	1.000	-0.300
71.000	0.040	0.750	1.540	1.000	-1.080
67.000	0.300	0.750	1.320	1.000	-0.490
56.000	0.300	0.750	1.320	1.000	-0.300
78.000	0.300	0.750	1.320	1.000	-0.790
82.000	0.300	0.750	1.320	1.000	-1.090
35.000	0.300	0.750	1.320	1.000	0.0
64.000	0.040	0.750	1.540	1.000	-0.790
21.000	0.040	0.750	1.040	1.000	-1.090
16.000	0.040	0.750	1.040	1.000	-0.480
13.000	0.040	0.750	1.040	1.000	-0.300
20.000	0.040	0.750	1.040	1.000	-0.790
66.000	0.0	0.900	1.480	1.000	-0.490
53.000	0.0	0.900	1.340	1.000	-0.490
36.000	0.0	0.900	1.200	1.000	-0.490
24.000	0.0	0.900	1.090	1.000	-0.490
15.000	0.0	0.900	0.930	1.000	-0.490
37.000	-0.300	0.900	1.480	1.000	-0.480
26.000	-0.300	0.900	1.340	1.000	-0.480
16.000	-0.300	0.900	1.200	1.000	-0.480
12.000	-0.300	0.900	1.080	1.000	-0.490
83.000	0.300	0.900	1.480	1.000	-0.490
73.000	0.300	0.900	1.340	1.000	-0.480
40.000	0.300	0.900	1.080	1.000	-0.480
85.000	0.490	0.900	1.340	1.000	-0.490
53.000	0.490	0.900	1.080	1.000	-0.490
68.000	0.480	0.900	1.200	1.000	-0.490
38.000	0.480	0.900	0.930	1.000	-0.490
75.000	0.900	0.900	1.080	1.000	-0.480
61.000	0.900	0.900	0.930	1.000	-0.490
78.000	0.040	0.900	1.480	0.760	-0.480
48.000	0.040	0.900	1.200	0.760	-0.480
78.000	0.480	0.900	1.200	0.760	-0.490
28.000	0.040	0.900	1.340	1.190	-0.480
57.000	0.710	0.900	1.080	1.190	-0.480
51.000	0.040	0.750	1.320	1.000	-1.080

TABLE 4-2

$R_M$	$\log \frac{HM_d^{2.5}}{U^{1.8} L^{0.8}}$	$\log k$
65.000	4.558	-0.470
54.000	4.013	-0.470
38.000	3.341	-0.470
69.000	4.314	-0.470
90.000	5.157	-0.470
61.000	3.943	-0.470
90.000	5.070	-0.470
76.000	4.620	-0.600
79.000	4.745	-0.600
70.000	4.444	-0.600
78.000	4.990	-0.600
43.000	3.773	-0.600
90.000	5.274	-0.600

TABLE 4-3

$R_M$	$\log \frac{M_{w,0}^{1.25}}{U_{L,0}^{0.4}}$
93.000	3.827
92.000	3.821
55.000	3.890
79.000	3.924
66.000	3.753
96.000	3.747
69.000	3.250
30.000	2.957
85.000	4.045
20.000	2.622
39.000	2.793
14.000	2.437
39.000	3.025
66.000	3.392
61.000	3.307
74.000	3.739
52.000	3.166
35.000	2.876
30.000	2.725
19.000	2.494
45.000	3.117
50.000	3.430
39.000	3.289
71.000	3.912
67.000	3.395
56.000	3.254
78.000	3.626
92.000	3.877
25.000	3.013
64.000	3.617
21.000	2.655
16.000	2.174
13.000	2.032
20.000	2.414
66.000	3.366
53.000	3.029
36.000	2.684
24.000	2.372
15.000	1.997
37.000	2.764
26.000	2.427
16.000	2.082
12.000	1.769
93.000	3.968
73.000	3.631
40.000	2.973
95.000	4.012
53.000	3.345
69.000	3.638
35.000	2.951
75.000	4.177
61.000	3.941
78.000	3.890
49.000	3.198
78.000	4.069
25.000	2.757
57.000	3.431
51.000	3.357
65.000	3.919
54.000	3.393
39.000	2.725
67.000	3.684
90.000	4.516
61.000	3.327
90.000	4.449
76.000	3.831
77.000	3.956
78.000	4.190
43.000	2.927
90.000	4.484
70.000	3.655

TABLE 4-4

P/1.

$R_M$	$\log H$	$\log k$	$\log d$	$\log U$	$\log L_m$
22.000	-0.300	0.900	1.200	1.000	-0.190
51.000	0.040	0.900	1.200	1.000	-0.190
70.000	0.300	0.900	1.200	1.000	-0.190
81.000	0.400	0.900	1.200	1.000	-0.190
90.000	0.590	0.900	1.200	1.000	-0.190
62.000	0.0	0.900	1.340	1.000	-0.180
90.000	0.520	0.900	1.340	1.000	-0.190
67.000	0.0	0.900	1.480	1.000	-0.190
84.000	0.280	0.900	1.480	1.000	-0.180
38.000	0.0	0.900	1.080	1.000	-0.190
70.000	0.520	0.900	1.080	1.000	-0.180
56.000	0.530	0.900	0.930	1.000	-0.180
57.000	0.150	0.900	1.200	1.000	-0.190
38.000	0.150	0.900	1.080	1.000	-0.190
33.000	-0.300	0.750	1.320	0.200	-0.190
55.000	0.180	0.750	1.320	0.780	-0.180
49.000	0.190	0.750	1.320	0.780	-0.180
58.000	0.180	0.750	1.320	0.780	-0.190
15.000	-0.100	0.750	1.320	1.000	-0.180
31.000	0.180	0.750	1.320	1.000	-0.180
55.000	0.320	0.750	1.320	1.000	-0.190
71.000	0.420	0.750	1.320	1.000	-0.190
88.000	0.600	0.750	1.320	1.000	-0.190
31.000	-0.100	0.750	1.680	1.000	-0.190
25.000	-0.100	0.750	1.600	1.000	-0.180
10.000	-0.100	0.750	1.040	1.000	-0.180
88.000	0.490	0.750	1.680	1.000	-0.180
87.000	0.490	0.750	1.600	1.000	-0.180
50.000	0.490	0.750	1.040	1.000	-0.180
78.000	0.200	0.750	1.320	0.200	-0.190
55.000	0.110	0.750	1.320	0.780	-0.180
41.000	0.420	0.750	1.320	1.200	-0.180
63.000	0.610	0.750	1.320	1.200	-0.180
44.530	0.530	0.750	1.320	1.340	-0.180
80.000	0.860	0.750	1.320	1.340	-0.180
71.000	0.150	0.750	1.320	0.780	-0.180
73.000	0.150	0.750	1.320	0.780	-0.180
60.000	0.640	0.750	1.040	1.000	-0.180
63.000	0.640	0.750	1.040	1.000	-0.190
9.000	-0.050	0.750	1.320	1.000	0.300
21.000	0.280	0.750	1.320	1.000	0.300
57.000	0.600	0.750	1.320	1.000	0.300
70.000	0.600	0.750	1.320	1.000	0.0
30.000	0.300	0.750	1.320	1.000	0.0
14.000	0.0	0.750	1.320	1.000	0.0
21.000	0.0	0.750	1.320	1.000	-0.190
42.000	0.300	0.750	1.320	1.000	-0.180
41.000	0.300	0.750	1.320	1.000	-0.190
95.000	0.600	0.750	1.320	1.000	-0.190
92.000	0.600	0.750	1.320	1.000	-0.480
66.000	0.300	0.750	1.320	1.000	-0.490
51.000	0.0	0.750	1.320	1.000	-0.780
40.000	0.0	0.750	1.320	1.000	-0.490
95.000	0.600	0.750	1.320	1.000	-0.780
79.000	0.300	0.750	1.320	1.000	-0.780
10.000	0.0	0.750	1.320	0.780	0.300
36.000	0.0	0.750	1.320	0.780	0.0
50.000	0.0	0.750	1.320	0.780	-0.490
13.000	0.300	0.750	1.040	1.000	0.0
40.000	0.300	0.750	1.040	1.000	-0.490
26.000	0.300	0.750	1.040	1.000	-0.180

TABLE 4-5

$R_M$	$\log \frac{HM_{wd}^4}{\lambda_m^3}$	$\log k$
22.000	0.210	0.900
51.000	0.900	0.900
70.000	1.420	0.900
81.000	1.800	0.900
90.000	2.020	0.900
62.000	1.040	0.900
90.000	2.070	0.900
67.000	1.250	0.900
84.000	1.820	0.900
38.000	0.620	0.900
70.000	1.630	0.900
56.000	1.440	0.900
57.000	1.110	0.900
33.000	0.910	0.900
33.000	1.310	0.750
55.000	1.650	0.750
49.000	1.650	0.750
58.000	1.650	0.750
15.000	0.810	0.750
31.000	1.260	0.750
55.000	1.650	0.750
71.000	1.870	0.750
89.000	2.210	0.750
31.000	1.290	0.750
25.000	1.260	0.750
10.000	0.360	0.750
88.000	2.560	0.750
37.000	2.440	0.750
56.000	1.540	0.750
79.000	2.320	0.750
55.000	1.520	0.750
41.000	1.530	0.750
63.000	1.970	0.750
44.000	1.630	0.750
80.000	2.290	0.750
50.000	3.600	-0.600
94.000	4.000	-0.600
36.000	3.150	-0.600
14.000	2.550	-0.470
46.000	3.570	-0.470
50.000	3.960	-0.470
41.000	3.150	-0.470
76.000	3.950	-0.600
26.000	3.530	-0.600
49.000	4.290	-0.600
54.000	3.950	-0.470
33.000	3.530	-0.470
70.000	4.290	-0.470
19.000	3.350	-0.470

TABLE 4-6

$R_M$	$\log \frac{M_{0.1} - M_{0.9}}{U_{0.1} - U_{0.9}}$
22.000	1.840
51.000	2.530
70.000	3.050
91.000	3.430
90.000	3.450
62.000	3.470
90.000	3.700
67.000	3.780
84.000	3.440
29.000	2.250
70.000	3.210
57.000	2.740
29.000	2.540
33.000	2.660
55.000	3.000
40.000	3.000
59.000	3.000
15.000	2.160
21.000	2.710
55.000	3.000
71.000	3.220
88.000	3.500
31.000	2.740
25.000	2.610
10.000	1.710
89.000	3.210
87.000	3.790
56.000	2.990
78.000	3.470
55.000	2.970
41.000	2.930
63.000	3.320
44.000	2.990
80.000	3.640
60.000	3.190
63.000	3.190
9.000	1.740
21.000	2.390
51.000	2.640
70.000	3.370
20.000	2.770
14.000	2.170
21.000	2.260
42.000	2.960
41.000	2.960
85.000	3.560
92.000	3.900
66.000	3.300
51.000	3.040
40.000	2.700
95.000	4.240
79.000	3.640
10.000	2.130
36.000	2.460
50.000	2.990
18.000	2.320
40.000	2.950
26.000	2.510
50.000	2.520
36.000	2.070
14.000	1.710
46.000	2.730
50.000	3.120
41.000	2.310
76.000	2.970
26.000	2.000
40.000	2.320
54.000	2.720
23.000	2.300
70.000	3.000
19.000	2.120

TABLE 4-7

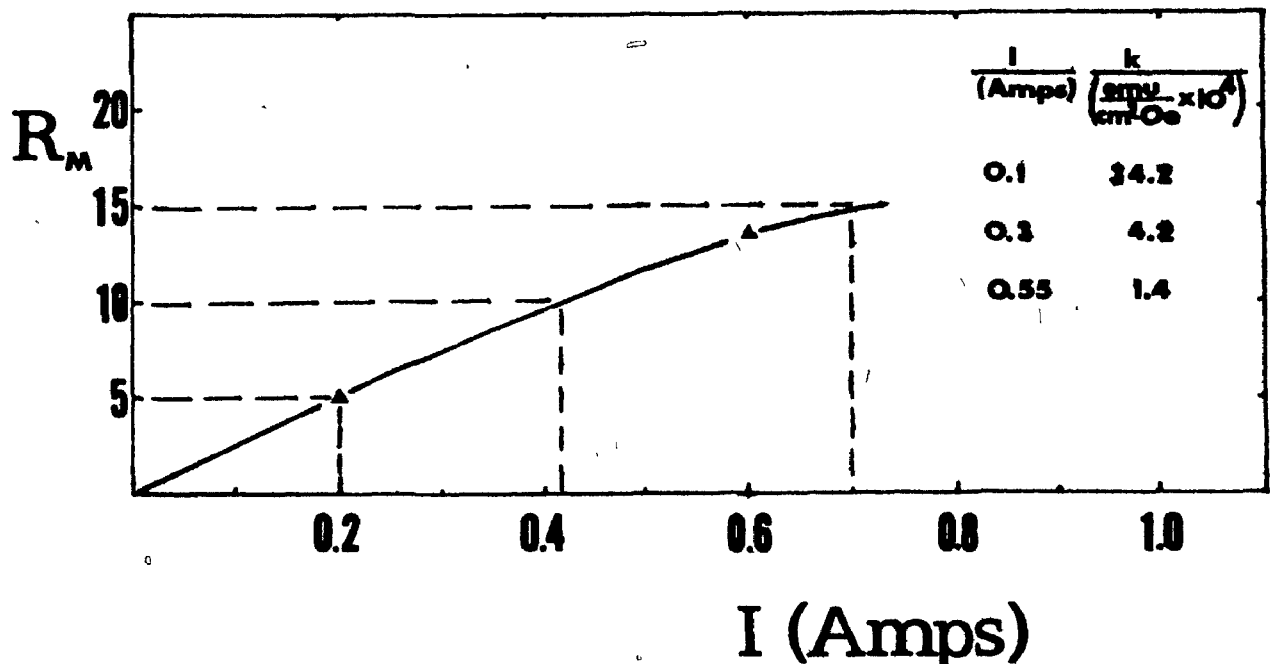
$R_M$	$\log \frac{HM_{w,1}^{3.5} d^{1.4}}{U_{1,1}^{1.5}}$
22.000	3.730
51.000	4.420
70.000	4.940
81.000	5.320
90.000	5.540
62.000	4.560
90.000	5.570
67.000	4.770
84.000	5.330
38.000	4.140
70.000	5.200
50.000	4.900
57.000	4.630
38.000	4.430
22.000	4.230
55.000	4.570
49.000	4.570
58.000	4.570
15.000	3.730
31.000	4.280
55.000	4.570
71.000	4.790
83.000	5.130
31.000	4.310
25.000	4.130
10.000	3.280
88.000	5.480
87.000	5.260
56.000	4.460
78.000	5.240
55.000	4.440
41.000	4.500
63.000	4.890
44.000	4.550
80.000	5.210
60.000	4.760
63.000	4.760
9.000	3.310
21.000	3.960
51.000	4.610
70.000	4.940
30.000	4.340
14.000	3.740
21.000	3.930
42.000	4.530
41.000	4.530
85.000	5.130
92.000	5.470
66.000	4.970
51.000	4.610
40.000	4.270
95.000	5.810
79.000	5.210
10.000	3.700
36.000	4.030
50.000	4.560
18.000	3.890
40.000	4.420
26.000	4.090

APPENDIX 5

I. METHODOLOGY FOR PREDICTING METALLURGY FROM TIN CONCENTRATE SEPARATIONS

Size and pyrrhotite distribution of the sample is given in Table 8.

The susceptibility of the sample was described by 3 k values. The magnetic response curve, below, shows that ~15% of the sample could be magnetically recovered. Each k value accounted for 5% of the sample, or 1/3rd of the magnetically recoverable material. Approximately 1/3rd of the magnetic material was recovered between 0 and 0.2 Amp, another 1/3rd between 0.2 and 0.4, and the final third between 0.4 and 0.7. Each was therefore characterized by the median value -0.1, 0.3 and 0.55 Amp, respectively. These were then used as the  $I_{50\%}$  in determining the susceptibility of the fraction of the sample that it represented (using Eq (24)). The volume susceptibilities and the specific gravities used to calculate them are given in Table 12.



Feed weight for four of the tests was 20 gms and estimated magnetically recoverable fraction for the tests was 10 to 15%. Therefore the average, 12.5%, of 20 gms represents an  $L_m = 0.04$ . Feed weight for a fifth test (Test #4) was 40 gms, or  $L_m = 0.08$ . If the predicted recovery was considerably different from 10 to 15%, then a new  $L_m$  would be selected and the prediction repeated.

$R_m$  for each d and k interval was determined with Eq (27).

$R_T$  was determined with Eq (33),  $R_{SnO_2T}$  with Eq (34),  $G_{Fe_7S_8}$  Mags with Eq (32), and  $G_{Fe_7S_8}$  Non-Mags with Eq (35).

#### SUMMARY OF GENERAL CONDITIONS

$d_{Fe_7S_8}$	$f_d$	% $Fe_7S_8$	$f_{Fe_7S_8}$
38.0	0.404	6.1	0.0246
28.0	0.505	10.3	0.0505
21.2	0.065	10.0	0.0065
15.0	0.041	10.0	0.0041

Test 1 - TIN CONCENTRATE SEPARATION

$$\begin{aligned}
 H &= 3.9 \text{ kG} \\
 U &= 15.6 \text{ cm/sec} \\
 L_m &= 0.04
 \end{aligned}$$

$\frac{d_{\text{Fe}_7\text{S}_8}}{(\mu\text{m})}$	$f_{\text{Fe}_7\text{S}_8}$	$R_M$ at $k =$			$R_{\text{fract}}$ at $k =$		
		34.2	4.2	1.4	34.2	4.2	1.4
38	0.0246	100	100	88	.0246	.0246	.0216
28	0.0505	100	94	74	.0505	.0475	.0373
21.2	0.0065	100	86	66	.0065	.0056	.0043
15	<u>0.0041</u>	100	73	53	<u>.0041</u>	<u>.0030</u>	<u>.0022</u>
	0.0857				.0857	.0806	.0654

$$R_{\text{fract } T} = \frac{1}{3}(.0857 + 0.806 + 0.0654) = .0772$$

$$R_{\text{Fe}_7\text{S}_8 M} = \frac{.0772}{.0857} \times 100 = 90.1 \therefore R_{\text{Fe}_7\text{S}_8 T} = 91.1\%$$

$$R_T \sim (13.5 \times \frac{90.1}{94.4}) + 2 = 15.0\%$$

$$R_{\text{SnO}_2 T} = 15.0 - (91.1)(.0857) = 7.3$$

$$G_{\text{Fe}_7\text{S}_8 \text{ Mags}} = \frac{(91.1)(8.57) \times 100}{(91.1)(8.57) + (7.3)(91.4)} = 53.9\%$$

$$G_{\text{Fe}_7\text{S}_8 \text{ Non-Mags}} = \frac{(8.9)(8.57) \times 100}{(8.9)(8.57) + (92.7)(91.4)} = 0.89$$

Test 2 - TIN CONCENTRATE SEPARATION

$$\begin{aligned}
 H &= 2.0 \text{ kG} \\
 U &= 15.6 \text{ cm/sec} \\
 L_m &= 0.04
 \end{aligned}$$

$d_{\text{Fe}_7\text{S}_8}$ ( $\mu\text{m}$ )	$f_{\text{Fe}_7\text{S}_8}$	$R_M$ at $k =$			$R_{\text{fract}}$ at $k =$		
		34.2	4.2	1.4	34.2	4.2	1.4
38	0.0246	100	88	68	.0246	.0216	.0167
28	0.0505	100	74	54	.0505	.0373	.0272
21.2	0.0065	100	66	46	.0065	.0043	.0030
15	0.0041	91	53	33	.0037	.0022	.0014
	0.0857				.0853	.0654	.0483

$$R_{\text{fract } T} = \frac{1}{3}(.0853 + .0654 + .0483) = .0663$$

$$R_{\text{Fe}_7\text{S}_8 M} = \left( \frac{.0663}{.0857} \right) \times 100 = 77.4\% \therefore R_{\text{Fe}_7\text{S}_8 T} = 78.4\%$$

$$R_T \sim \left( 13.5 \times \frac{77.4}{94.4} \right) + 2 = 13.0\%$$

$$R_{\text{SnO}_2 T} = 13.0 - (78.4)(.0857) = 6.4\%$$

$$G_{\text{Fe}_7\text{S}_8 \text{ Mags}} = \frac{(78.4)(.857) \times 100}{(78.4)(8.57) + (6.4)(91.4)} = 53.0\%$$

$$G_{\text{Fe}_7\text{S}_8 \text{ Non-Mags}} = \frac{(21.6)(8.57) \times 100}{(21.6)(8.57) + (93.6)(91.4)} = 2.12\%$$

Test 3 - TIN CONCENTRATE SEPARATION

$$\begin{aligned}
 H &= 1.2 \text{ kG} \\
 U &= 15.6 \text{ cm/sec} \\
 L_m &= 0.04
 \end{aligned}$$

$d_{\text{Fe}_7\text{S}_8}$ ( $\mu\text{m}$ )	$f_{\text{Fe}_7\text{S}_8}$	$R_M$ at $k =$			$R_{\text{fract}}$ at $k =$		
		34.2	4.2	1.4	34.2	4.2	1.4
38	0.0246	100	73	53	.0246	.0180	.0130
28	0.0505	97	59	39	.0490	.0230	.0197
21.2	0.0065	89	51	31	.0058	.0033	.0020
15	0.0041	76	38	18	.0031	.0016	.0007
	0.0857				.0825	.0459	.0354

$$R_{\text{fract } T} = \frac{1}{3}(.0825 + .0459 + .0354) = .0546$$

$$R_{\text{Fe}_7\text{S}_8 M} = \frac{.0546}{.0857} \times 100 = 63.7\% \quad \therefore R_{\text{Fe}_7\text{S}_8 T} = 64.7\%$$

$$R_T = (13.5 \times \frac{63.7}{94.4}) + 2 = 11.0\%$$

$$R_{\text{SnO}_2 T} = 11.0 - (64.7)(.0857) = 5.5\%$$

$$G_{\text{Fe}_7\text{S}_8 \text{ Mags}} = \frac{(64.7)(8.57) \times 100}{(64.7)(8.57) + (5.5)(91.4)} = 51.8$$

$$G_{\text{Fe}_7\text{S}_8 \text{ Non-Mags}} = \frac{(35.3)(8.57) \times 100}{(35.3)(8.57) + (94.5)(91.4)} = 3.38$$

Test 4 - TIN CONCENTRATE SEPARATION

$$\begin{aligned}
 H &= 2.0 \text{ kG} \\
 U &= 15.6 \text{ cm/sec} \\
 L_m &= 0.08
 \end{aligned}$$

$d_{\text{Fe}_7\text{S}_8}$ ( $\mu\text{m}$ )	$f_{\text{Fe}_7\text{S}_8}$	$R_M$ at $k =$			$R_{\text{fract}}$ at $k =$		
		34.2	4.2	1.4	34.2	4.2	1.4
38	.0246	100	80	60	.0246	.0197	.0148
28	.0505	100	66	46	.0505	.0333	.0232
21.2	.0065	96	58	38	.0062	.0038	.0025
15	.0041	83	45	25	.0034	.0018	.0010
	.0857				.0847	.0586	.0415

$$\begin{aligned}
 R_{\text{fract } T} &= \frac{1}{3}(.0847 + .0586 + .0415) \\
 &= .0616
 \end{aligned}$$

$$R_{\text{Fe}_7\text{S}_8 M} = \frac{.0616}{.0857} \times 100 = 71.9\% \quad \therefore R_{\text{Fe}_7\text{S}_8 T} = 72.9\%$$

$$R_T = (13.5 \times \frac{71.9}{94.4}) + 2 = 12.3\%$$

$$R_{\text{SnO}_2 T} = 12.3 - (72.9)(.0857) = 6.1\%$$

$$G_{\text{Fe}_7\text{S}_8 \text{ Mags}} = \frac{(72.9)(8.57) \times 100}{(72.9)(8.57) + (6.1)(91.4)} = 52.2\%$$

$$G_{\text{Fe}_7\text{S}_8 \text{ Non-mags}} = \frac{(27.1)(8.57) \times 100}{(27.1)(8.57) + (93.9)(91.4)} = 2.63\%$$

Test 5 - TIN CONCENTRATE SEPARATION

$$\begin{aligned}
 H &= 2.1 \text{ kG} \\
 U &= 22 \text{ cm/sec} \\
 L_m &= 0.04
 \end{aligned}$$

$d_{\text{Fe}_7\text{S}_8}$ ( $\mu\text{m}$ )	$d_{\text{Fe}_7\text{S}_8}$	$R_M$ at $k =$			$R_{\text{fract}}$ at $k =$		
		34.2	4.2	1.4	34.2	4.2	1.4
38	.0246	100	80	60	.0246	.0197	.0148
28	.0505	100	66	46	.0505	.0333	.0232
21.2	.0065	96	58	38	.0062	.0038	.0025
15	.0041	83	45	25	.0034	.0018	.0010
					.0847	.0586	.0415

$$\begin{aligned}
 R_{\text{fract T}} &= \frac{1}{3}(.0847 + .0586 + .0415) \\
 &= .0616
 \end{aligned}$$

$$R_{\text{Fe}_7\text{S}_8 \text{ M}} = \frac{.0616}{.0857} \times 100 = 71.9\% \quad \therefore R_{\text{Fe}_7\text{S}_8 \text{ T}} = 72.9\%$$

$$R_T = (13.5 \times \frac{71.9}{94.4}) + 2 = 12.3\%$$

$$R_{\text{SnO}_2 \text{ T}} = 12.3 - (72.9)(.0857) = 6.1\%$$

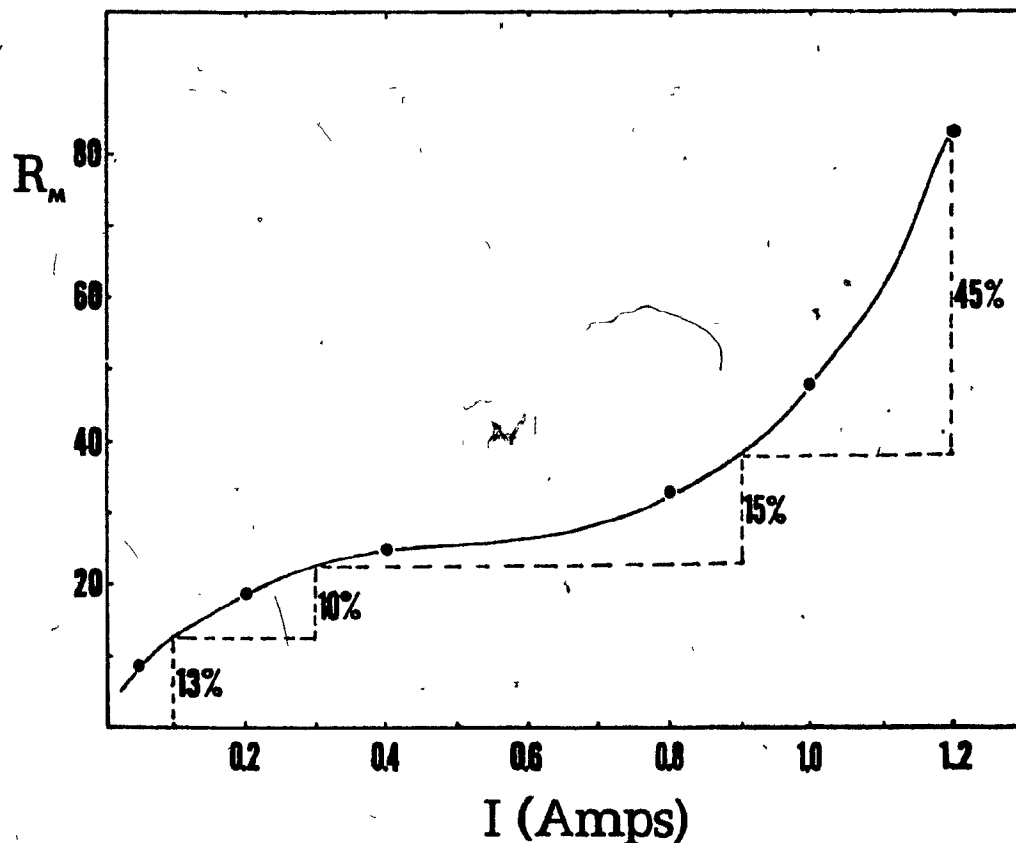
$$G_{\text{Fe}_7\text{S}_8 \text{ Mags}} = \frac{(72.9)(8.57) \times 100}{(72.9)(8.57) + (6.1)(91.4)} = 52.3\%$$

$$G_{\text{Fe}_7\text{S}_8 \text{ Non-mags}} = \frac{(27.1)(8.57) \times 100}{(27.1)(8.57) + (93.9)(91.4)} = 2.63\%$$

## II. METHODOLOGY FOR PREDICTING METALLURGY FROM COPPER CONCENTRATE SEPARATIONS

The particle size distribution of the cyclone U/F, -325m sample is shown in Figure 26.

The susceptibility of the sample was described by 4 values. The magnetic response curve, below, is an average of the response curves of the 2nd



and 3rd cyclosizer cones, Figure 27, which represent 53% of the sample. As can be seen from the response curve, 13% of the sample was recovered between 0 and 0.1 Amp, 10% between 0.1 and 0.3 Amp, 15% between 0.3 and 0.9 Amp, and 45% between 0.9 and 1.2 Amp. The median of each current range was applied to characterize the susceptibility of each range.

Feed weight for the four samples was 20 gms, and estimated magnetic recovery for the tests was 20 to 30%. Therefore, the average, 15%, of 20 gms represents an  $L_m = 0.084$ .

$R_M$  for each d and k interval was determined using Eq (27).

<u>Current range</u> (Amp)	<u>Median Current (<math>I_{50\%}</math>)</u> (Amp)	$k$ $\left(\frac{\text{emu}}{\text{cm}^3} \times 10^4\right)$	<u>Wt %</u>
0 ▶ 0.1	0.05	125	13
0.1 ▶ 0.3	0.20	7.8	10
0.3 ▶ 0.9	0.60	0.86	15
0.9 ▶ 1.2	1.05	0.29	45

Test 1 - COPPER CONCENTRATE SEPARATION

$$\begin{aligned}
 H &= 2.1 \text{ kG} \\
 U &= 22 \text{ cm/sec} \\
 L_m &= 0.084
 \end{aligned}$$

$\frac{d}{(\mu\text{m})}$	$\frac{f}{d}$	$R_M$ at $k =$				$R_{\text{fract}}$ at $k =$			
		125	7.8	0.86	0.29	125	7.8	0.86	0.29
35	.072	100	79	39	19	.072	.057	.028	.014
28	.271	100	70	30	10	.271	.190	.081	.027
21	.259	100	59	19	0	.259	.153	.049	0
15	.182	97	47	7	0	.177	.086	.013	0
11	.061	85	35	0	0	.052	.021	0	0
7	.155	68	18	0	0	.105	.028	0	0
						.936	.535	.171	.041

$$R_M = .13(93.6) + .10(53.5) + .15(17.1) + .45(4.1)$$

$$= 21.9\%$$

$$R_p \sim 1\%$$

$$R_T = 23\%$$

Test 2 - COPPER CONCENTRATE SEPARATION

$$\begin{aligned}
 H &= 1.1 \text{ kG} \\
 U &= 15.6 \text{ cm/sec} \\
 L_m &= 0.084
 \end{aligned}$$

<u>d</u>	<u>f<sub>d</sub></u>	<u>R<sub>M</sub> at k =</u>				<u>R<sub>fract</sub> at k =</u>			
		<u>125</u>	<u>7.8</u>	<u>0.86</u>	<u>0.29</u>	<u>125</u>	<u>7.8</u>	<u>0.86</u>	<u>0.29</u>
35	.072	100	69	29	9	.072	.050	.021	.007
28	.271	100	60	20	0	.271	.163	.054	0
21	.259	99	49	9	0	.256	.127	.023	0
15	.182	87	37	0	0	.158	.067	0	0
11	.061	75	25	0	0	.046	.015	0	0
7	.155	58	8	0	0	.090	.012	0	0
						.893	.434	.098	.007

$$R_M = .13(89.3) + .10(43.4) + .15(9.8) + .45(0.7)$$

$$= 17.7\%$$

$$R_p \sim 1\%$$

$$R_T = 19\%$$

Test 3 - COPPER CONCENTRATE SEPARATION

$$\begin{aligned}
 H &= 2.1 \text{ kG} \\
 U &= 15.6 \text{ cm/sec} \\
 L_m &= 0.084
 \end{aligned}$$

$\frac{d}{(\mu\text{m})}$	$f_d$	$R_M$ at $k =$				$R_{\text{fract}}$ at $k =$			
		125	7.8	0.86	0.29	125	7.8	0.86	0.29
35	.072	100	89	49	29	.072	.064	.035	.021
28	.271	100	80	40	20	.271	.217	.108	.054
21	.259	100	69	29	9	.259	.179	.075	.023
15	.182	100	57	17	0	.182	.104	.031	0
11	.061	95	45	5	0	.058	.028	.003	0
7	.155	78	28	0	0	.121	.043	0	0
						.963	.635	.252	.098

$$R_M = .13(96.3) + .10(63.5) + .15(25.2) + .45(9.8)$$

$$= 27.0$$

$$R_P \sim 1\%$$

$$R_T = 28\%$$

Test 4 - COPPER CONCENTRATE SEPARATION

$$\begin{aligned}
 H &= 4.0 \text{ kG} \\
 U &= 15.6 \text{ cm/sec} \\
 L_m &= 0.084
 \end{aligned}$$

$\frac{d}{(\mu\text{m})}$	$f_d$	$R_M$ at $k =$				$R_{\text{fract}}$ at $k =$			
		125	7.8	0.86	0.29	125	7.8	0.86	0.29
35	.072	100	100	69	42	.072	.072	.050	.030
28	.271	100	100	60	33	.271	.271	.163	.089
21	.259	100	89	49	22	.259	.231	.123	.057
15	.182	100	77	37	10	.182	.140	.067	.018
11	.061	100	65	25	0	.061	.040	.015	0
7	.155	100	48	8	0	.155	.074	.012	0
						1.000	.828	.430	.194

$$R_M = .13(100) + .10(82.8) + .15(43.0) + .45(19.4)$$

$$= 36.3\%$$

$$R_P \sim 1\%$$

$$R_T = 37\% \quad \equiv L_m = 0.12$$

$R_T$  in this case is greater than the expected  $L_m$  would be. Therefore, the prediction was repeated, except using an  $L_m = 0.11$  (33% capture).

Test 4 - COPPER CONCENTRATE SEPARATION

$$\begin{aligned}
 H &= 4.0 \text{ kG} \\
 U &= 15.6 \text{ cm/sec} \\
 \underline{L_m} &= 0.11
 \end{aligned}$$

$\frac{d}{(\mu\text{m})}$	$f_d$	$R_M$ at $k =$				$R_{\text{fract}}$ at $k =$			
		125	7.8	0.86	0.29	125	7.8	0.86	0.29
35	.072	100	100	66	39	.072	.072	.047	.028
28	.271	100	97	57	30	.271	.263	.154	.081
21	.259	100	86	46	19	.259	.222	.119	.049
15	.182	100	74	34	7	.182	.135	.062	.013
11	.061	100	62	22	0	.061	.037	.013	0
7	.155	95	45	5	0	<u>.147</u>	<u>.070</u>	<u>.003</u>	<u>0</u>
						.992	.799	.398	.171

$$\begin{aligned}
 R_M &= .13(99.2) + .10(79.9) + .15(39.8) + .45(17.1) \\
 &= 34.3
 \end{aligned}$$

$$R_P \approx 1\%$$

$$R_T = 35\%$$

Thus, the  $L_m$  chosen corresponds with the predicted weight recovery.

APPENDIX 6  
PRECISION OF SEPARATION

I. CONSTANT HEAD SYSTEM

$$R_M = -60.6 + 34.8 \log \left[ \frac{HM_w k^{1.2} d^{2.5}}{U^{1.8} L_m^{0.8}} \right] \quad (27)$$

Since  $H$ ,  $M_w$ ,  $U$  and  $L_m$  are constant, let

$$\left( \frac{HM_w}{U^{1.8} L_m^{0.8}} \right) = C$$

When  $R_M = 90\%$  let  $k = k_1$  and  $d = d_1$

Then,

$$\log \left[ k_1^{1.2} d_1^{2.5} C \right] = \frac{90 + 60.6}{34.8} = 4.33$$

$$\text{Therefore, } \left[ k_1^{1.2} d_1^{2.5} C \right] = 2.14 \times 10^4$$

When  $R_M = 10\%$  let  $k = k_2$ , and  $d = d_2$

$$\text{Then, } \log \left[ k_2^{1.2} d_2^{2.5} C \right] = \frac{10 + 60.6}{34.8} = 2.03$$

$$\text{Therefore, } \left[ k_2^{1.2} d_2^{2.5} C \right] = 1.07 \times 10^2$$

$$\text{Therefore, } \frac{k_1^{1.2} d_1^{2.5}}{k_2^{1.2} d_2^{2.5}} = \frac{2.14 \times 10^4}{1.07 \times 10^2} = 200$$

(a) Let  $d_1 = d_2$

Then,  $\left(\frac{k_1}{k_2}\right)^{1.2} = 200$

$1.2 \log \left(\frac{k_1}{k_2}\right) = \log 200$

$\log \left(\frac{k_1}{k_2}\right) = \frac{\log 200}{1.2} = 1.92$

Therefore,  $\frac{k_1}{k_2} = 83$

(b) Let  $k_1 = k_2$

Then,  $\left(\frac{d_1}{d_2}\right)^{2.5} = 200$

$2.5 \log \left(\frac{d_1}{d_2}\right) = \log 200$

$\log \left(\frac{d_1}{d_2}\right) = \frac{\log 200}{2.5} = 0.92$

Therefore,  $\frac{d_1}{d_2} = 8.3$

## II. DRAINAGE SYSTEM

$$R_M = -58.9 + 38.3 \log \left[ \frac{HM_w k^{1.8} d^{1.6}}{U^{1.3} L_m^{1.1}} \right] \quad (28)$$

$$\text{Let } \left( \frac{HM_w}{U^{1.3} L_m^{1.1}} \right) = C$$

When  $R_M = 90\%$ , let  $k = k_1$ , and  $d = d_1$

$$\begin{aligned} \text{Then, } \log \left[ k_1^{1.8} d_1^{1.6} C \right] &= \frac{90 + 58.9}{38.3} \\ &= 3.88 \end{aligned}$$

$$\text{Therefore, } \left[ k_1^{1.8} d_1^{1.6} C \right] = 7.59 \times 10^3$$

When  $R_M = 10\%$ , let  $k = k_2$ , and  $d = d_2$

$$\text{Then, } \log \left[ k_2^{1.8} d_2^{1.6} C \right] = \frac{10 + 58.9}{38.3}$$

$$= 1.80$$

$$\text{Therefore, } \left[ k_2^{1.8} d_2^{1.6} C \right] = 6.3 \times 10$$

$$\text{Therefore, } \frac{k_1^{1.8} d_1^{1.6}}{k_2^{1.8} d_2^{1.6}} = \frac{7.59 \times 10^3}{6.3 \times 10} = 120$$

(a) Let  $d_1 = d_2$

$$\text{Then, } \left( \frac{k_1}{k_2} \right)^{1.8} = 120$$

$$1.8 \log \left( \frac{k_1}{k_2} \right) = \log 120$$

$$\log \left( \frac{k_1}{k_2} \right) = \frac{\log 120}{1.8} = 1.16$$

$$\text{Therefore, } \frac{k_1}{k_2} = 14.3$$

(b) Let  $k_1 = k_2$

$$\text{Then, } \left( \frac{d_1}{d_2} \right)^{1.6} = 120$$

$$1.6 \log \left( \frac{d_1}{d_2} \right) = \log 120$$

$$\log \left( \frac{d_1}{d_2} \right) = \frac{\log 120}{1.6} = 1.30$$

$$\text{Therefore, } \frac{d_1}{d_2} = 20.0$$

REFERENCES

1. Taggart, A.F., "Handbook of Mineral Dressing", John Wiley and Sons, Inc., New York, Sect. 13 (1944).
2. Gaudin, A.M., "Principles of Mineral Dressing", McGraw-Hill Book Co., New York, Chap. 18 (1939).
3. Lawver, J.E. and Hopstock, D.M., Minerals Sci. Engng. 6 (3), 154 (1974).
4. Oberteuffer, J.A., IEEE Trans. MAG - 10, No. 2, 223 (1974).
5. British Patent No. 768,451 (1955).
6. Jones, G.H., Proc. 5th Int. Min. Proc. Congress, London, 717 (1960).
7. Stone, W.J.D., Proc. 5th Int. Min. Proc. Congress, London, 733 (1960).
8. Bartnik, J.A., Zabel, W.H. and Hopstock, D.M., Int. J. of Min. Processing 2 (2), 117 (1975).
9. Stone, W.J.D., Can. Min. J. 92 (6), 56 (1971).
10. Jones, G.H., Proc. 7th Int. Min. Proc. Congress, New York, 405 (1964).
11. Carpenter, J.H., Proc. 7th Int. Min. Proc. Congress, New York, 399 (1964).
12. Lawver, J.E., Wright, J.L. and Kokal, H.R., Trans. A.I.M.E. 241, 194 (1968).
13. Cullity, B.D., "Introduction to Magnetic Materials", Addison-Wesley Publishing Co., Chap. 1 and 2 (1972).
14. Oberteuffer, J.A. and Kelland, D.R. (Eds.), Proc. HGMS Symposium, M.I.T., May 22, 1973.
15. Kolm, H.H., Oberteuffer, J.A. and Kelland, D.R., Scientific American 233 (5), 46 (1975).
16. U.S. Patent No. 3,627,678 (1971).
17. Kelland, D.R. and Maxwell, E., IEEE Trans. MAG-11, No. 5, 1582 (1975).
18. Kelland, D.R. and Maxwell, E., 104th Annual Meeting, A.I.M.E. (1975).
19. Watson, J.H.P., Clark, N.O. and Windle W., 11th Int. Min. Proc. Congress, Paper 29, Cagliari (1975)

20. Trindade, S.C. and Kolm, H.H., IEEE Trans. MAG-9, No. 3, 310 (1973).
21. deLatour, C., IEEE Trans. MAG-9, No. 3, 314 (1973).
22. Oberteuffer, J.A. et al, IEEE Trans. MAG-11, No. 5, 1591 (1975).
23. Collins, D.N. and Read, A.D., Minerals Sci. Engng. 3 (2), 19 (1971).
24. Klassen, V.I. and Mokrousov, V.A., "An Introduction to the Theory of Flotation", Butterworth, Chapter 18, (1963).
25. Gaudin, A.M. and Malozemoff, P., J. Phys. Chem. 37, 597 (1933).
26. Gaudin, A.M. and Malozemoff, P., Trans. A.I.M.E. 112, 303 (1934).
27. Read, A.D. and Whitehead, A., 10th Int. Min. Proc. Congress, London Paper 1 (1973).
28. Yarar, B. and Kitchener, J.A., Trans. Inst. Min. Metall. 79, C23, (1970).
29. Mozley, R.H., Inter. Tin Council, London 1, 79 (1968).
30. Bean, C.P., Bull Am. Phys. Soc. 16, 350 (1971).
31. Watson, J.H.P., J. Appl. Phys. 44 (9), 4209 (1973).
32. Watson, J.H.P., IEEE Trans. MAG-11, No. 5, 1597 (1975).
33. Luborsky, F.E. and Drummond, B.J., IEEE Trans. MAG-11, No. 6, 1969 (1975).
34. Stratton, J.A., "Electromagnetic Theory", McGraw-Hill, New York (1941).
35. Oberteuffer, J.A., IEEE Trans. MAG-9, No. 3, 303 (1973).
36. Kelsall, D.F., Trans. Inst. Min. & Metall. 70, 191 (1961).
37. Maxwell, E., Cryogenics 15 (4), 179 (1975).
38. Hein, R.A., Science 185 (4147), 211 (1974).
39. Stekly, Z. J.J., IEEE Trans. MAG-11, No. 5, 1594 (1975).
40. M.V.E. Cryogenics, "Safe Handling and Operating Instructions for USHE Liquid Helium Containers".
41. Ref. 13, p. 43.
42. Hess, H.H., Notes on Operation of Frantz Isodynamic Separator; S.G. Frantz Co.
43. Gaudin, A.M. and Spedden, H.R., Trans. A.I.M.E. 153, 563 (1943).
44. Partridge, A.C., Flotation and Absorption Characteristics of the Hematite-Dodecylamine-Starch System, M. Sc. Thesis, McGill University, p.23 (1970).

45. Smith, S.L., "Ore Microscopy", Sturm & Smith, Tucson, Arizona,  
p. 109 (1957).

46. Ref. 13, p. 108.